

DISSERTATION

FROM *RETROVIRIDAE* TO *FLAVIVIRIDAE*: ADVENTURES IN MOLECULAR
VIROLOGY

Submitted by

Molly Butler

Department of Microbiology, Immunology, and Pathology

In partial fulfillment of the requirements

For the Degree of Doctor of Philosophy

Colorado State University

Fort Collins, Colorado

Spring 2021

Doctoral Committee:

Advisor: Joel Rovnak

Sandra Quackenbush
Julie Moreno
Mark Stenglein

Copyright by Molly Butler 2021

All Rights Reserved

ABSTRACT

FROM *RETROVIRIDAE* TO *FLAVIVIRIDAE*: ADVENTURES IN MOLECULAR VIROLOGY

The work presented here encompasses two avenues of investigation: the first, regarding the identification of a novel retrovirus in Gunnison's prairie dogs, and the second regarding the role of cyclin-dependent kinases 8 and 19 (CDK8 and CDK19) as transcriptional regulators during infection with dengue virus serotype 2 (DENV2) and during the innate immune response.

Part I: During the course of research and wildlife disease surveillance efforts, we identified three cases of thymic lymphoma in free-ranging Gunnison's prairie dogs (*Cynomys gunnisoni*). As Gunnison's prairie dogs are keystone species, that is, critical for the maintenance of their ecosystems, we investigated the potential for an association between the observed thymic lymphomas and retroviral infection. We identified a novel retroviral sequence which exhibits genetic organization consistent with a type D betaretrovirus and which was highly associated with thymic lymphoma in Gunnison's prairie dogs. The proposed name of this virus is Gunnison's prairie dog retrovirus (GPDRV).

Part II: CDK8 and CDK19 are transcriptional regulators which are critical for modulating gene expression changes during induced states such as hypoxia and starvation. We investigated the role of CDK8 and CDK19 in two distinct but related induced states: infection with DENV2 and the type I interferon response. We found that

in the context of DENV2 infection, CDK8/19 regulate metabolic gene expression changes, the result of which is a reshaping of the host cell metabolic environment which is ultimately beneficial to viral replication. Therefore, chemical inhibition or reduced expression of CDK8 or CDK19 significantly restricted viral replication. Both within the context of DENV2 infection and with non-viral stimulation of innate immunity, we identified a role for CDK8 and CDK19 as regulators of the type I interferon response. CDK8 and CDK19 have distinct and overlapping functions as regulators of IFN- β expression dependent on the nature of the stimulus. This work not only furthers our understanding of host transcriptional regulation during DENV2 infection and within innate immunity, but also the diverse and complex functions of CDK8 and CDK19 as key modulators of cellular stress responses.

ACKNOWLEDGEMENTS

I would like to start by acknowledging the first person I met at CSU, Heidi Runge. My meeting with Heidi was the first step on the road that brought me to today, and I cannot thank her enough for her generosity, kindness, and excellent advice. I also cannot overstate how reassuring it is to have someone who knows the answer to every question and is patient and kind and willing to respond to even the most frazzled graduate student with grace. Thank you, Heidi.

Speaking of important mentors at CSU – thank you to my committee. I want to thank Mark Stenglein, for taking me on as a rotation student, allowing me to continue a project I had already started – a project which ultimately became a chapter in this dissertation. Mark also gave me some very constructive feedback on my rotation evaluation: that I should focus on what I need to do, instead of trying to do a million things at once. I think about that a lot – and know that he was absolutely right. Because whenever I remember to follow that advice, things magically go much better. I also want to thank Jennifer Nyborg for being an invaluable member of my committee, for asking insightful and important questions, again, which I think about a lot, and which made my work stronger.

I also want to especially thank Julie Moreno, not only for being a committee member, but also a mentor and a friend. I had the immense privilege of working with Julie in leading a Career Issues group, and I am so grateful for that opportunity. Not only is Julie amazingly kind and supportive, she is brilliant and accomplished and someone I look up to as a scientist and as a human being.

Next, I am so grateful for my cohort. I want to thank Megan Miller, Shaun Cross, Bridget Eklund, Dan Hartman, and Kristy Burkhalter so much for being such wonderful classmates, study buddies, co-complainers, listeners, and friends. They say the best place to be is surrounded by people who are smarter than you, and I feel so lucky that that is exactly where I got to be. I am so excited to see what incredible lives this amazing group of individuals go on to have.

I want to thank Jasmine Donkoh for being the best “partner-in-the-lab” I could ever ask for. I am so grateful for her presence in my life for the last three years. Sharing a lab, an office, and large chunks of my life with Jasmine was an absolute joy. I am so grateful for the laughs, the snacks, and the shared complaints. She celebrated with me during the best times and commiserated during the worst times, in all cases with candy and wine. My life is so much better for her in it.

I am so thankful for Connie Brewster, who taught me so much - much more than I could ever say here. She was so patient and kind and thoughtful and the first person that truly made me feel like I belonged in science. Just as important as the many lab techniques she taught me, I will never forget Connie’s Rules of Molecular Biology: (1) Don’t panic and (2) Don’t get greedy. Excellent advice, in science and life. I also can’t express how grateful I was to have a someone that I knew I could come to with any question no matter how basic and any idea no matter how crazy, or “unencumbered by data,” it may have been. Thank you, Connie.

Everything that has happened in my life in the last five years would not have been possible without Sandra Quackenbush and Joel Rovnak. When I was thinking about applying for graduate school, I sent an email to almost the entire list of MIP

faculty, asking for a chance to volunteer in their labs. Q and Joel responded. It is not lost on me that their one email completely changed my life for the better. Q and Joel took a chance on me – a part-time, non-traditional student without any research experience and with a full-time job outside of school. I am so amazingly grateful for them, that not only did they take a chance on me, but that they also cared enough to make it work. This crazy idea I had to get a PhD without having any clue what I was doing could have gone so many different ways, and it only worked because of Q and Joel. Thank you so much for teaching me everything I know.

I also need to acknowledge my family for their unending support, love, and encouragement. I am so grateful for my dad, who made me believe I could do anything I set my mind to and who has always supported my most outlandish ambitions. Thank you to Carrie, Leslee, and Eric, my siblings, for always holding the door open for me as we moved through life and teaching me all the things that they had to learn the hard way. And finally, I cannot express how grateful I am for my mom. I always thought that I was going to turn into my mom as I grew up, and now I know that I would be incredibly lucky to be half as good, half as kind, and half as wonderful of a mother as she is to me.

Finally, I cannot say enough about the light of my life, my husband Tommy. I feel so lucky to have such a wonderful best friend to spend with my life with, who makes me laugh, and who makes me a better person, and who makes me so proud. Thank you for always being by my side, and I am so excited to see what's next.

TABLE OF CONTENTS

ABSTRACT.....	ii
ACKNOWLEDGEMENTS.....	iii
PART I: Identification of a Novel Retrovirus in Gunnison’s Prairie Dogs.....	1
Chapter 1: Overview of Literature, Part I.....	2
1.1 Gunnison’s Prairie Dogs.....	2
1.1a Geographic Distribution and Ecological Importance.....	2
1.1b Health Threats to Prairie Dogs.....	2
1.2 Retroviruses.....	3
1.2a Retrovirus Genome Organization.....	3
1.2b Characteristic Features of Betaretroviruses.....	5
1.2c Retrovirus Replication Cycle.....	6
1.3 Oncogenic Retroviruses.....	8
1.3a Overview of Oncogenic Retroviruses.....	8
1.3b Mechanisms of Retroviral Oncogenesis.....	9
Chapter 2: Identification of a Novel Retrovirus (Gunnison’s Prairie Dog Retrovirus) Associated with Thymic Lymphoma in Gunnison’s Prairie Dogs in Colorado, USA.....	12
2.1 Summary	12
2.2 Introduction.....	13
2.3 Materials and Methods.....	14
2.3a Necropsy, Histopathology, and Immunohistochemistry.....	14
2.3b PCR for <i>Yersinia pestis</i> and <i>Francisella tularensis</i>	16
2.3c RNA Extraction and RT-PCR.....	17
2.3d Library Preparation, NextGen Sequencing, Genome Assembly and Analysis.....	19
2.3e Phylogenetics	21
2.3f Integration Site Analysis.....	22
2.3g PCR Screening for GPDRV and ERV-PDRV.1- <i>Cynomys ludovicianus</i>	23
2.3h Deposition of Sequences and of Expression Data.....	24
2.4 Results	25
2.4a Thymic Lymphoma in Gunnison’s Prairie Dogs.....	25
2.4b Identification of Prairie Dog Retroviral Sequence Associated with Thymic Lymphoma	28
2.4c Prairie Dog Endogenous Retroviral Sequence.....	30
2.4d Features of the Gunnison’s Prairie Dog Retrovirus Sequence, Predicted Proteins, and Phylogenetic Analysis.....	30
2.4e Integration Site Analysis.....	38
2.4f Screening for GPDRV with Virus-Specific Primers.....	38
2.5 Discussion	40
PART II: The Role of Cyclin-Dependent Kinases 8 and 19 as Transcriptional Regulators during Viral Infection and in the Innate Immune Response.....	45
Chapter 3: Overview of Literature, Part II.....	46

3.1 Dengue Viruses.....	46
3.1a Dengue Virus Serotype 2 (DENV2) Genome and Proteins.....	47
3.1b DENV2 Replication.....	54
3.1c Metabolism Changes during DENV2 Infection.....	58
3.2 The Type I Interferon Response.....	63
3.2a Type I IFN Induction and Signaling Pathways.....	64
3.2b Type I IFN Evasion by DENV2.....	67
3.2c Transcriptional Regulation of IFN- β Expression.....	67
3.3 Cyclin-dependent Kinases 8 and 19.....	69
3.3a Mechanisms of Transcriptional Regulation by CDK8/19.....	70
3.3b CDK8/19 Chemical Inhibition.....	74
3.3c Viral Manipulation of CDK8/19.....	75
3.4 Summary and Introduction to Research Aims.....	76
3.4a Introduction to Research Aims, Chapter 4.....	76
3.4b Introduction to Research Aims, Chapter 5.....	77
Chapter 4: Cyclin-dependent Kinases 8 and 19 Regulate Host Cell Metabolism during Dengue Virus Serotype 2 Infection.....	79
4.1 Summary	79
4.2 Introduction.....	80
4.3 Materials and Methods.....	83
4.3a Cell Culture and DENV2 Infection.....	83
4.3b CDK8/19 Small-Molecule Inhibition and Cell Viability Assay.....	84
4.3c qRT-PCR Analysis.....	84
4.3d Plaque-forming Unit and Extracellular Genome Equivalent Analysis.....	85
4.3e Lentivirus-mediated shRNA Gene Knockdown.....	86
4.3f Subcellular Extracts and Protein Analysis.....	87
4.3g Mitochondrial and Glycolytic Stress Tests.....	89
4.3h Statistics	91
4.4 Results	91
4.4a Cyclin-dependent Kinase 8 is Upregulated during DENV2 Infection	91
4.4b Knockdowns of CDK8 and CDK19 Reduce DENV2 Replication	94
4.4c CDK8/19 Chemical Inhibition Reduces DENV2 Replication.....	96
4.4d Metabolic Gene Expression is Dependent on CDK8/19 Kinase Activity	99
4.4e Senexin A Reduces Induction of Lipophagic Gene Expression	102
4.4f Senexin A Inhibits Mitochondrial Respiration	105
4.5 Discussion.....	109
Chapter 5: Cyclin-dependent Kinases 8 and 19 Differentially Regulate the Early Phase of the Type I Interferon Response	115
5.1 Summary.....	115
5.2 Introduction.....	116
5.3 Materials and Methods.....	118
5.3a Cell Culture, DENV2 Infection, and Poly(I:C) Treatment.....	118
5.3b qRT-PCR Analysis.....	119

5.3c Establishment of Knockdown Cell Lines.....	120
5.3d Subcellular Extracts and Protein Analysis.....	121
5.3e Statistics.....	122
5.4 Results	122
5.4a CDK8/19 Chemical Inhibition Reduces IFN- β and OAS1 Expression during DENV Infection.....	122
5.4b The DENV2 Requirement for CDK8 is Independent of the Type I Interferon Response.....	124
5.4c CDK19 is a Negative Regulator of the Type I IFN Response during DENV2 Infection.....	127
5.4d CDK8 and CDK19 Have Distinct Regulatory Roles in Induction of the Type I IFN Response.....	129
5.5 Discussion	131
Conclusion	136
References	140

PART I: IDENTIFICATION OF A NOVEL RETROVIRUS IN GUNNISON'S PRAIRIE
DOGS

CHAPTER 1: OVERVIEW OF LITERATURE, PART I

1.1 Gunnison's Prairie Dogs

1.1a Geographic Distribution and Ecological Importance

Colorado is home to three of the five free-ranging prairie dog species native to North America: the white-tailed prairie dog (*Cynomys leucurus*), the black-tailed prairie dog (*Cynomys ludovicianus*), and the Gunnison's prairie dog (*Cynomys gunnisoni*). Prairie dogs are a member of the *Sciuridae* family, along with squirrels and other burrowing rodents. Prairie dogs are considered "keystone" species in that prairie dogs and their burrows provide prey and habitat for a number of wild birds and mammals which supports diverse plant and pollinator communities, and the health of the local ecosystem often depends on the health of prairie dog populations (Hardwicke, 2006; Miller et al., 2007a).

1.1b Health Threats to Gunnison's Prairie Dogs

Disease threats from plague (caused by *Yersinia pestis*) are well understood in prairie dogs which are highly susceptible to fatal infections from *Y. pestis* (Richgels et al., 2016). However, the roles of other infectious agents in the health of free-ranging prairie dog colonies have not been extensively considered.

Much of the available information about prairie dog health, including the incidence of cancer, comes from studies in prairie dogs that are kept in captivity either as pets or for research. The most commonly reported tumors of captive prairie dogs are elodontoma and hepatocellular adenocarcinoma, of which hepatocellular carcinoma may be associated with infection by a hepadnavirus (Thas and Garner, 2012; Wright et al., 2017). Other tumors are less commonly encountered in captive prairie dogs but do include lymphoma and thymoma (Matsumoto et al., 2017; Miwa et al., 2006; Thas and Garner, 2012). An infectious cause for lymphoid tumors in prairie dogs has not been investigated, although retroviruses are a well-known cause of several human and veterinary lymphoid cancers (Hardy et al., 1973; Mammerickx et al., 1987; Miwa et al., 2006; Poiesz et al., 1980; Xu et al., 2013).

1.2 Retroviruses

1.2a Retrovirus Genome Organization

Retroviral genomes are single-stranded, positive-sense RNA genomes and contain at a minimum *gag*, *pro-pol*, and *env* coding regions. *Gag* and *env* encode structural and envelope proteins while *pro-pol* encodes for the viral enzymes required for replication including protease, reverse transcriptase, and integrase.

Retroviruses employ mechanisms to regulate the translation of viral mRNA transcripts due to the demand for a much greater amount of Gag proteins compared to enzymatic proteins. Differential expression is achieved by completing translation after

production of Gag with much greater frequency than allowing translation to progress through *pro-pol* (LeBlanc et al., 2013). The two primary mechanisms are frameshifting and termination suppression. Frameshifts occur when *gag* and *pro-pol* are in different reading frames, separated by a “slippery” A-U rich sequence. Ribosomes pause on the “slippery” sequence and then “slip” back one nucleotide, therefore entering into the -1 reading frame, avoiding the stop codon, and allowing translation of Pro-pol. This is a low-frequency event, allowing much more robust translation of Gag than Gag-pro-pol (LeBlanc et al., 2013). Termination suppression occurs when *gag* and *pro-pol* are in the same reading frame and separated by a stop codon. Termination suppression after translation of Gag is achieved with an insertion of a glutamine tRNA at the *gag* stop codon, allowing readthrough into the *pro-pol* sequence (LeBlanc et al., 2013). Like frameshifts, termination suppression is a low-frequency event and thereby a mechanism for differentially regulating Gag and Pro-pol expression from the same mRNA transcripts (LeBlanc et al., 2013).

In addition to the essential components of *gag*, *pro-pol*, and *env*, many retroviral genomes encode additional proteins which serve accessory functions in viral replication. Complex retroviral genomes, such as those of lentiviruses and deltaretroviruses, encode many accessory genes which aid in viral replication and host immune evasion. For example, the lentivirus human immunodeficiency virus 1 (HIV-1) encodes six accessory proteins: transactivator of transcription (Tat), regulator of virion (Rev), viral protein R (Vpr), viral protein U (Vpu), viral infectivity factor (Vif), and negative regulatory factor (Nef) (Frankel and Young, 1998). These six accessory proteins are responsible for functions essential for viral replication including transport into the nucleus upon

infection (Vpr), transcription initiation and processivity (Tat), export of unspliced viral transcripts out of the nucleus (Rev), host immune evasion (Vif and Nef), and viral particle release (Vpu) (Frankel and Young, 1998).

1.2b Characteristic Features of Betaretroviruses

Betaretroviruses, such as mouse mammary tumor virus (MMTV), jaagsiekte sheep retrovirus (JSRV), and enzootic nasal tumor virus (ENTV), have characteristic features, which while individually are not completely exclusive to the genus, in combination allow for classification distinct from other genera of retroviruses in accordance with sequence similarity in highly conserved regions such as *pro-pol*. In betaretroviruses, regulation of expression of structural versus enzymatic viral proteins is achieved through two frameshift events (one between *gag* and *pro* and one between *pro* and *pol*) where a translating ribosome slips back one base and allows the translation of Pro-pol at lower frequency than Gag (Hizi and Herschhorn, 2008; Hizi et al., 1987). Additionally, a classic feature of betaretroviral genomes is a coding sequence for a viral dUTPase which, by limiting the ratio of dUTP to dTTP, functions to prevent the erroneous incorporation of dUTP into DNA products (Hizi and Herzig, 2015). Additionally, some, but not all, betaretroviruses encode an immunosuppressive domain in the Env protein, as exhibited by Mason-Pfizer monkey virus (Sonigo et al., 1986). Betaretroviral genome organization is summarized in Figure 1.1.

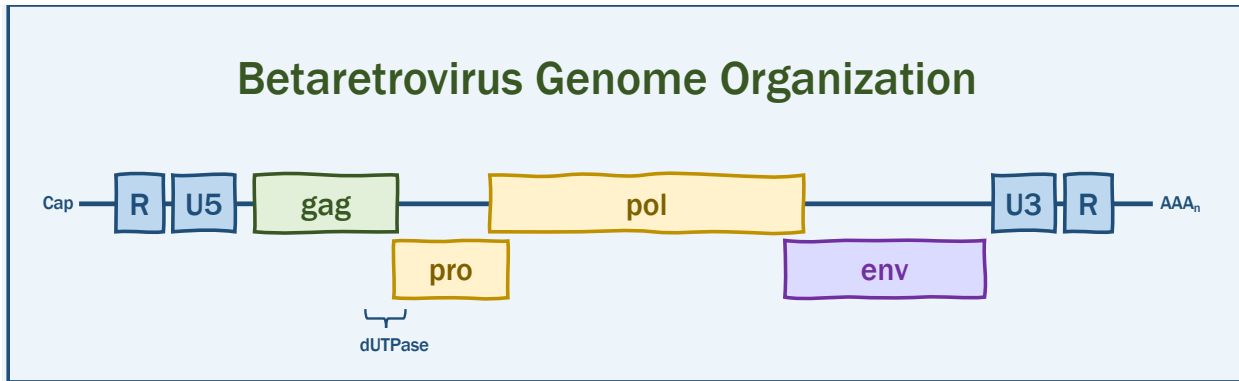


Figure 1.1 Betaretrovirus Genome Organization. Untranslated elements (cap, R, U5, U3, polyA tail) are indicated in blue. Frameshifts allow differential translation of Gag and Pro-pol and are indicated in overlap in coding regions in betaretroviral genomes. The dUTPase, characteristic of betaretroviruses, is encoded by the 3' end of *gag* and the 5' end of *pro*.

1.2c Retrovirus Replication Cycle

Retroviral particles contain two copies of the RNA genome, as well as the viral proteins reverse transcriptase (RT) and integrase. Upon cellular receptor binding, the contents of the viral particle enter the cytoplasm and reverse transcription is initiated. Viral RT, which has RNA-dependent DNA polymerase and RNase H activity, transcribes the single-stranded RNA genome into double-stranded DNA, which then translocates to the nucleus and is inserted into the host genome through the activity of viral integrase. The provirus is transcribed by host transcription machinery. Full-length transcripts, which are capped and polyadenylated by host machinery, may serve as viral genome copies while others are spliced to yield Env transcripts. Gag-pol and Gag precursor polypeptides are translated and processed into individual viral proteins in the cytoplasm. Viral particles assemble and then bud through the plasma membrane (Flint et al., 2015). The retroviral replication cycle is summarized in Figure 1.2.

Retroviral Replication Cycle

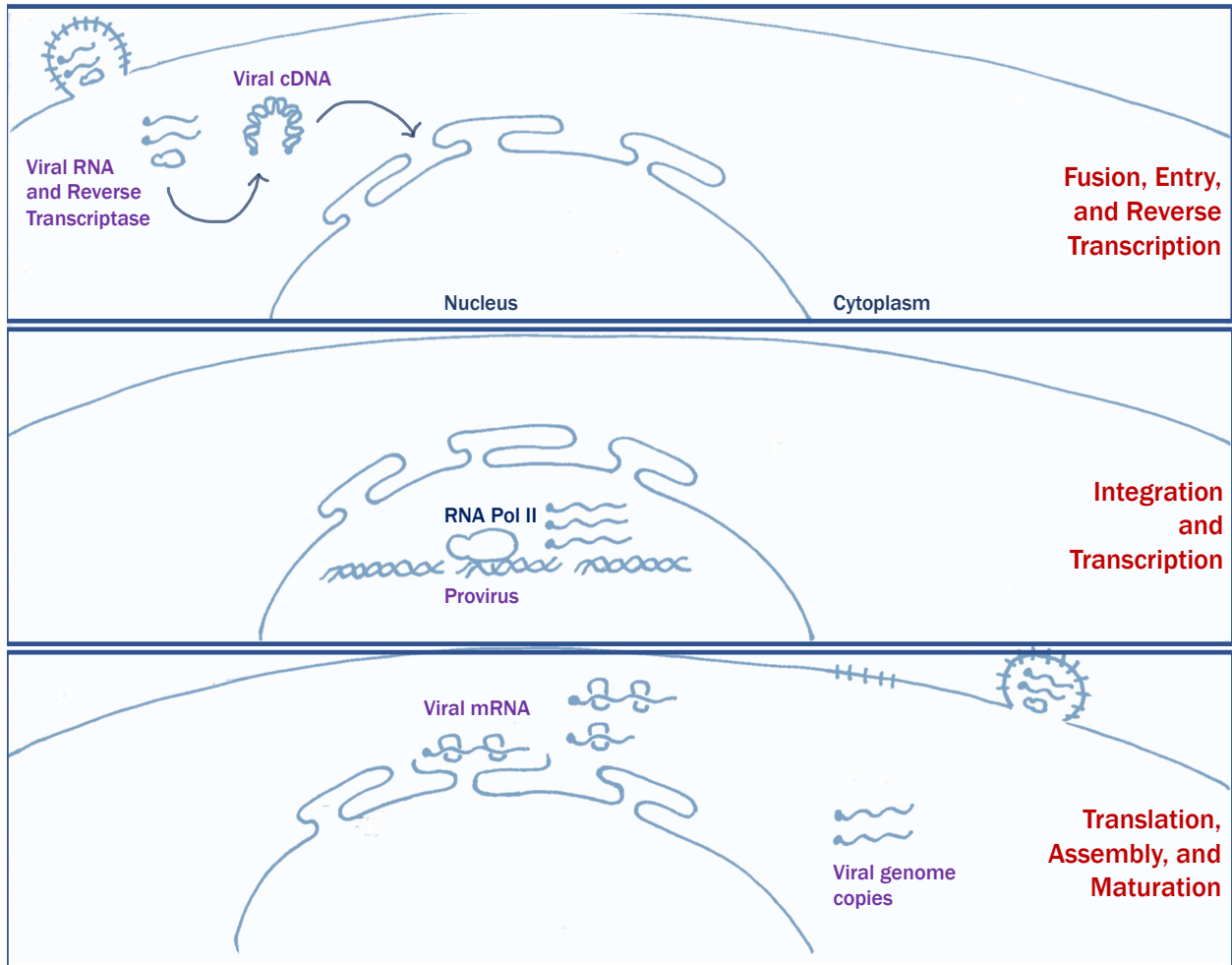


Figure 1.2 Retroviral Replication Cycle. Top panel: Fusion of the viral envelope with the plasma membrane allows release of viral particle contents into the cytoplasm. Viral mRNA is reverse transcribed into cDNA by viral reverse transcriptase, forming the pre-integration complex which then translocates to the nucleus. Middle panel: Viral cDNA integrates into the host DNA through the action of viral integrase. The provirus is transcribed by host transcription machinery. Bottom panel: Full-length viral transcripts are translated by host machinery to produce Gag and Pro-pol, spliced transcripts are translated on the ER to produce Env. Additional full-length capped and polyadenylated viral transcripts function as viral genome copies. Particle assembly occurs at the plasma membrane, and viral particles bud out of the host cell.

1.3 Oncogenic Retroviruses

1.3a Overview of Oncogenic Retroviruses

Since the initial discovery by Rous in 1911 of transmissibility of tumors through inoculation of cell-free filtrates, many oncogenic retroviruses have been identified in a wide range of species (Burmeister, 2001; Rous, 1911; Rubin, 2011). Representative members of all genera of retroviruses with the exception of *Spumaretrovirus* are associated with malignant disease, summarized in Table 1.1.

Malignancies associated with retroviral infection can arise from a wide variety of cell types and manifest as a diverse array of disease states. Lymphocytes are common targets of retroviral oncogenesis, manifesting in the form of lymphoma and/or leukemia. Development of lymphoma is associated with feline leukemia virus (FeLV) infection and feline immunodeficiency virus (FIV) infection, as well as infection with murine leukemia and avian leukosis viruses (Burmeister, 2001).

In some cases, such as infection with FeLV and FIV, possible sequela of retroviral infection also include immune suppression (Beatty et al., 1998; Hartmann, 2012; Hoover et al., 1987; Magden et al., 2013). This immunosuppression is an indirect mechanism by which retroviral infection can lead to neoplastic disease, as is primarily the case for lymphomas associated with FIV infection (Beatty et al., 1998; Magden et al., 2013).

Table 1.1 Representative Sample of Oncogenic Animal Retroviruses

Genus	Representative Virus	Associated Malignant Disease	References
<i>Epsilonretrovirus</i>	Walleye dermal sarcoma virus	Sarcoma	(Rovnak and Quackenbush, 2010)
<i>Gammaretrovirus</i>	Feline leukemia virus	Leukemia/lymphoma, predominately T-cell	(Hardy et al., 1973; Hoover et al., 1987; Tsatsanis et al., 1994)
<i>Deltaretrovirus</i>	Bovine leukemia virus	Leukosis	(Mammerickx et al., 1987)
<i>Alpharetrovirus</i>	Rous sarcoma virus	Sarcoma	(Rous, 1911)
<i>Betaretrovirus</i>	Mouse mammary tumor virus	Mammary adenocarcinoma	(Graff et al., 1949; Theodorou et al., 2007)
<i>Lentivirus</i>	Feline immunodeficiency virus	Lymphoma, predominately B-cell	(Beatty et al., 1998; Magden et al., 2013; Poli et al., 1994)

1.3b Mechanisms of Retroviral Oncogenesis

In addition to indirect oncogenesis through immunosuppression, there are several other mechanisms by which retroviral infection can lead to neoplastic disease. These fall broadly into four categories: insertional mutagenesis, cellular oncogene capture, virally encoded regulatory or accessory genes which contribute to oncogenesis, and dysregulation of cellular signaling pathways (Maeda et al., 2008).

Insertional mutagenesis refers to the process by which retroviral genome insertion into the host genome disrupts transcription at the site of insertion. Insertional mutagenesis can be the result of insertion of a long terminal repeat (LTR) element near a transcription start site, resulting in increased promoter activity off of the LTR to promote increased transcription of whichever cellular genes is regulated by said

promoter. Likewise, enhancer activity can be promoted by insertion of LTR elements, also leading to increased host gene expression. Dependent on the site of insertion, both of these events have the potential for cellular proto-oncogenes to become overexpressed and lead to uncontrolled cellular proliferation (Maeda et al., 2008).

Avian leukosis virus (ALV) provides a classic example of insertional mutagenesis in which a large majority of lymphomas associated with ALV viral genome integration is adjacent to the cellular gene *c-myc* (Hayward et al., 1981). Insertion of the LTR element immediately upstream of *c-myc* results in overexpression of *myc* and uncontrolled cellular proliferation (Hayward et al., 1981). Similarly, insertion sites of MMTV are commonly adjacent to cellular proliferation pathway components including components of the Wnt, fibroblast growth factor (FGF), Notch, and Ras signaling pathways (Theodorou et al., 2007).

Cellular oncogene capture occurs when a cellular gene is “captured” into a retroviral genome as a replication error. Recombination between the genome copy which contains the cellular gene and a typical viral genome generally results in a replication defective virus but allows expression of the cellular gene during transcription of the provirus, resulting in overexpression of the oncogene (Maeda et al., 2008). The capture of avian *c-src* by avian sarcoma virus (ASV) is the classic example of cellular oncogene capture, by which *c-src* is incorporated into a replication-defective ASV genome and then expressed upon integration (Stehelin et al., 1976).

Virally encoded genes are also known to contribute to retroviral oncogenesis. Tax, a transcriptional regulator expressed by human T-cell leukemia virus type I (HTLV-I), has transforming capability, as inoculation of Tax-expressing but uninfected cells into

naïve animals results in tumor formation (Tanaka et al., 1990). Additionally, the envelope protein (Env) of both JSRV and ENTV has been shown to be a primary driver of bronchioalveolar tumor formation in infected animals (Alberti et al., 2002; Palmarini et al., 1999; Wootton et al., 2006; Zavala et al., 2003). This is primarily thought to be the result of disruption of cellular proliferation pathway activation by Env (Alberti et al., 2002; Zavala et al., 2003). In addition to JSRV and ENTV, other retroviruses are known to contribute to oncogenesis through dysregulation of cell signaling. Friend spleen focus-forming virus (SFFV) infection leads to constitutive activation of MAPK, overexpression of *c-jun*, and constitutive Ras-GTP binding, resulting in a constitutive cellular state which mimics the typically transient cellular response to growth factors (Muszynski et al., 1998, 2000).

CHAPTER 2: A NOVEL RETROVIRUS (GUNNISON'S PRAIRIE
DOG RETROVIRUS) ASSOCIATED WITH THYMIC LYMPHOMA IN GUNNISON'S
PRAIRIE DOGS IN COLORADO, USA¹

2.1 Summary

As part of research and wildlife disease surveillance efforts, we performed necropsy examinations of 125 free-ranging ($n = 114$) and captive ($n = 11$) prairie dogs in Colorado from 2009 to 2017. From these cases, we identified three cases of thymic lymphoma in free-ranging Gunnison's prairie dogs (*Cynomys gunnisoni*), and we identified a novel retroviral sequence associated with these tumors. The viral sequence is 7700 nucleotides in length and exhibits a genetic organization that is consistent with the characteristics of a type D betaretrovirus. The proposed name of this virus is Gunnison's prairie dog retrovirus (GPDRV). We screened all 125 prairie dogs for the presence of GPDRV using PCR with envelope-specific primers and DNA extracted from spleen samples. Samples were from Gunnison's prairie dogs ($n = 59$), black-tailed prairie dogs (*Cynomys ludovicianus*) ($n = 40$), and white-tailed prairie dogs (*Cynomys leucurus*) ($n = 26$). We identified GPDRV in a total of 7/125 (5.6%) samples including all three of the prairie dogs with thymic lymphoma, as well as spleen from an additional four Gunnison's prairie dogs with no tumors recognized at necropsy. None of the GPDRV-negative Gunnison's prairie dogs had thymic lymphomas. We also identified a

¹Butler, M.D.; Griffin, K.; Brewster, C.D.; Kapuscinski, M.L.; Stenglein, M.D.; Tripp, D.W.; Quackenbush, S.L.; Fox, K.A. (2020). A Novel Retrovirus (Gunnison's Prairie Dog Retrovirus) Associated With Thymic Lymphoma in Gunnison's Prairie Dogs in Colorado, USA. *Viruses*. 12, 606

related, apparently endogenous retroviral sequence in all prairie dog samples. These results suggest that GPDRV infection may lead to development of thymic lymphoma in Gunnison's prairie dogs.

2.2 Introduction

Colorado is home to three of the five free-ranging prairie dog species native to North America: the white-tailed prairie dog (*Cynomys leucurus*), the black-tailed prairie dog (*Cynomys ludovicianus*), and the Gunnison's prairie dog (*Cynomys gunnisoni*). Prairie dogs are a member of the *Sciuridae* family, along with squirrels and other burrowing rodents. Prairie dogs are considered "keystone" species in that prairie dogs and their burrows provide prey and habitat for a number of wild birds and mammals, they support diverse plant and pollinator communities, and the health of the local ecosystem often depends on the health of prairie dog populations (Hardwicke, 2006; Kotliar et al., 2006). Disease threats from plague (caused by *Yersinia pestis*) are well understood in prairie dogs (Ecke and Johnson; Richgels et al., 2016) which are highly susceptible to fatal infections from *Y. pestis*. However, the roles of other infectious agents in the health of free-ranging prairie dog colonies have not been extensively considered.

Much of the available information about prairie dog health, including the incidence of cancer, comes from studies in prairie dogs that are kept in captivity either as pets or for research. The most commonly reported tumors of captive prairie dogs are elodontoma and hepatocellular adenocarcinoma, of which hepatocellular carcinoma

may be associated with infection by a hepadnavirus (Thas and Garner, 2012; Wright et al., 2017). Other tumors are less commonly encountered in captive prairie dogs but do include lymphoma and thymoma (Matsumoto et al., 2017; Miwa et al., 2006; Thas and Garner, 2012). An infectious cause for lymphoid tumors in prairie dogs has not been investigated, although retroviruses are a well-known cause of several human and veterinary lymphoid cancers (Hardy et al., 1973; Jarrett et al., 1964; Mammerickx et al., 1987; Poiesz et al., 1980; Rosenberg and Jolicoeur, 1997; Xu et al., 2013). In some cases, such as infection with feline leukemia virus and feline immunodeficiency virus, possible sequela of retroviral infection also include immune suppression (Beatty et al., 1998; Hartmann, 2012; Hoover et al., 1987; Magden et al., 2013; Orosz et al., 1985).

During the course of wildlife disease research and surveillance activities in Colorado, USA, we identified three free-ranging Gunnison's prairie dogs with thymic lymphoma, and a novel type D betaretrovirus associated with these tumors. Based on the known sensitivity of prairie dogs to sylvatic plague, we also considered retroviral infections as a possible source of immune suppression that could contribute to mortality.

2.3 Materials and Methods

2.3a Necropsy, Histopathology, and Immunohistochemistry

From 2009 to 2017, we necropsied 125 free-ranging ($n = 114$) and captive ($n = 11$) prairie dogs from Colorado. Species examined included Gunnison's ($n = 59$), black-tailed ($n = 40$), and white-tailed ($n = 26$) prairie dogs. Animals examined were either

found dead ($n = 118$), died during processing ($n = 3$), or were euthanized due to disease concerns ($n = 4$). Research methods included trapping and brief anesthesia with isoflurane gas (Tripp et al., 2017) and were approved (06/06/2013) by the Colorado Parks and Wildlife Animal Care and Use Committee #06-2013.

Gross necropsy was performed for all 125 prairie dogs to determine cause of death, and we pursued histopathology if cause of death was not apparent from gross necropsy and tissues were suitable. Prior to necropsy, the carcasses were either frozen at -20 C to preserve the carcass and to kill fleas, or fresh carcasses were treated with insecticide (Deltamethrin/DeltaDust, Bayer Environmental Science, Cary, NC, USA) prior to necropsy to kill fleas without the need for freezing. Necropsies were conducted in a biological safety cabinet (NU-S813-400, Nuair, Plymouth, MN, USA) with additional personal protective equipment in accordance with BSL-2 biosafety practices.

After necropsy, carcasses were frozen at -20 C until *Y. pestis* PCR results were obtained, and any carcasses with tissues confirmed positive for *Y. pestis* or *Francisella tularensis* were disposed of by chemical digestion. For histopathology, tissues were fixed in 10% neutral buffered formalin, embedded in paraffin wax, sectioned by microtome to approximately 8 micrometers, affixed to glass slides, and stained with hematoxylin and eosin.

We used immunohistochemistry to identify T-lymphocytes (CD-3 (LN10, Leica Biosystems, Buffalo Grove, IL, USA)), B-lymphocytes (PAX-5 (1EW, Leica Biosystems, Buffalo Grove, IL, USA)), and epithelial cells/cytokeratin (MCK (AE1/AE3, Leica Biosystems, Buffalo Grove, IL, USA)) in formalin-fixed paraffin embedded tissues. The above monoclonal mouse anti-human antibodies were applied using a Leica BOND-

MAX automated IHC staining platform (Leica Biosystems, Buffalo Grove, IL, USA), with chromogen Poly-AP anti-mouse (PV6110, PowerVision, Leica Biosystems, Buffalo Grove, IL, USA) used for PAX-5 and MCF, and chromogen Poly-HRP anti-mouse (PV6113, PowerVision, Leica Biosystems, Buffalo Grove, IL, USA) used for CD-3. Slides were counterstained with hematoxylin. Negative controls of duplicate tissue sections were incubated in antibody diluent and homologous nonimmune sera. Non-specific staining was not observed.

To confirm efficacy in prairie dog tissues, we applied IHC stains to control tissues, including thymus, spleen, and skin from a yearling prairie dog that died from enteric disease. These control tissues demonstrated expected staining properties including robust staining of T-lymphocytes in the thymus with CD-3, scattered staining of B-lymphocytes in the thymus with PAX-5, and staining of epithelial cords and nests (Hassall's corpuscles) in the thymus with MCK. Control prairie dog spleen demonstrated robust staining with PAX-5, highlighting follicular structure, and skin epithelium demonstrated robust staining with MCK.

2.3b PCR for *Yersinia pestis* and *Francisella tularensis*

We extracted DNA from spleen tissue of all (n = 125) prairie dogs, under BSL-2 conditions, using a DNeasy blood and tissue kit (Qiagen, Valencia, CA, USA). Each sample was tested for presence of *Y. pestis* by PCR using primers caf 1-F/caf 1-R (Table 2.1) (Begier et al., 2006) and cycling conditions as previously described (Griffin et al., 2010). Primers (50 μ M) and DNA template (50–250 ng) were added to a 0.2 mL

PCR tube containing a puReTaq Ready-To-Go PCR bead (Illustra, GE Healthcare Bio-Sciences Corp, Piscataway, NJ, USA) for a final volume of 25 μ L. Cycling conditions were: 94 C for 10 min (1 cycle), followed by 94 C for 1 min, 55 C for 1 min, 72 C for 30 s (35 cycles), and 72°C for 10 min (1 cycle). The final product was visualized on a 2% agarose gel. DNA extracted from spleen (see above) was also tested for *F. tularensis* using primers P2/P3 (Table 2.1) and cycling conditions as previously described (Junhui et al., 1996). Primers (20 μ M) and DNA template (50–250 ng) were added to a 0.2 mL PCR tube containing a puReTaq Ready-To-Go PCR bead (Illustra, GE Healthcare Bio-Sciences Corp, Piscataway, NJ, USA) for a final volume of 25 μ L. Cycling conditions were: 97 C for 10 min (1 cycle), followed by 94 C for 1 min, 55 C for 1 min, 75 C for 1 min (35 cycles), and 75 C for 10 min (1 cycle). The final product was visualized on a 2% agarose gel.

2.3c. RNA Extraction and RT-PCR

Total RNA was extracted from fresh-frozen spleen (case nos. 11-1310, 14-1342, 15-1406) and thymic tumor (case nos. 14-1342, 15-1406) tissue samples using TRIzol (ThermoFisher Scientific, Waltham, MA, USA) according to the manufacturer's instructions. One microgram of DNase (Ambion Turbo DNase; ThermoFisher Scientific, Waltham, MA, USA) RNA was reverse transcribed into cDNA using SuperScript III (ThermoFisher, Scientific, Waltham, MA, USA) according to the manufacturer's protocol. A 3:1 mix of random hexamers and oligo-dT or the degenerate primer, YMDD, was used as the reverse primer (Table 2.1). PCR was performed using

Taq DNA polymerase (ThermoScientific, Waltham, MA) with the degenerate primers LPQG and YMDD (Table 2.1). PCR reactions contained 2 μ L cDNA in reaction buffer comprised of 200 nM of each primer, 2 mM MgCl₂, 0.2 mM dNTPs and 0.5 units of Fermentas *Taq* DNA polymerase (ThermoFisher Scientific, Waltham, MA, USA) in a total volume of 50 μ L. The cycling conditions were as follows for cycles 1–10: 94 C for 1 min, 37 C for 2 min, and 72 C for 3 min. The conditions for cycles 11–40 were: 94 C for 30 s, 55 C for 1 min, and 72 C for 1 min (Donehower et al., 1990). The PCR product was purified (QIAquick PCR Purification Kit (Qiagen, Valencia, CA, USA)), cloned into the pCR2.1 TOPO vector (ThermoFisher Scientific, Waltham, MA, USA) and submitted for sequencing.

Table 2.1 PCR primers

Primer Designation	Primer Sequence
<i>caf1-F</i>	5' ATA CTG CAG ATG AAA AAA ATC AGT TCC 3'
<i>caf1-R</i>	5' ATA AAG CTT TTA TTG GTT AGA TAC GGT 3'
P2	5' TAG GAT CCC ATT AGC TGT CCA CTT ACC 3'
P3	5' GGA ATT CGT TAG GTG GCT CTG ATG AT 3'
YMDD	5' ATC AGA TCC TAC TAA CDR TCR TCC ATR TA 3'
LPQG	5' TAC CAG TGG AAT GTT CTA CCN 3'
LTR-F	5' GAC CGT GAC TTG TTT ATC TAA CCA CAA 3'
Env-7073	5' AGA CTG CAA TCT TTG GTA ATG AAC CTG 3'
SP3	5' AAG GTT CTT CAT CCA GGA GGT ATA TCT C 3'
SP4	5' TTT GGA CTT CAA CCA TGG GGA AAA TAC 3'
SP5	5' TTC CGT ACT TAC CCC TTC TTT CCG AT 3'
LTR-R	5' CCA AGG TTC TTC ATC CAG GAG GTA TAT 3'
494F	5' AAG GAT GTG AAG GAA CTA TAC AGC CAT 3'
591R	5' TCG GGG TGA ATT GGA ATT GAA AAG AAA 3'
393F	5' ATG CTG ACT GGG ATA TGG TCA AAA ATG 3'
1961R	5' GTA TCG GGT TTC CTT GGA CAT CAA ATT 3'
5729F	5' GGA TGG CAA ATC GTA TTA TCA GGC TAC 3'
5840R	5' TAG AGT TCC CAC TGA GGT ACC TAA GAT 3'

2.3d Library Preparation, NextGen Sequencing, Genome Assembly and Analysis

The KAPA Biosystems RNA HyperPrep Kit (Roche, Pleasanton, CA, USA) was used to prepare sequencing libraries from 100 ng total RNA isolated from the lymphoma and spleen from two Gunnison's prairie dogs (14-1342, 15-1406) with tumors, the spleen from two Gunnison's prairie dogs (15-656, 15-671) without tumor, and the spleen from a Black-tailed prairie dog (14-1382) without tumor according to the manufacturer's protocol using half-scale reactions without fragmentation. Pooled libraries were length-selected for 300–500-bp fragments using a BluePippin 2% cassette (Sage Biosciences, Beverly, MA, USA). Length-selected libraries were cleaned using a 1:1.4 ratio of solid phase reversible immobilization (Caspritz and Hadden, 1987) beads (Kapa Biosystems, Roche, Pleasanton, CA, USA). Individual libraries were then pooled for sequencing. The library pool was diluted to 4 nM based on fluorometric DNA quantification (Qubit High Sensitivity DNA Assay; ThermoFisher Scientific, Waltham, MA, USA) and quantified by qPCR using the KAPA Library Quantification Kit (Kapa Biosystems, Roche, Pleasanton, CA, USA). Paired-end 2 × 150 bp sequencing was performed on an Illumina NextSeq, producing an average of 5×10^6 read pairs per dataset.

Datasets were processed as previously described, with the goal of taxonomically categorizing all non-prairie dog reads (Cross et al., 2018). Briefly, first low-quality and adapter sequences were filtered using Cutadapt v1.18 (Martin, 2011). Duplicate read pairs (reads that shared >96% pairwise identity) were removed using cd-hit v4.8.1 (Fu et al., 2012). Bowtie2 was used to remove host-derived reads by mapping to a combined index built from the *Marmota marmota* (European marmot;

GCF_001458135.1) and *Ictidomys tridecemlineatus* (thirteen-lined ground squirrel; GCF_000236235.1) genomes and transcriptomes (Gossmann et al., 2019; Langmead and Salzberg, 2012). Reads with an alignment score >60 were removed. Remaining reads were assembled using the SPAdes assembler (Bankevich et al., 2012). Contigs were taxonomically assigned by searching the NCBI nt database using BLASTN and then by searching the NCBI nr database using diamond (Buchfink et al., 2015; Camacho et al., 2009). Candidate retrovirus-derived contigs were manually inspected in Geneious Prime 2020.0.3 (<https://www.geneious.com>) and validated by re-mapping reads using bowtie2 as above. This analysis pipeline is available at https://github.com/stenglein-lab/taxonomy_pipeline. Libraries from HeLa cell total RNA and water were constructed and analyzed in parallel as positive and negative controls.

PCR and Sanger sequencing confirmation of the Gunnison's prairie dog retrovirus (GPDRV) genome assembly was performed on high-molecular weight splenic DNA from a tumor-negative but GPDRV sequence positive prairie dog using a forward primer in the LTR (LTR-F) and a reverse primer in env (Env-7073) (Table 2.1). PCR conditions were as follows: 98 C for 30 s, then 30 cycles of 98 C for 10 s, 66 C for 20 s, and 72 C for 4min, followed by 72 C for 5 min. A single PCR product of the expected size (7266 bp) was cloned into Strataclone Blunt vector (Agilent Technologies, LaJolla, CA, USA) Plasmid DNA was isolated from individual colonies. Samples were confirmed positive for the insert by restriction digest and sent for Sanger sequencing. The sequence was confirmed using primer walking. Fisher's exact test was performed as implemented in R (RC Team, 2017).

2.3e Phylogenetics

To collect relevant Pol sequences, we used two strategies. First, we queried the GPDRV Pol sequence against the NCBI nr protein database using BLASTP (Altschul et al., 1990) and retrieved all aligning sequences that produced alignments with E-values lower than 10^{-40} . We removed sequences shorter than 600 amino acids and used cd-hit to collapse sequences that shared >95% pairwise identity (Fu et al., 2012; Martin, 2011). Secondly, we collected all Pol sequences in the NCBI RefSeq protein database annotated under the family *Retroviridae* (taxid 11632). To collect Env transmembrane protein (TM) domain sequences, we collected all Env sequences in the NCBI RefSeq protein database annotated under the family *Retroviridae*. Because of the high level of sequence divergence between retrovirus Env sequences, we selected the subset of these Env TM refseqs that produced a blastp alignment with an E-value $<10^{-40}$.

In all of these cases, we aligned collected sequences using the MAFFT aligner v7.407 with default parameters and trimmed alignments using TrimAL v1.4.rev15 (Capella-Gutierrez et al., 2009; Katoh and Standley, 2013). The best model for tree inference was selected using modeltest-ng and trees were created using RaxML-ng v. 0.9.0 with standard parameters (Darriba et al., 2020; Stamatakis, 2014). Trees were visualized using the Interactive Tree Of Life (iTOL) v4 (Letunic and Bork, 2019).

2.3f Integration Site Analysis

We performed an integration site analysis using Retro-X Integration Site Analysis Kit (Clontech, Mountain View, CA, USA) according to the manufacturer's instructions. Briefly, high molecular weight genomic DNA was isolated from tumor tissue and then digested with restriction enzymes *Ssp1*, *Hpa1*, or *Dra1*. Digested DNA was purified and then ligated to GenomeWalker (Clontech, Mountain View, CA, USA) adaptors using T4 DNA ligase. A primary PCR reaction was performed on the adaptor-ligated DNA using an outer, adaptor-specific forward primer AP1, and an outer, GPDRV sequence-specific reverse primer (SP3, SP4, or SP5, Table 2.1). A secondary, or nested PCR reaction was performed using the primary PCR reaction amplicons as template, a nested adaptor-specific primer AP2, and a nested GPDRV sequence-specific reverse primer (SP3 or LTR-R, Table 2.1). Secondary PCR products were visualized by electrophoresis on an agarose gel to confirm a single, predominant PCR product. PCR products were cloned (Topo TA (ThermoFisher, Waltham, MA, USA)) and plasmid DNA was isolated from individual colonies. Samples were confirmed positive for inserts by restriction digest and submitted for Sanger sequencing. Sequences that partially overlapped on the 3' end with the 5' end of the GPDRV sequence, but that diverged upstream were identified as integration sites.

2.3g PCR Screening for GPDRV and ERV-PDRV.1-*Cynomys ludovicianus*

Endogenous pro/pol: Primers 494F/591R (Table 2.1) were used to screen DNA extracted from 42 prairie dog spleen samples (DNeasy blood and tissue kit (Qiagen, Valencia, CA, USA)). These samples were selected to include captive ($n = 7$) and free-ranging ($n = 35$) animals representing the timespan of the entire project, and originating from carcasses with minimal to mild autolysis suggesting good DNA quality. DNA template (10 ng) was added to a PCR mixture containing 5 μ L 10x Taq buffer with $(\text{NH}_4)_2\text{SO}_4$, 0.5 μ L Taq polymerase (Fermentas, ThermoFisher Scientific, Waltham MA, USA), 200 μ M (each) dNTPs, 500 pmol (each primer), 1 mM MgCl_2 , and sterile water to a final volume of 50 μ L. Cycling conditions were: 95 C for 3 min (1 cycle), followed by 95 C for 30 s, 53.7 C for 30 s, 72 C for 30 s (30 cycles), and 72 C for 5 min. The final product was visualized on a 1% agarose gel.

GPDRV gag gene: Primers 393F/1961R (Table 2.1) were used to screen DNA extracted from 42 prairie dog spleen samples (DNeasy blood and tissue kit (Qiagen, Valencia, CA, USA)). DNA template (10 ng) was added to a PCR mixture containing 5 μ L 10x Taq buffer with $(\text{NH}_4)_2\text{SO}_4$, 0.5 μ L Taq polymerase (Fermentas, ThermoFisher Scientific, Waltham, MA, USA), 200 μ M (each) dNTPs, 500 pmol (each primer), 1 mM MgCl_2 , and sterile water to a final volume of 50 μ L. Cycling conditions were: 95 C for 3 min (1 cycle), followed by 95 C for 30 s, 51 C for 45 s, 72 C for 30 s (30cycles), and 72 C for 5 min. The final product was visualized on a 1% agarose gel.

GPDRV env gene: Primers 5729F/5840R (Table 2.1) were used to screen DNA extracted from prairie dog spleen samples (DNeasy blood and tissue kit (Qiagen,

Valencia, CA, USA)). DNA template (10 ng) was added to a PCR mixture containing 5 μ L 10 \times Taq buffer with (NH₄)₂SO₄, 0.5 μ L Taq polymerase (Fermentas, ThermoFisher Scientific, Waltham, MA, USA), 200 μ M (each) dNTPs, 500 pmol (each primer), 1 mM MgCl₂, and sterile water to a final volume of 50 μ L. Cycling conditions were: 95 C for 3 min (1 cycle), followed by 95 C for 30 s, 54.3 C for 30 s, 72 C for 30 s (30 cycles), and 72 C for 5 min. The final product was visualized on a 1% agarose gel.

Primers 5729F/5840R (Table 2.1) were also used to screen DNA extracted from an additional 83 prairie dog spleen samples (DNeasy blood and tissue kit (Qiagen, Valencia, CA, USA)). Primers (0.5 μ M) and DNA template (50–250 ng) were added to a 0.2 mL PCR tube containing a puReTaq Ready-To-Go PCR bead (Illustra, GE Healthcare Bio-Sciences Corp, Piscataway, NJ, USA) for a final volume of 25 μ L. Cycling conditions were: 95 C for 3 min (1 cycle), followed by 95 C for 30 s, 54.3 C for 30 s, 72 C for 30 s (30 cycles), and 72 C for 5 min (1 cycle). The final product was visualized on a 2% agarose gel.

2.3h Deposition of Sequences and of Expression Data

Sequences have been deposited in GenBank under accession numbers MT361316, MT361317, and MT316318. The data have been deposited with links to BioProject accession number PRJNA631279 in the NCBI BioProject database (<https://www.ncbi.nlm.nih.gov/bioproject/>).

2.4 Results

2.4a Thymic Lymphoma in Gunnison's Prairie Dogs

Causes of death in prairie dogs included bacteremia, trauma, capture-related factors, environmental factors, intraspecific aggression, euthanasia for disease concern, and thymic lymphoma (Table 2.2). Plague, caused by *Y. pestis*, accounted for nearly all (49/54; 91%) of the cases of bacterial disease. Two prairie dogs had severe lesions of tularemia, caused by *F. tularensis*. Three Gunnison's prairie dogs were affected by thymic lymphoma. No other tumors were observed in any of the other 122 prairie dogs examined. The three cases of thymic lymphoma are further described below.

Table 2.2 Causes of death in 125 prairie dogs in Colorado from 2009 to 2018.

Cause of Death	#	G^a	BT^b	WT^c	TL^d	GPDRV^e
Thymic lymphoma only	2	2	0	0	2	2
Bacterial	54	21	23	10	0	3
Plague	49	20	19	10	0	2
Tularemia	2	1	1	0	0	1
Other bacteremia	3	0	3	0	0	0
Trauma	21	14	3	4	0	0
Capture related	10	9	1	0	1	2
Environmental	8	3	5	0	0	0
Intraspecific aggression	6	2	1	3	0	0
Euthanized for disease concern	4	1	3	0	0	0
Undetermined	20	7	4	9	0	0
^a G Gunnison's prairie dog ^b BT black-tailed prairie dog ^c WT white-tailed prairie dog ^d TL thymic lymphoma ^e GPDRV Gunnison's prairie dog retrovirus						

Thymic lymphoma case number 11-1310 was a free-ranging yearling female Gunnison's prairie dog found dead lying half-way out of a burrow with no evidence of trauma. The chest was filled with cloudy fluid and few fibrin strands. The lungs were mottled and the heart was dilated. The thymus was enlarged to approximately 10× normal size by a soft, white mass with a mottled appearance suggesting multifocal hemorrhage and necrosis. Histopathology was complicated by freeze/thaw artifacts but demonstrated uniform infiltrates of neoplastic lymphocytes determined to be T-cells by immunohistochemistry for CD-3. The tumor did not contain a significant population of B-cells or epithelial cells as determined by immunohistochemistry for Pax5 and MCK. Neoplastic cells invaded beyond the tissue capsule of the mass and infiltrated the surrounding adipose tissue. The tumor was diagnosed as T-cell lymphoma. Metastasis was not observed. The spleen and liver were PCR negative for *Y. pestis* and *F. tularensis*.

Thymic lymphoma case number 14-1342 was a free-ranging, lactating adult female Gunnison's prairie dog trapped as part of research and management activities. The prairie dog was observed to have slightly labored breathing when found in the trap but did not raise concern for illness. The same prairie dog had been captured approximately one-year prior without complications. While anesthetized, the prairie dog was noted to have stopped breathing. Oxygen was administered but the prairie dog never recovered from anesthesia. At necropsy, erythema of the skin was observed on the vulva and lower limbs. An approximately 1 cm diameter granuloma was present within the mesenteric adipose tissue of the abdomen. Firmly adhered to the base of the trachea was an approximately 3 cm diameter mass that displaced the heart caudally

(Figure 2.1). The mass was white and firm, with a mottled appearance on cut surface suggesting hemorrhage and necrosis. Histopathology was complicated by freeze/thaw artifacts but demonstrated uniform infiltrates of neoplastic lymphocytes (Figure 2.1) determined to be T-cells by immunohistochemistry for CD-3 (Figure 2.1). The tumor did not contain a significant population of B-cells or epithelial cells as determined by immunohistochemistry for Pax5 and MCK. The tumor was diagnosed as T-cell lymphoma. Metastasis was not observed. PCR of liver and spleen were negative for *Y. pestis* and *F. tularensis*.

Thymic lymphoma case number 15-1406 was a free-ranging, approximately 1–2 year-old female Gunnison's prairie dog found dead in a burrow with no evidence of trauma. Body condition was good, with plentiful fat stores in the abdomen. The chest contained an approximately 4 cm diameter mass, with red-tinged fluid filling the chest cavity. The mass was white, soft, and contained multifocal hemorrhages on cut surface. The spleen was moderately enlarged, and the inguinal lymph nodes were dark red. Histopathology was complicated by freeze/thaw artifacts but the thymic mass demonstrated uniform infiltrates of neoplastic lymphocytes determined to be T-cells by immunohistochemistry for CD-3. The tumor did not contain a significant population of B-cells or epithelial cells as determined by immunohistochemistry for Pax5 and MCK. The tumor was diagnosed as T-cell lymphoma. Metastasis was not observed. PCR of liver and spleen were negative for *Y. pestis* and *F. tularensis*.

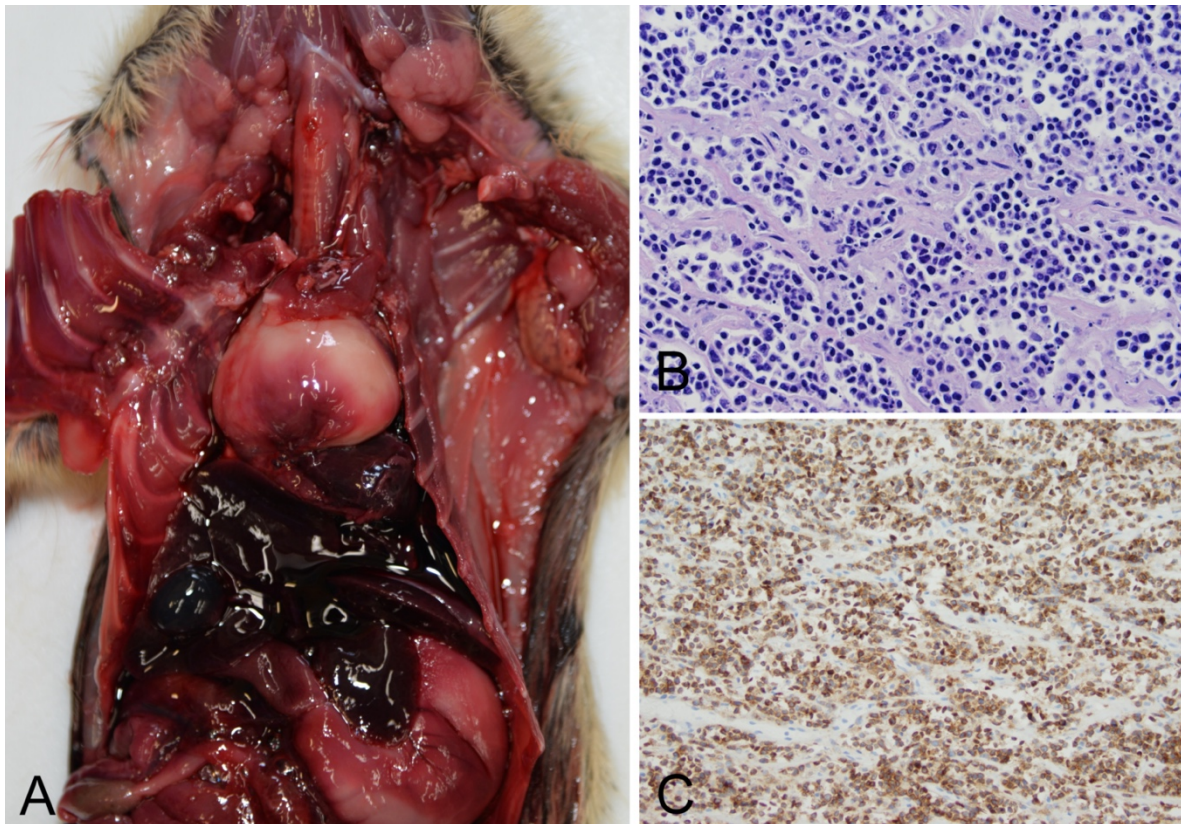


Figure 2.1 Thymic lymphoma identified in a Gunnison's prairie dog (Case 14-1342). (A) An approximately 3 cm diameter, soft, white mass displaces the heart caudally. (B) Histologic findings included uniform infiltrates of neoplastic lymphocytes (hematoxylin and eosin). (C) Immunohistochemical staining with anti-CD3 identified neoplastic cells as T-lymphocytes.

2.4b Identification of Prairie Dog Retroviral Sequences Associated with Thymic Lymphoma

Initial investigation for a possible retroviral etiology involved use of reverse transcription polymerase chain reaction (RT-PCR) with degenerate retrovirus primers (LPQG and YMDD) targeting a well-conserved region in the reverse transcriptase gene (Donehower et al., 1990). Sequencing of the PCR products from tumors 14-1342 and 15-1406 identified two unique sequences with homology to known retroviruses.

To obtain additional sequences of these two potential viruses we utilized a metagenomics approach. Total RNA was isolated from the lymphoma and spleen from two Gunnison's prairie dogs (14-1342, 15-1406) with tumors, the spleen from two Gunnison's prairie dogs (15-656, 15-671) without tumor, and the spleen from a black-tailed prairie dog (14-1382) without tumor. An individual library was prepared from each sample and sequenced on an Illumina NextSeq. Sequencing produced an average of 5×10^6 2×150 read pairs per sample. Following removal of low-quality reads, adapter sequences, duplicate reads, and host-derived reads, an average of 2.4×10^4 read pairs remained in each dataset (0.5% of starting datasets). These remaining reads were assembled and the resulting contigs were taxonomically classified.

Retroviral sequences were identified in the lymphoma and spleen from the two tumor-positive animals but not in the spleens from the three tumor negative animals. A complete sequence of 7700 nucleotides (nt) in length was assembled from both tumors. The organization of the assembled genome appeared to be similar to that of betaretroviruses with *gag*, *pro*, *pol* and *env* genes (Figure 2.2). The nucleotide sequences of the two assembled genomes were 99.2% identical. The two sequences differ at 57 nucleotides resulting in eight amino acid changes in Gag, two in Pro, one in Pol and five in Env. The *pro* and *pol* genes are predicted to utilize ribosomal frameshifting for expression of *gag-pro* and *gag-pro-pol* precursors. The *env* transcript is likely generated by splicing. These data represent the first report of retroviral sequences associated with lymphoma in Gunnison's prairie dogs, with the provisional name Gunnison's prairie dog retrovirus (GPDRV).

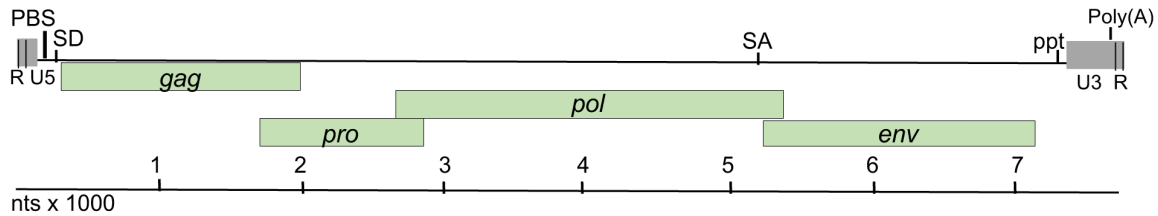


Figure 2.2 Gunnison's prairie dog retrovirus genome organization. Diagram of the assembled GPDRV genome from tumors from prairie dogs 14-1342 and 15-1406. The Gag-Pro-Pol polyprotein is predicted to be translated from the genome by ribosomal frameshifting. Location of predicted sites-PBS-primer binding site, SD-splice donor, SA-splice acceptor, polypurine tract (ppt), and polyadenylation (poly(A)) sequence.

2.4c Prairie Dog Endogenous Retroviral Sequence

A second, distinct retroviral sequence was identified and a consensus contig was assembled from the black-tailed prairie dog (14-1382) spleen sample. This sequence is 6132 nucleotides in length and includes predicted *gag*, *pro*, and *pol* genes. An *env*-coding region and LTR sequences were not definitively identified. Sequence reads from the tumors and all spleen samples (animals 14-1342, 15-1406, 15-656, 15-671 and 14-1382) align with the 14-1382 consensus contig suggesting this sequence is likely an endogenous retrovirus, provisionally named ERV- PDRV.1-*Cynomys ludovicianus*. This sequence shares 54% nucleotide identity with the GPDRV *gag-pro-pol* sequence.

2.4d Features of the Gunnison's Prairie Dog Retrovirus Sequence, Predicted Proteins, and Phylogenetic Analysis

The long terminal repeat (LTR) and the 5' and 3' untranslated regions of retroviral genomes contain regulatory sequences that are central for viral replication. The LTR of

GPDRV is 403 bases in length and is bound by inverted repeat sequences CAAG (nt 94–97) and CTTG (nt 7376–7379) that are essential for integration. U3 is 308 bp, R is 15 bp and U5 is 79 bp (Figure 2.2). The U3 region is preceded by a polypurine tract (nt 7358–7375), the site for initiation of plus-strand synthesis of viral DNA during retroviral replication. The U3 region in the 5' LTR serves as the promoter and enhancer for transcription of viral RNA. A consensus TATA box (TATATAA) is located 29 bp upstream of the predicted transcription initiation site. Binding sites for the transcription factors, NF1, AP1, Elk1, and NF-AT are present in the U3 region. The highly conserved polyadenylation signal, AATAAA, is located in the 3' LTR at nt 7680–7686, similar in position to that of the betaretroviruses, jaagsiekte sheep retrovirus (JSRV), and enzootic nasal tumor virus (ENTV) (Cousens et al., 1999; York et al., 1992).

The 5' untranslated region harbors a predicted primer-binding site (PBS) with sequence complementary to the 15 bases at the 3' end of tRNA^{Gln} that would serve as the site for reverse transcriptase to initiate minus-strand DNA synthesis. A predicted splice donor site for the generation of the subgenomic *env* transcript is located at nt 124–131 in the untranslated region between the PBS and start of *gag*.

The *gag* open reading frame (nt 212–1915) is predicted to encode a 567 amino acid (aa), 62.8 kDa polyprotein. The *n* terminus of GPDRV Gag contains a consensus myristylation motif (Met-Gly) like that of many retroviruses. The GPDRV capsid protein (CA) is predicted to be a 206 aa, 22.8 kDa protein. A highly conserved major homology region (MHR), QGPSESYSDFIGRLMQSA, is located in CA. Two Cys-His motifs (Cys-X₂-Cys-X₄-His-X₄-Cys) separated by 14 amino acids are located in the nucleocapsid

protein (NC) at nt positions 1565–1607 and 1649–1690. The NC protein is predicted to be 14.3 kDa.

The *pro* open reading frame (nt 1705–2712) is predicted to encode a 334 aa, 35.7 kDa protein expressed as a Gag-Pro fusion polypeptide generated by ribosomal frameshifting. The protein encoded by the *pro* open reading frame is comprised of two domains, similar to that of betaretroviruses: a pseudoprotease domain with dUTPase activity and the active protease (Figure 2.3). GPDRV dUTPase exhibits 54–57% amino acid identity with other betaretroviruses. The active protease site with a core aspartyl protease sequence, Leu-Asp-Thr-Gly, is located at amino acid 198-201 (nt 2296–2307). A glycine-rich G patch domain similar in sequence to that found in betaretroviruses is present near the C-terminus of protease (Aravind and Koonin, 1999; Gifford et al., 2005).

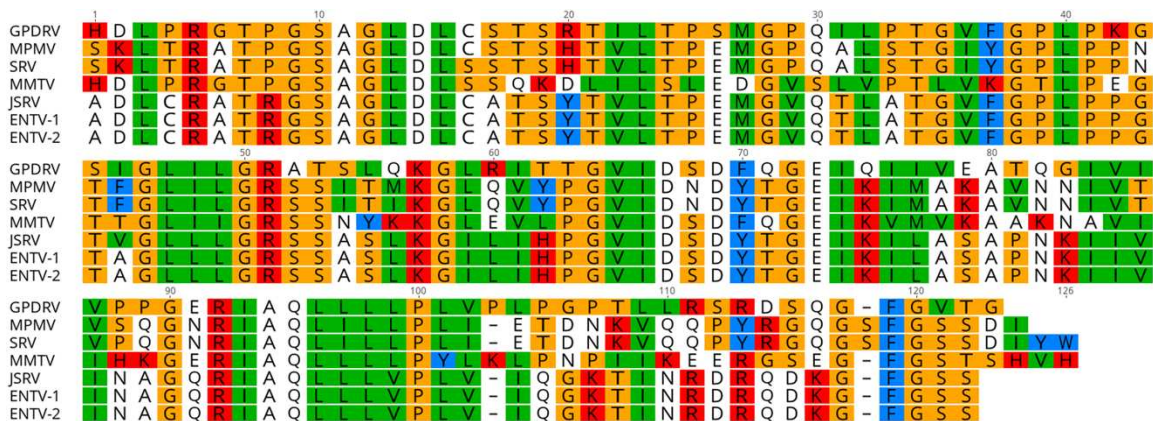


Figure 2.3 Amino acid alignment of the dUTPase domain from several betaretroviruses. Amino acid alignment was constructed using sequences GPDRV- Gunnison’s prairie dog retrovirus (this manuscript), MPMV- Mason-Pfizer monkey virus (NC_001550), SRV (M11841), MMTV (NC_001503), JSRV (NC_001494), ENTV-1 (NC_007015), and ENTV-2 (NC_00494) with Geneious Prime 2019.2.3.

The *pol* open reading frame (nt 2685–5375) is predicted to encode a peptide of 896 aa with a molecular mass of 101.8 kDa. Pol is predicted to be expressed as a Gag-

Pro-Pol polypeptide generated by ribosomal frameshifting. The Pol polypeptide encodes reverse transcriptase and integrase activity. The conserved polymerase sequences LPQG and YMDD are located at amino acids 157 and 191 (nt 3153 and 3255), respectively. RT contains an RNase H domain with a conserved active site (DEDD). There is an N-terminal Zn⁺ binding domain present in the integrase protein.

To determine the relationship between GPDRV and members of established retrovirus subfamilies and genera, the entire Pol amino acid sequence was used to infer phylogenies. We took a two-fold approach to identify closely related sequences. First, we created a tree using all of the Pol sequences in the NCBI RefSeq protein database that were annotated as belonging to viruses in the family *Retroviridae* (Figure 2.4). In this tree, GPDRV and ERV- PDRV.1 clustered within betaretrovirus Pol sequences (genus *Betaretrovirus*) (Figure 2.4). Second, we used BLASTP to identify the most closely related protein sequences in the NCBI protein database: those producing alignments with E-values less than 10^{-40} (Figure 2.5). The most closely related sequences were a mixture of retroviral and endogenous retroviral-like sequences from mammalian genome assemblies. The GPDRV Pol sequences clustered with sequences present in the alpine marmot (*Marmota marmota*) genome assembly (Gossmann et al., 2019). In fact, GPDRV Pol was more closely related to these marmot sequences than to ERV- PDRV.1 Pol (Figure 2.5).

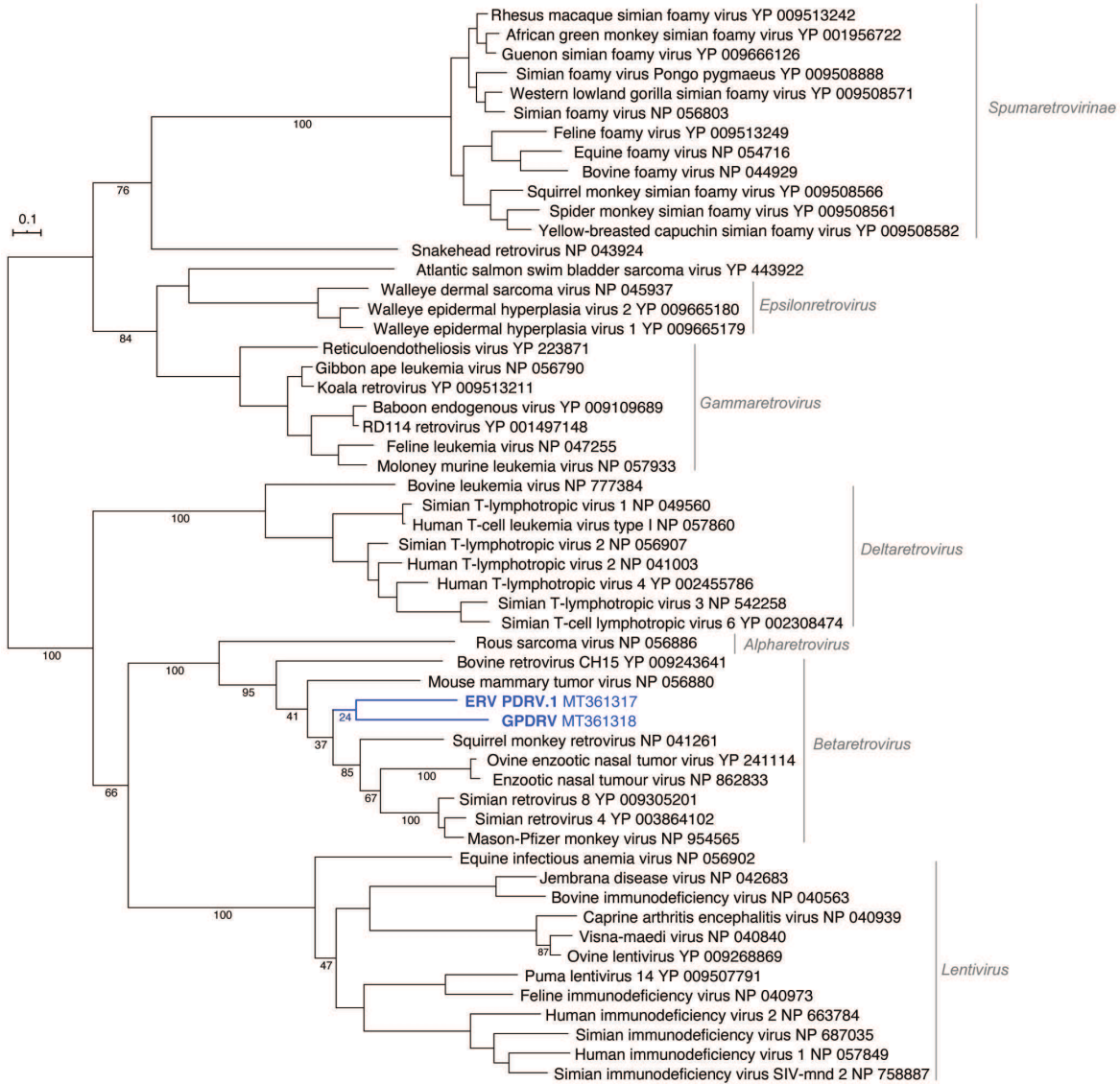


Figure 2.4 GPDRV is a betaretrovirus. All Pol sequences in the NCBI RefSeq protein database annotated as belonging to the *Retroviridae* family longer than 600 amino acids were used to infer a maximum-likelihood tree. The Felsenstein bootstrap (FBP) support values of select branches are indicated. Retrovirus genera and subfamilies (except for *Spumaretrovirinae*) are indicated. The tree is unrooted and was arbitrary midpoint rooted.

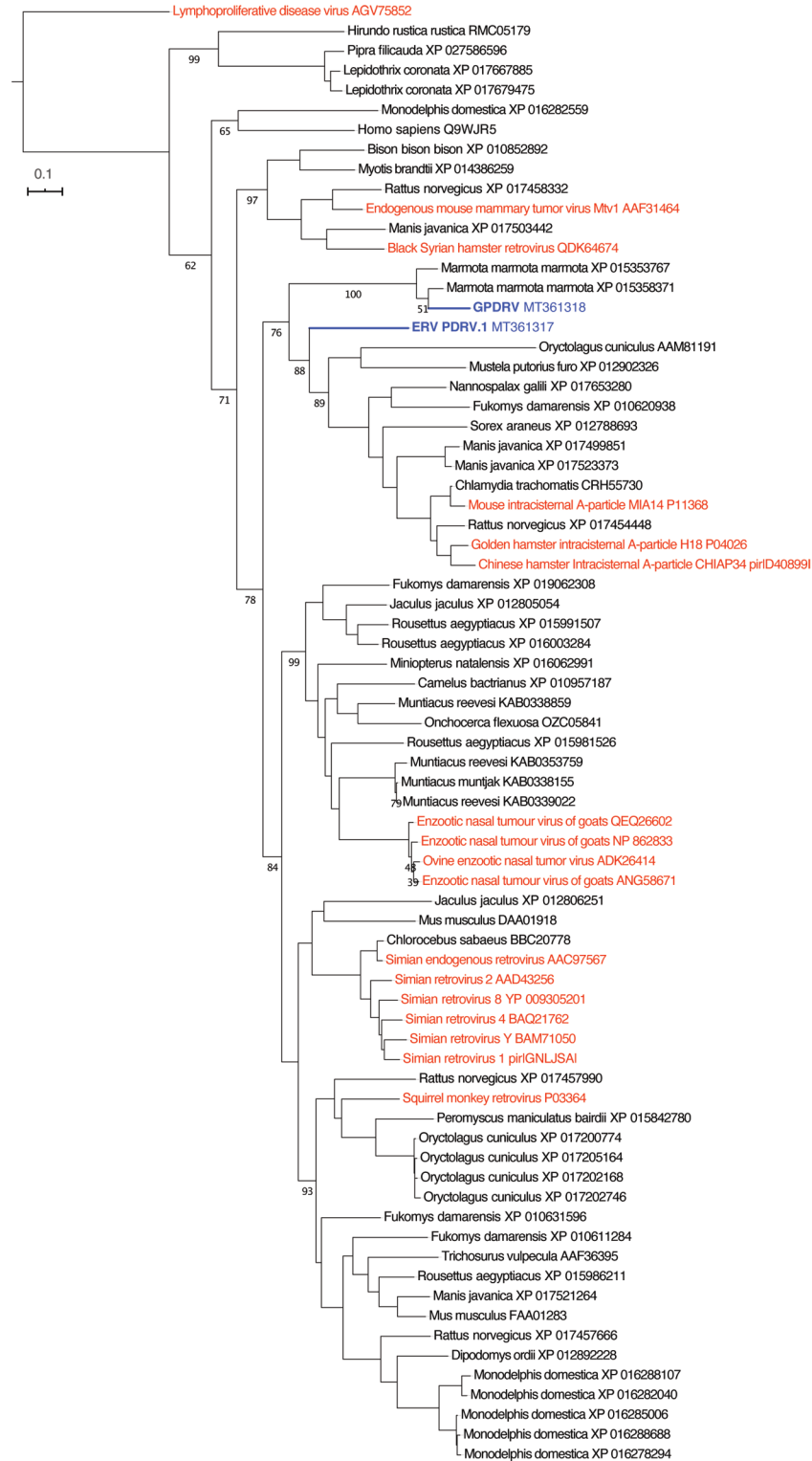


Figure 2.5 GPDRV is most closely related to retroviral-like sequences in the marmot genome. A tree was made from the sequences in the NCBI protein database most closely related to GPDRV Pol as determined by a BLASTP search. The Felsenstein bootstrap (FBP) support values of select branches are indicated. The GPDRV and GPD

ERV Pol sequences are colored blue. Sequences annotated as belonging to the *Retroviridae* family are colored red. The rest of the sequences are annotated as belonging to the indicated mammalian species and are present in the corresponding genome assemblies. The tree was rooted using lymphoproliferative disease virus Pol, which was included as an outgroup.

The envelope protein is likely translated from a spliced transcript that utilizes a splice acceptor site located at nucleotide 5209. The *env* open reading frame (nt 5275–7092) is predicted to encode a 605 amino acid, 64.9 kDa protein. A hydrophobic region located from nt 5275 to 5388 would serve as the signal peptide. Proteolytic cleavage at the furin cleavage consensus recognition site (RHRR) in Env would generate a 410 aa, 43.7 kDa surface protein (SU) and 195 aa, 21.2 kDa transmembrane protein (TM). The TM subunit contains two heptad repeats (HR1 and HR2) that form a coiled coil structure. Located between HR1 and HR2 resides a conserved immunosuppressive domain (ISD) (Figure 2.6) followed by a cysteine-rich region (CX₆CC), which is predicted to form a covalent disulfide bond with SU. The GPDRV ISD is 94% identical to that found in Mason-Pfizer monkey virus (Sonigo et al., 1986). A 21 aa hydrophobic region within TM (nt 6850–6945) likely serves as the transmembrane anchor with a 43 amino acid cytoplasmic region. There are ten predicted N-linked glycosylation sites, nine in SU and one in TM. Phylogenetic analysis of the TM subunit demonstrates GPDRV TM is found in the branch of retroviruses that have an ISD and covalent TM (Figure 2.7). The group that includes GPDRV TM includes sequences from betaretroviruses and gammaretroviruses, but due to the relatively short length of the TM domain, branches of the tree generally had low support values.

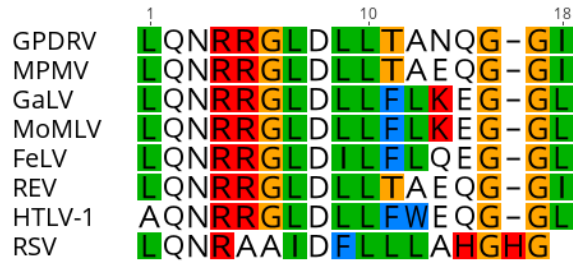
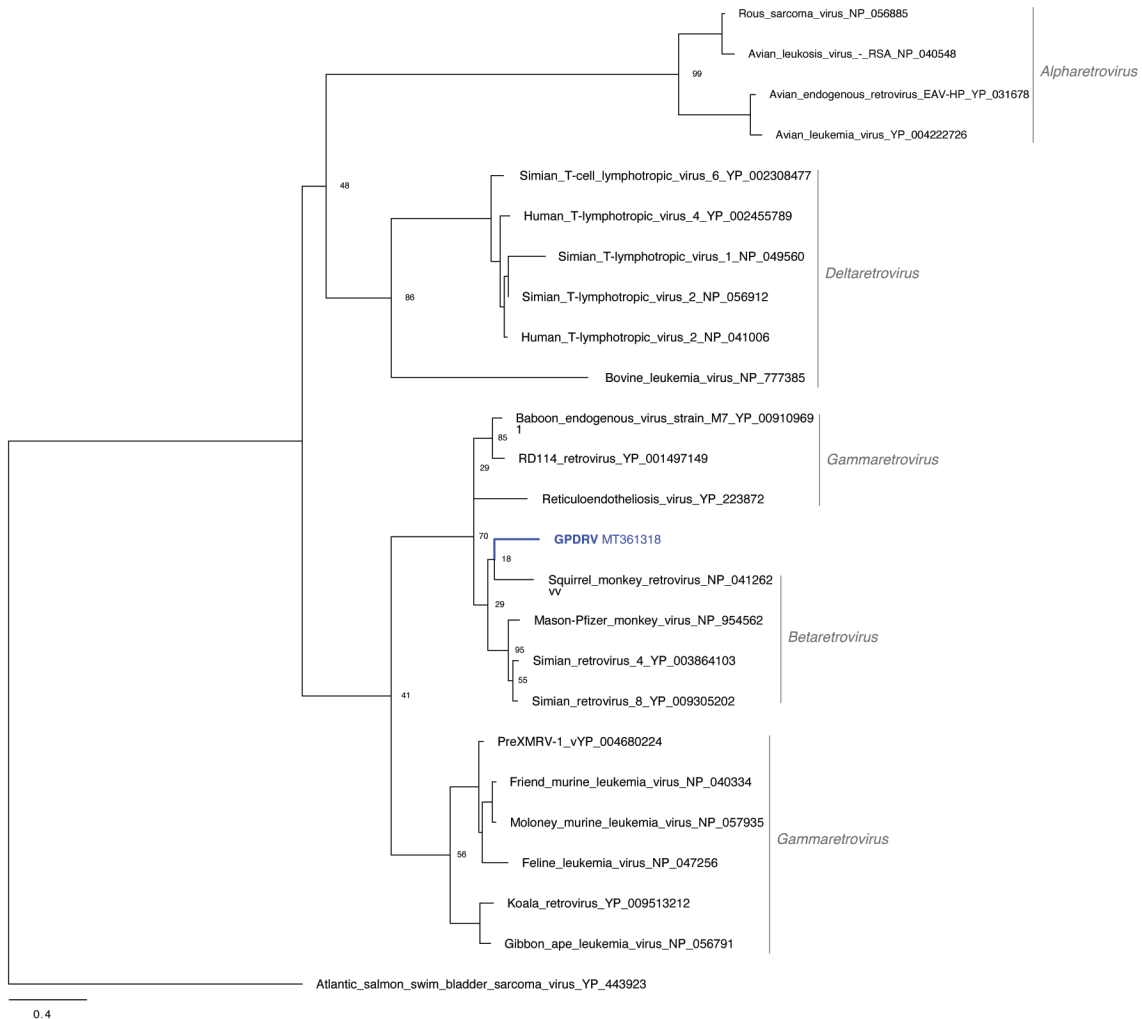


Figure 2.6 Alignment of the immunosuppressive domain from retroviral transmembrane protein sequences. Amino acid alignment was constructed using sequences GPDRV- Gunnison’s prairie dog retrovirus (this manuscript), MPMV- Mason-Pfizer monkey virus (NC_001550), GaLV- Gibbon ape leukemia virus (NC_001885), MoMLV- Moloney murine leukemia virus (NC_001501), FeLV- feline leukemia virus (NC_001940), REV- reticuloendotheliosis virus NC_006934), HTLV-1- human T cell leukemia virus (NC_001436), and RSV- Rous sarcoma virus (NC_001407) with Geneious Prime 2019.2.3.



0.4

Figure 2.7 GPDRV Env transmembrane protein (TM) clusters with gamma and betaretrovirus sequences. All ENV TM sequences in the NCBI RefSeq protein database annotated as belonging to the *Retroviridae* family were used to infer a maximum-likelihood tree. The Felsenstein bootstrap (FBP) support values of select branches are indicated. Retrovirus genera are indicated. The tree is unrooted and was arbitrary midpoint rooted.

2.4e Integration Site Analysis

Identification of integration sites in tumor DNA resulted in four unique sites: two sites were identified in the 14-1342 tumor and two in the 15-1406 tumor. The Gunnison's prairie dog genome sequence recently became available (Tsuchiya et al., 2020) which enabled identification of the genome location of the four integration sites. The GPDRV sequence in the 14-1342 tumor was integrated at positions 309,469 (+ orientation) and 81,902 (– orientation) and the GPDRV sequence in the 15-1406 tumor was integrated at positions 1,301,104 (+ orientation) and 629,910 (– orientation).

2.4f Screening for GPDRV with Virus-Specific Primers

Following the identification of two retroviral sequences with the metagenomics approach we developed virus specific primers to screen additional samples. We selected 42 prairie dog spleen samples to screen for the presence of ERV-PDRV.1-*Cynomys ludovicianus* using virus-specific primers (494F/591R, Table 2.1) that amplify a region spanning *pro-pol*. This sequence was detected in DNA from all ($n = 42$) prairie dog spleen samples tested, strongly supporting this as an endogenous retroviral

sequence. These samples represented Gunnison's ($n = 25$), black-tailed ($n = 14$), and white-tailed ($n = 2$) prairie dogs.

Alignment of the endogenous and exogenous sequences was used to identify primers that specifically amplify only *gag* from the exogenous GPDRV. Of the 42 prairie dog spleen samples, GPDRV was only detected in the spleen (and tumor) from 14-1342 and 15-1406 and in the spleen of a Gunnison's prairie dog (14-1344) without a tumor. Animal 14-1344 was from the same colony as 14-1342.

Spleen tissues from all 125 prairie dogs in this study were screened for GPDRV using *env*-specific primers 5729F/5840R (Table 2.1). GPDRV was detected only in Gunnison's prairie dogs, including detection in thymus from 11-1310 and spleen and thymus from 14-1342 and 15-1406. We also detected GPDRV in spleen from four additional Gunnison's prairie dogs that did not have tumors observed at necropsy. Causes of death in these four prairie dogs included: plague (16-633 and 16-778), tularemia (16-675), and suspected stress-related capture mortality (14-1344). Detection of GPDRV RNA is therefore significantly associated with presence of thymic lymphomas (Fisher's exact test; $p = 0.002$).

Using primers located in U3 and *env* we were able to amplify a 7.14 kb fragment from the spleen of animal 14-1344. Sequencing of this product confirmed the presence of GPDRV with 99.7% and 99.1% nucleotide identity with the assembled genomes from 14-1342 and 15-1406, respectively.

2.5 Discussion

In any population, clusters of tumor cases can suggest an underlying or predisposing factor (Chang et al., 2017; Hardy et al., 1977; Parkin, 2006) and three cases of thymic lymphoma in Gunnison's prairie dogs in Colorado, USA warranted further investigation. We specifically investigated a possible retroviral etiology due to similar retrovirus-associated lymphoid tumors in other species (Hoover et al., 1980; Jarrett et al., 1964; Kozak and Ruscetti, 1992; Rosenberg and Jolicoeur, 1997; Xu et al., 2013). Using PCR and next-generation sequencing, we identified and were able to assemble two unique retroviral sequences from lymphoid tissue of prairie dogs.

One of the sequences was identified in DNA from all samples screened, which included members from each of three species of prairie dogs included in the study. This widespread occurrence is consistent with the expected distribution of an endogenous viral sequence (Boeke and Stoye, 1997; Gifford et al., 2005; Mager and Stoye). This sequence lacked an apparent *env*-coding region, suggesting a possible mutation/deletion typical of endogenous viruses (Boeke and Stoye, 1997; Mager and Stoye). We suspect that this consensus sequence likely represents endogenous retroviral sequence(s) of prairie dogs, and we propose the name ERV-PDRV.1-*Cynomys ludovicianus* (Gifford et al., 2018). The presence of ERV-PDRV.1-*Cynomys ludovicianus* in all three species of prairie dogs suggests that endogenization occurred prior to evolutionary divergence of these species (Arnaud et al., 2007; Boeke and Stoye, 1997; Gifford et al., 2005). Screening of other prairie dog species and other *Sciuridae* species may provide further insights as to when this viral sequence was acquired.

Gifford et al. (Gifford et al., 2005) screened for the presence of class II endogenous retroviral sequences using conserved PR and RT primers and identified a sequence from a black-tailed prairie dog that is 62% identical to the ERV-PDRV.1-*Cynomys ludovicianus* and 59% identical to GPDRV nucleotide sequences identified in this study.

A second retroviral sequence identified in thymic tissue and spleen of two prairie dogs with thymic lymphoma included *gag-pro-pol-env* coding regions. Using *env*-specific primers this sequence was identified in thymic tissue and spleen from all (3/3) of the prairie dogs with thymic lymphoma, and from splenic tissue of only 3.3% (4/122) of prairie dogs that did not have tumors identified grossly. All of the *env*-positive animals were from prairie dog colonies located in the Gunnison Basin in Colorado, USA. Gunnison's prairie dogs located outside the Gunnison Basin were all negative for GPDRV. This consistent association with tumors and infrequent occurrence in the overall population of animals examined in the study is an expected pattern for an infectious, exogenous oncogenic virus. Isolation of virus in culture was not pursued in this study. The finding of multiple integration sites supports classification as an exogenous infectious virus. We suggest that this sequence represents the first exogenous retroviral sequence identified in prairie dogs and propose the name Gunnison's prairie dog retrovirus (GPDRV).

As we were finalizing this paper, a Gunnison's prairie dog genome assembly was published (Tsuchiya et al., 2020). This assembly contained multiple contigs with sequences similar to both GPRDV and to ERV-PDRV.1-*Cynomys ludovicianus*. A BLASTN search of the assembly with ERV-PDRV.1-*Cynomys ludovicianus* yielded 3156 alignments with E-values less than 10^{-10} . Many of these are nearly identical to the

ERV-PDRV.1 sequence over more or less its entire length: 652 of the alignments cover >80% of the ERV sequence with >90% identity. The highest scoring alignment was 95.9% identical over 100% of the ERV-PDRV.1 sequence, which represents a consensus sequence assembled from our metagenomic datasets. A similar BLAST search with GPDRV produced 759 alignments with *E*-values less than 10^{-10} . For these, the highest scoring alignment was on 84.9% identical to GPDRV, over 99% of the GPDRV sequence. We conclude that the Gunnison's prairie dog genome contains a large number of sequences related to both GPDRV and to ERV-PDRV.1 that may represent endogenized retrovirus sequences and possibly proviruses from other exogenous retroviruses.

The genetic organization of GPDRV is typical of a betaretrovirus. The protease and polymerase proteins are expected to be expressed as Gag-Pro and Gag-Pro-Pol polypeptides by ribosomal frameshifting. The protein encoded by *pro* harbors dUTPase and active protease domains. Phylogenetic analysis based on Pol amino acid sequences supported the classification of GPDRV as a betaretrovirus.

The retrovirus envelope protein is cleaved by cellular furin to generate SU and TM subunits. The SU and TM subunits remain associated after cleavage either through noncovalent interactions or formation of a covalent bond, which is determined by the cysteine motif located between the heptad repeats within TM (Opstelten et al., 1998; Wallin et al., 2004). The betaretroviruses, MMTV, JSRV and ENTV, contain a CX₇C motif, which forms noncovalent interactions (Henzy and Coffin, 2013). The TM subunit found in alpha-, gamma- and delta- retroviruses contain a cysteine motif, CX₆CC that forms a covalent bond with a cysteine in the SU subunit (Johnston and Radke, 2000;

Leamson and Halpern, 1976; Li et al., 2008a; Opstelten et al., 1998). The TM subunit of alpha-, gamma-, delta-retroviruses and the D-type betaretrovirus, Mason-Pfizer monkey virus (MPMV), also contain an immunosuppressive domain (Bénit et al., 2001; Cianciolo et al., 1985; Sonigo et al., 1986). The envelope gene of MPMV was derived by a recombination event, which resulted in the acquisition of an envelope gene from a gammaretrovirus (Barker et al., 1986; Sonigo et al., 1986). The GPDRV TM harbors a CX₆CC and an immunosuppressive domain similar to that of MPMV suggesting GPDRV is a D-type betaretrovirus that may have undergone a similar recombination event.

The significance of GPDRV to prairie dog populations is uncertain. For all three cases with thymic lymphoma, the tumor was determined to be the cause of death or related to the cause of death by compromising cardiovascular function under anesthesia. However, overall occurrence of thymic lymphoma was low (3/125) and not considered to be a significant source of mortality at the population level. Of the four prairie dogs which tested positive for GPDRV but were unaffected by thymic lymphoma, three died from bacterial infections. Based on the immunosuppressive effects of other retroviruses, we considered possible population effects due to increased susceptibility to bacterial infections. However, prairie dogs positive for GPDRV were not over-represented among animals that died from bacteremia. Although three of the seven (43%) prairie dogs with GPDRV died from bacterial infections, 51 of the 118 (43%) prairie dogs without GPDRV also died from bacterial infections. One prairie dog that was positive for GPRDV but unaffected by thymic lymphoma died from capture-related factors (heat stress) with no signs of immune suppression. This rare complication of trapping is unfortunate but GPDRV was not suspected to be associated with the cause

of death in this animal. No other lesions observed were suggestive of immune suppression. The small proportion of animals testing positive for GPDRV prevented further analysis of possible effects of the virus.

GPDRV is statistically associated with thymic lymphoma in Gunnison's prairie dogs. Future investigations could include isolation of virus, experimental infection studies, and corroboration of the association with larger sample sets. Further analysis of integration sites may yield insight into potential mechanisms of oncogenesis. Surveillance areas were limited to the state of Colorado, with access to only three prairie dog species. GPDRV sequences were only found in Gunnison's prairie dogs. This could suggest either species specificity or lack of exposure in other species. Continued surveillance of other prairie dog species may help understand the species host range of the virus.

PART II: THE ROLE OF CYCLIN-DEPENDENT KINASES 8 AND 19 AS
TRANSCRIPTIONAL REGULATORS DURING VIRAL INFECTION AND IN THE
INNATE IMMUNE RESPONSE

CHAPTER 3: OVERVIEW OF LITERATURE, PART II

3.1 Dengue Viruses

Global incidence of dengue disease has increased dramatically since 2000, with an estimated 390 million cases annually and approximately one third of the world's population at risk for infection each year (Bhatt et al., 2013; Pang et al., 2017; World Health Organization, 2020). Reported cases represent only a small fraction of actual infections due to asymptomatic, mildly symptomatic, and non-specific febrile clinical presentations that prevent diagnosis of all cases (World Health Organization, 2020). Dengue disease, caused by the four serotypes of dengue virus (DENV1-4), is the most aggressive arthropod-borne disease currently in circulation (Bhatt et al., 2013; Pang et al., 2017). While the majority of dengue cases result in asymptomatic or self-limiting flu-like illness, some will progress to severe dengue, characterized by plasma leakage resulting in hemodynamic instability and organ dysfunction (Pang et al., 2017; Wilder-Smith et al., 2019; World Health Organization, 2020). Current treatment is limited to supportive care, and vaccine development remains challenging due to subtle but important differences among serotypes and the potential for exposure to one serotype, by vaccination or infection, to contribute to more severe disease upon exposure to a second serotype (Guzman and Harris, 2015).

Infections caused by the four serotypes of dengue viruses (DENV1-4) represent a significant, ongoing public health concern (Guzman and Harris, 2015). Understanding both the molecular virology of DENV2 and the host requirements for efficient dengue

replication may provide insight into potential avenues of therapeutic interdiction. Key among these requirements of the host cell that DENV2 relies on is a metabolic environment which supports viral replication (Abernathy et al., 2019; Fernandes-Siqueira et al., 2018; Fontaine et al., 2015; Gullberg et al., 2018; Heaton et al., 2010; Jordan and Randall, 2017; Zhang et al., 2018).

3.1a Dengue Virus Serotype 2 (DENV2) Genome and Proteins

DENV2, family *Flaviviridae*, genus *Flavivirus*, has a 10.72 kb positive-sense, single-stranded RNA genome which is translated into a single polypeptide and subsequently cleaved into three structural (C, prM, E), and seven nonstructural proteins (NS1, NS2A, NS2B, NS3, NS4A, NS4B, and NS5) The genomic organization of DENV2 is shown in Figure 3.1.

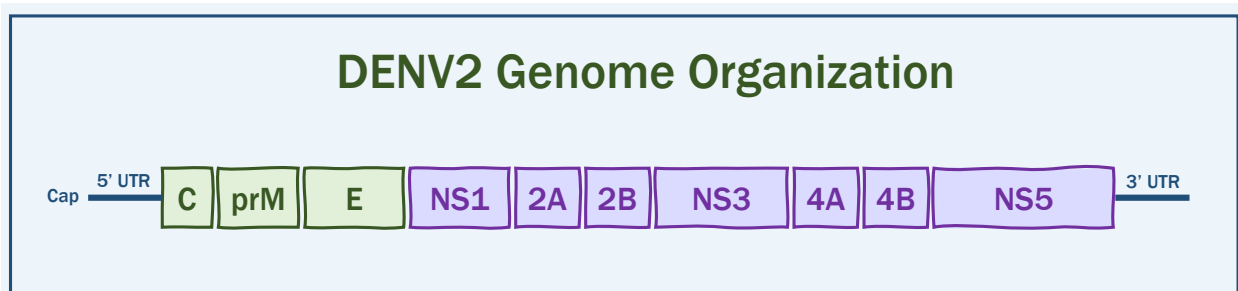


Figure 3.1 DENV2 Genome Organization. Untranslated, structural elements (cap, 5' untranslated region (UTR), 3' UTR) are indicated in blue, structural proteins in green, and nonstructural proteins in purple.

Capsid (C) is a highly basic 12 kDa protein and is the least conserved protein among dengue serotypes (Byk and Gamarnik, 2016; Markoff et al., 1997). Capsid

functions as a homodimer, with each monomer comprised of four alpha helices (Byk and Gamarnik, 2016; Ma et al., 2004). The capsid homodimer associates with viral RNA, presumably through hydrostatic interactions, to form the nucleocapsid (NC). This association is critical for viral particle assembly, and the reversal of this association is required for viral genome release upon infection of a new host cell (Byk and Gamarnik, 2016).

A hydrophobic signal peptide on the C-terminal end of capsid serves as an anchor within the ER membrane (Markoff et al., 1997). Capsid is first cleaved from the anchor on the cytoplasmic surface by the viral protease NS2B-3 (Lobigs, 1993; Stocks and Lobigs, 1998). On the C-terminal end of the signal peptide anchor is the cleavage site for the host protease signal peptidase, which cleaves the anchor from the N-terminus of prM, leaving prM in the lumen of the ER (Stocks and Lobigs, 1998).

While capsid is therefore primarily cytoplasmic or associated with ER membranes, capsid has also been found to localize to lipid droplets and the nucleus (Samsa et al., 2009; Sangiambut et al., 2008; Wang et al., 2002). The functional purpose of this localization is not well understood, though it has been proposed that capsid localization to lipid droplets may serve to temporarily sequester capsid protein until viral particle assembly commences, or that lipid droplets may serve as a platform for viral particle assembly (Miyanari et al., 2007; Samsa et al., 2009).

The remaining two structural proteins, prM (pre-membrane or precursor membrane) and E (envelope) are also processed by host signal peptidase but remain associated with the ER membrane. In the cell-associated, immature particle conformation, prM and E associate as heterodimers arranged in a trimeric, spiky

conformation (Li et al., 2008b; Yu et al., 2008). The pr-M junction contains a conserved furin cleavage site flanked by basic residues which allow regulation of the timing and efficiency of furin-mediated cleavage of prM (Junjhon et al., 2008). Following furin-mediated cleavage, soluble pr is no longer associated with the viral particle, and M remains associated with the viral envelope but is no longer exposed on the surface of the virion (Kuhn et al., 2014; Li et al., 2008b; Yu et al., 2008). The surface arrangement of E then shifts to homodimers arranged in a trimeric, smooth, herringbone arrangement characteristic of mature viral particles (Kuhn et al., 2014; Li et al., 2008b; Yu et al., 2008). E mediates attachment to cellular receptors to initiate viral infection and upon entry into slightly acidic endosomes changes conformation, revealing the fusion peptide and allowing release of the viral genome into the cytoplasm (Fritz et al., 2008; Liao et al., 2010; Modis et al., 2003, 2004, 2005).

The seven non-structural proteins of DENV2 serve a diverse array of functions required for viral replication and immune evasion. Non-structural protein 1 (NS1) is a 48 kDa glycoprotein which can be associated with viral replication complexes in a monomeric form, with cellular membranes in a dimeric form, or can be secreted from infected cells in a hexameric form (Chen et al., 2018; Mackenzie et al., 1996). Intracellular NS1 contributes to viral genome replication and viral particle assembly (Płaszczycza et al., 2019; Scaturro et al., 2015). The secreted form of NS1 is thought to contribute to dengue pathogenesis by promoting endothelial hyperpermeability resulting in vascular leakage (Beatty et al., 2015; Chen et al., 2016) and platelet activation and apoptosis resulting in thrombocytopenia and coagulopathy (Chao et al., 2019). In

addition, endocytosis of NS1 by dendritic cells (DCs) increases DC susceptibility to infection and enhances viral replication in DCs (Alayli and Scholle, 2016).

Non-structural protein 2A (NS2A) is associated with the ER membrane through five transmembrane domains, with NS2A cleaved from NS1 by a host protease in the ER lumen, while the C-terminal end is cleaved in the cytoplasm by viral NS2B-NS3 protease (Xie et al., 2013). NS2A functions in viral replication by recruiting structural proteins and viral RNA to sites of virion assembly (Wu et al., 2015; Xie et al., 2013, 2015, 2019). In addition, NS2A is known to interfere in the host antiviral response by reducing type I interferon (IFN) signaling and production of IFN- β (Munoz-Jordan et al., 2003).

Non-structural protein 2B (NS2B) is an approximately 15 kDa protein with four transmembrane helices and a hydrophilic, cytoplasmic-facing domain (Li et al., 2015). This hydrophilic domain serves as a cofactor for the viral serine protease NS2B-NS3 (Arias et al., 1993; Clum et al., 1997; Falgout et al., 1991, 1993; Yusof et al., 2000). The NS2B-NS3 protease acts in *cis* and *trans* to mediate cleavage of NS2A/NS2B, NS2B/NS3, NS3/NS4A, and NS4B/NS5, as well as internal cleavages of C, NS2A, NS3, and NS4A (Reddy et al., 2018). As with several other DENV2 non-structural proteins, NS2B has been implicated in interference with the type I IFN response through inhibiting IRF3 phosphorylation and promoting degradation of the cytosolic DNA sensor, cyclic GMP-AMP synthase (cGAS) (Aguirre et al., 2017; Angleró-Rodríguez et al., 2014). Due to the absolute requirement of the NS2B-NS3 protease activity in viral replication, NS2B-NS3pro has been identified as a potential antiviral drug target (Luo et al., 2015; Nitsche, 2019).

In addition to its protease activity, NS3 also functions as an ssRNA-activated NTPase and helicase (Bartelma and Padmanabhan, 2002; Li et al., 1999). The N-terminal 168 amino acids of NS3 are essential for protease activity, followed by a 10 amino acid flexible linker, and the C-terminal helicase/NTPase (Luo et al., 2008a, 2008b, 2010). The essential functions in viral replication carried out by NS3 require association with NS2B, NS4B, and NS5 (Chatel-Chaix et al., 2015; Tay et al., 2015; Umareddy et al., 2006). NS3 has also been shown to be involved in virally-directed metabolic changes in the host cell by inducing relocalization of fatty acid synthase to sites of viral replication (Heaton et al., 2010).

Non-structural protein 4A (NS4A) is a small, 16 kDa, hydrophobic protein highly associated with the ER membrane through three transmembrane domains (Li et al., 2018; Miller et al., 2007b). NS4A localizes to viral replication complexes and induces membrane rearrangement through oligomerization in concert with the host protein reticulon 3.1 (Aktepe et al., 2017; Lee et al., 2015; Miller et al., 2007b; Stern et al., 2013). The formation of viral replication complexes is also supported by an interaction between NS4A and the host intermediate fiber protein vimentin, which provides a structural scaffold for the viral replication complexes (Teo and Chu, 2014).

Supplementary to this key role of NS4A in formation of viral replication complexes, NS4A interaction with host ancient ubiquitous protein 1 (AUP1) has been implicated as a key driver of DENV-induced lipophagy which supports infectious particle production (Heaton and Randall, 2010; Jordan and Randall, 2017; Zhang et al., 2018). NS4A is also known to manipulate the type I IFN response through binding to mitochondrial antiviral signaling protein (MAVS). MAVS is required for retinoic acid

inducible gene I (RIG-I) signaling and subsequent IRF3 translocation to the nucleus; therefore, MAVS inhibition reduces the production of IFN- β in response to DENV2 infection (He et al., 2016).

An approximately 2 kDa signal sequence (2K) separates NS4A and NS4B (approximately 27 kDa) and dictates that the N-terminus of NS4B is located in the lumen of the ER (Li et al., 2016; Miller et al., 2006). The highly hydrophobic NS4B remains associated with the ER membrane despite cleavage from the 2K fragment by host signalase due to several transmembrane domains (Li et al., 2016; Miller et al., 2006). During DENV infection, NS4B primarily localizes at sites of viral replication, in association with NS3 and dsRNA (Miller et al., 2006). The cytosolic loop of NS4B associates specifically with the helicase domain of NS3 and enhances helicase activity of NS3 by promoting disassociation of NS3 with ssRNA, allowing reinitiation of unwinding on a subsequent RNA molecule (Chatel-Chaix et al., 2015; Umareddy et al., 2006). In addition to NS3, NS4B is thought to homodimerize and to associate with DENV NS1 and NS4A to modulate viral replication (Giraldo et al., 2018; Płaszcyca et al., 2019; Zou et al., 2014, 2015).

NS4B interferes with the type I IFN response to reduce IFN- α/β signaling by preventing phosphorylation of signal transducer and activator of transcription 1 (STAT1) (Munoz-Jordan et al., 2003; Muñoz-Jordán et al., 2005). NS4B has also been implicated in disruption of mitochondrial dynamics during DENV2 infection which involves decreased mitochondrial fission, mitochondrial elongation, and presumed enhanced metabolic capacity of infected cells in combination with reduced mitochondrial-

membrane-dependent anti-viral signaling (Barbier et al., 2017; Chatel-Chaix et al., 2016).

The final non-structural protein encoded by the DENV2 genome is NS5 (approximately 105 kDa). The N-terminus of NS5 contains a methyltransferase (MTase) domain, required for $7^{\text{Me}}\text{GpppA}_{2'\text{OMe}}$ capping of nascent viral genomes to allow for efficient translation by host machinery (Egloff et al., 2002, 2007). The C-terminus of NS5 contains an RNA-dependent-RNA-polymerase (RdRp) domain responsible for viral RNA replication (Bartholomeusz and Wright, 1993; Iglesias et al., 2011; Yap et al., 2007). A flexible linker joins the MTase and RdRp domains which can adopt unique conformations resulting in different interfaces between the MTase and RdRp domain, providing a regulatory mechanism of viral capping and RNA replication (Klema et al., 2016; Zhao et al., 2015).

Despite cytoplasmic replication of DENV2, NS5 is known to localize to the nucleus in infected cells (Johansson et al., 2001; Kapoor et al., 1995; Kumar et al., 2013; Pryor et al., 2007; Tay et al., 2013, 2016). The functional significance of this nuclear localization is currently unclear, although NS5 has been implicated in disruption of splicing by interaction with components of the host spliceosome (De Maio et al., 2016). NS5 is also known to disrupt the type I IFN response through mediating degradation of STAT2, thereby reducing IFN- α/β signaling and production of interferon-stimulated genes (Ashour et al., 2009; Kumar et al., 2013).

3.1b DENV2 Replication

The DENV2 replication cycle begins with virion-cell surface interaction. While a definitive DENV2 receptor has not been identified, several host proteins have been implicated in DENV2 attachment and endocytosis. The cellular factors implicated in DENV2 attachment and entry fall broadly into two categories: C-type lectin receptor and TIM/TAM transmembrane receptor families. Of the C-type lectin receptors, dendritic cell-specific intracellular adhesion molecule-3-grabbing non-integrin (DC-SIGN) and mannose receptor (MR) mediate viral attachment (Lozach et al., 2005; Miller et al., 2008; Navarro-Sanchez et al., 2003; Pokidysheva et al., 2006; Tassaneetrithep et al., 2003). DC-SIGN is known to complex with the DENV2 E protein (Pokidysheva et al., 2006). In contrast, TIM-1 is thought to mediate DENV2 attachment through recognition of lipids in the viral envelope, rather than interaction with viral glycoproteins (Carnece et al., 2016; Dejarnac et al., 2018; Meertens et al., 2012; Richard et al., 2015). In addition to these two receptor families, cell surface expression of heparan sulfate facilitates virion-cell interaction and adsorption (Chen et al., 1997; Dalrymple and Mackow, 2011; Germi et al., 2002).

Following receptor-virion interaction, DENV particles enter the host cell through clathrin-mediated endocytosis (Acosta et al., 2008, 2011; Krishnan et al., 2007; Mosso et al., 2008; Peng et al., 2009; Suksanpaisan et al., 2009). Acidification of the endosomal compartment is required for fusion between the viral and endosomal membranes for release of the viral genome into the cytoplasm (Kao et al., 2018; Krishnan et al., 2007; Perreira et al., 2015; van der Schaar et al., 2007, 2008).

Transition from a neutral pH to low a pH in the endosome initiates a conformational change in the E glycoprotein, exposing the fusion loop and resulting a trimeric rather than dimeric conformation of E, the result of which is the viral and endosomal membranes entering into close proximity and fusing, opening a pore and releasing the viral nucleocapsid into the host cytoplasm (Modis et al., 2003, 2004).

Uncoating of the viral genome after release from the endosome occurs in the first 2-4 hours post infection and requires disassociation of viral RNA from capsid protein, which undergoes proteasome-mediated degradation (Byk et al., 2016). Viral RNA is then free to be translated by host ribosomes, which initiate translation of viral proteins 3-5 hours post infection (Byk et al., 2016). Translation initiation is aided by recognition of the 5' cap by host machinery, but translation of DENV RNA is not strictly dependent on the 5' cap (Edgil et al., 2006; Song et al., 2019). This not-fully-described cap-independent mechanism of translation initiation is likely achieved through an internal ribosome entry site located in the 5' UTR of the DENV genome and/or interaction between RNA structures in the 5' and 3' UTRs of the viral genome (Edgil et al., 2006; Song et al., 2019). Translation of the DENV2 genome into a multi-pass transmembrane polypeptide is exclusively carried out by ER-associated ribosomes, as opposed to cytosolic ribosomes, and requires host ER machinery to ensure proper topology (Ngo et al., 2019; Reid et al., 2018).

Viral non-structural proteins produced through this initial translation then induce massive restructuring of the ER membrane and formation of viral replication complexes (Aktepe et al., 2017; Miller et al., 2007b; Stern et al., 2013; Teo and Chu, 2014; Welsch et al., 2009). Because the positive-sense genome serves as the template

for both translation and viral genome replication, and the polymerase and ribosomes work in opposing directions, a switch from translation to replication is required to temporally regulate these two critical functions. This most likely involves a structural change in the positive-sense template from a linear form which is most efficiently used for translation, to a circularized form which is most efficiently used for negative-strand synthesis (Sanford et al., 2019). Interactions between secondary RNA structures in the 5' and 3' ends prevent effective ribosome scanning, thereby inhibiting translation on the circularized RNA (Sanford et al., 2019). The negative-strand then serves as a template for production of capped positive-sense genomes which are packaged into immature virions. Replication of the negative-strand template and production of the capped genome copies requires the RNA-dependent RNA-polymerase and methyltransferase activity of NS5, as well as the NTPase and helicase activity of NS3 (Bartelma and Padmanabhan, 2002; Bartholomeusz and Wright, 1993; Egloff et al., 2002, 2007; Iglesias et al., 2011; Li et al., 1999; Luo et al., 2008b; Sanford et al., 2019; Yap et al., 2007).

Viral structural proteins and viral genomes are recruited for assembly by NS2A (Xie et al., 2019). Immature viral particles bud into the ER and then are trafficked to the Golgi, a process dependent on host trafficking machinery (Neufeldt et al., 2019). Immature viral particles are characterized by a “spiky” conformation of E-prM heterodimers on the surface of the viral particle in neutral pH environments (Li et al., 2008b; Yu et al., 2008; Zhang et al., 2004). Upon entry into the acidic environment of the trans-Golgi network, M undergoes a conformational change which induces a “smooth,” dimeric conformation of E which exposes the furin cleavage site in prM (Li et

al., 2008b; Yu et al., 2008; Zhang et al., 2012, 2004). Cleaved pr remains associated with the viral particle until a subsequent pH change upon release from the cell (Yu et al., 2008, 2009). As pr obscures the fusion loop on E, this pH-dependent cleavage and dissociation is required to prevent premature exposure of the fusion loop in E which would initiate fusion with host membranes prior to release from the cell (Yu et al., 2008, 2009). A summary of DENV2 replication is represented in Figure 3.2.

DENV2 Replication Cycle

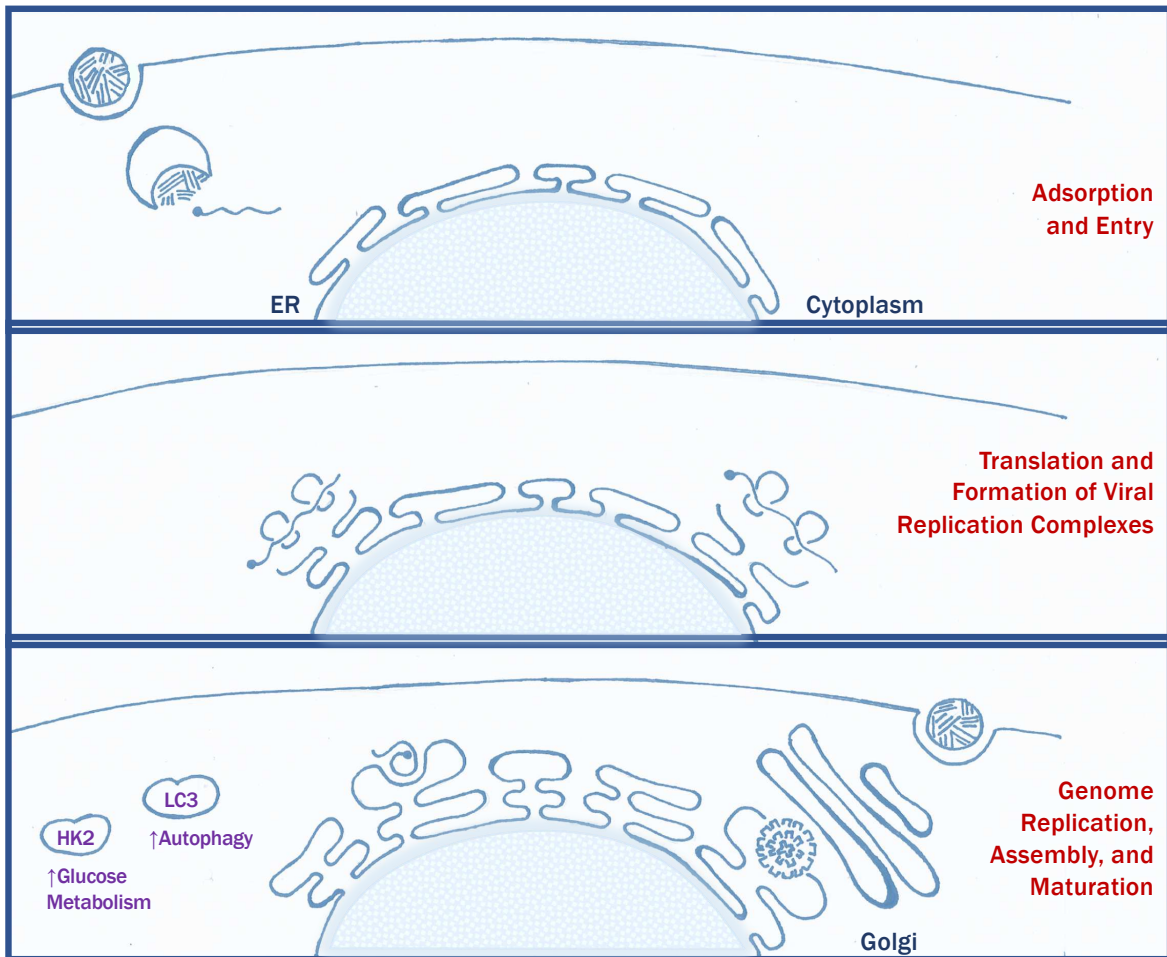


Figure 3.2 DENV2 Replication Cycle. Top panel: A DENV2 virion interacts with the cell surface, enters through an endosome, and then is released into the cytoplasm through fusion of the virion membrane with the endosomal membrane. Mid panel: The DENV2 genome is directly translated by host machinery to produce DENV2 proteins. The newly produced DENV2 proteins initiate membrane restructuring and formation of viral replication complexes on the ER membrane. Bottom panel: DENV2 genome copies are replicated and immature viral particles are assembled in the ER. Viral particles mature through the Golgi network and are released from the cell. The necessary membrane remodeling required for replication and viral particle assembly is supported by increases in glucose metabolism and autophagy.

3.1c Metabolism Changes during DENV2 Infection

Efficient infectious particle formation relies on coordinated completion of each step of the viral replication cycle and is heavily dependent on not only host cell machinery such as ribosomes and trafficking proteins, but the metabolic environment of the host cell. Key among the viral functions reliant on the cellular metabolic environment is the well-documented restructuring of cellular membranes that allows viral particle formation (Gillespie et al., 2010; Gullberg et al., 2018; Heaton and Randall, 2010; Jordan and Randall, 2017; Perera et al., 2012; Uchida et al., 2015; Welsch et al., 2009). Not only does the amount of lipids within the cell need to increase, the composition of these lipids is critical for infectious viral particle formation (Gullberg et al., 2018; Perera et al., 2012).

Acetyl-CoA and NADPH are two key metabolic intermediates required for fatty acid synthesis. Acetyl-CoA is the 2-carbon building block from which fatty acids are assembled while NADPH is required as a reducing agent. Acetyl-CoA and NADPH are products of glucose metabolism through the glycolytic and pentose phosphate pathways. Increased input and/or rate of either or both of these pathways would benefit

viral replication by providing the necessary metabolic intermediates for the upregulation of fatty acid synthesis required for viral particle assembly, as well as precursors for nucleotide synthesis and therefore viral genome replication. Glucose metabolism has been shown to be altered during DENV2 infection, including increased glucose uptake into infected cells (Fernandes-Siqueira et al., 2018; Fontaine et al., 2015). Virus-induced changes in lipogenesis are, at least in part, coordinated by DENV2 non-structural proteins; for example, host fatty acid synthase is relocalized to sites of viral replication by NS3 (Heaton et al., 2010).

Enhancement of glucose metabolism is thought to function in a primarily anaplerotic fashion in the context of DENV2 infection – that is, by functioning in the production of necessary metabolic intermediates rather than energy (Fernandes-Siqueira et al., 2018; Silva et al., 2019). This in contrast to an upregulation of glycolysis for ATP production. At least one described mechanism by which DENV2 infection results in an induction of these metabolic pathways is by the upregulation of hexokinase (HK) (Fontaine et al., 2015). HK is the first rate limiting enzyme in glycolysis and is responsible for the phosphorylation of glucose into glucose 6-phosphate (Wolf et al., 2011). Glucose 6-phosphate can then enter glycolysis or can be shunted into the pentose phosphate pathway. HK is therefore a key hub in the control of both glycolysis and the pentose phosphate pathway. The RNA and protein levels of HK were found to be upregulated during DENV2 infection (Fontaine et al., 2015). Glucose metabolism is summarized in Figure 3.3.

Glucose Metabolism

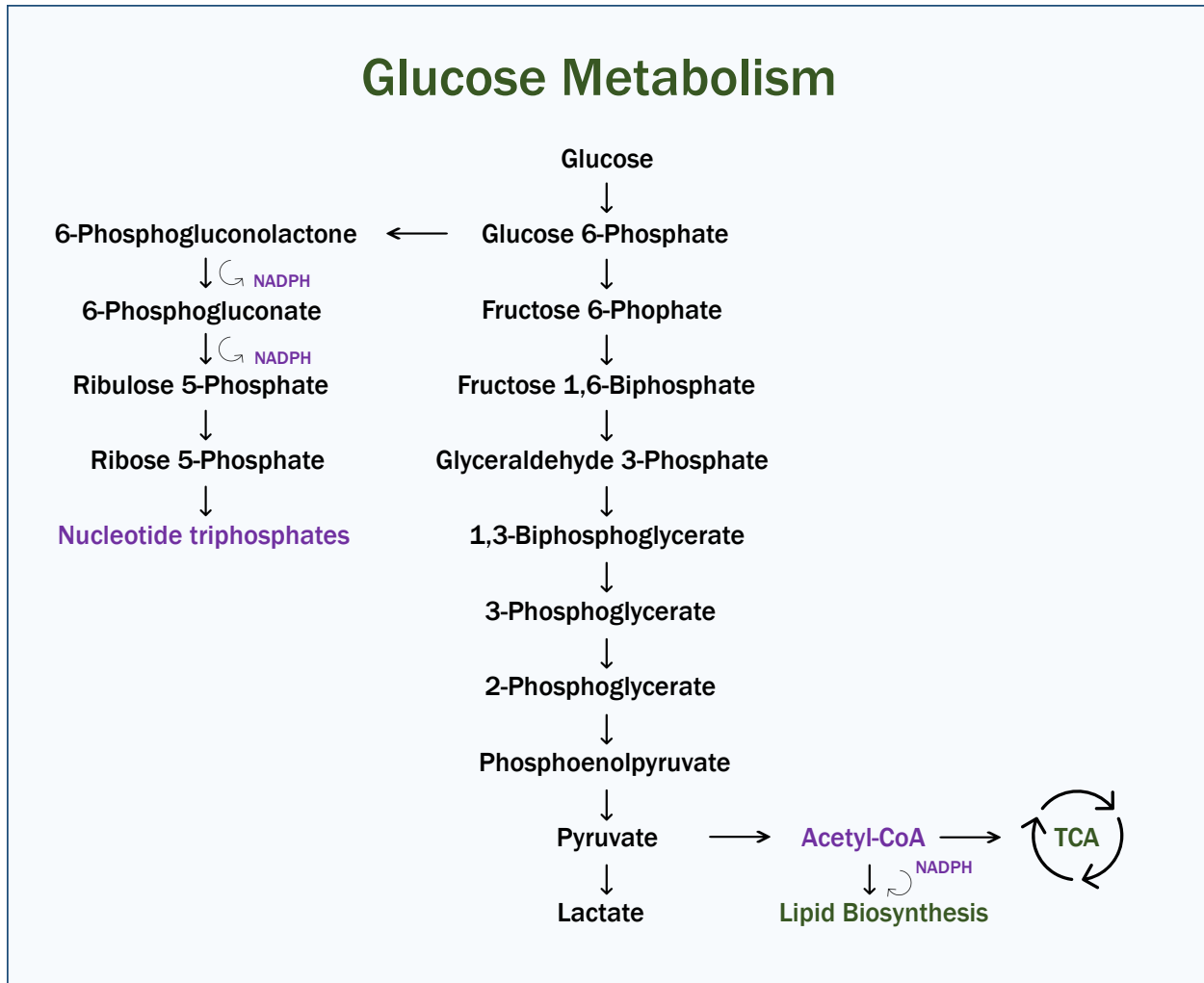


Figure 3.3 Glucose Metabolism. Key steps and intermediates in glucose metabolism. Glucose is phosphorylated to glucose 6-phosphate by hexokinase. Glucose 6-phosphate then progresses through glycolysis to produce pyruvate or is shuttled into the pentose phosphate pathway (left) to produce NADPH and NTPs. Pyruvate can be converted to lactate in anerobic conditions or into acetyl-CoA. Acetyl-CoA can enter the TCA cycle or can be used in lipid biosynthesis. Metabolic intermediates required for efficient DENV2 replication are indicated in purple.

In addition to an upregulation of glucose metabolism, DENV2 is known to induce changes in other metabolic pathways. Key among these is autophagy (Chen et al., 2016; Heaton and Randall, 2010; Jordan and Randall, 2017; Lee et al., 2008, 2013; Zhang et al., 2018). A pro-viral lipophagy induced during DENV2 infection promotes viral replication, presumably through the release of free fatty acids from lipid droplets for

entry into the mitochondria to undergo β -oxidation, ultimately supporting membrane restructuring and infectious particle production (Jordan and Randall, 2017; Zhang et al., 2018). This increased release in free fatty acids is matched with increased mitochondrial respiration during DENV2 infection, evident in both metabolic output (Fernandes-Siqueira et al., 2018) and changes in mitochondrial dynamics including increased fusion (Barbier et al., 2017). These mitochondrial changes carry important implications not only for metabolic outcomes, but also innate immune signaling (Chatel-Chaix et al., 2016).

Lipophagy is initiated with autophagosome component assembly on the lipid droplet, followed by formation of a limiting membrane, pinching off a portion of the lipid droplet with generation of the sealed autophagosome, and ultimately lysosomal fusion (Martinez-Lopez and Singh, 2015; Singh et al., 2009). Light chain 3 (LC3) is a membrane-associated protein which is often used as a marker for autophagosomes. LC3 is initially modified to LC3-I by the autophagy factor Atg4, and then subsequently modified to the membrane-associated, lipidated form LC3-II by autophagy factors Atg3 and Atg7 (Martinez-Lopez and Singh, 2015). Conversion of LC3-I to LC3-II is therefore considered a measure of autophagic activity (Martinez-Lopez and Singh, 2015; Singh et al., 2009). Increased conversion of LC3-I to LC3-II and subsequent depletion of lipid droplets has been noted in DENV2 infection (Heaton and Randall, 2010; Lee et al., 2008). Lipophagy is summarized in Figure 3.4.

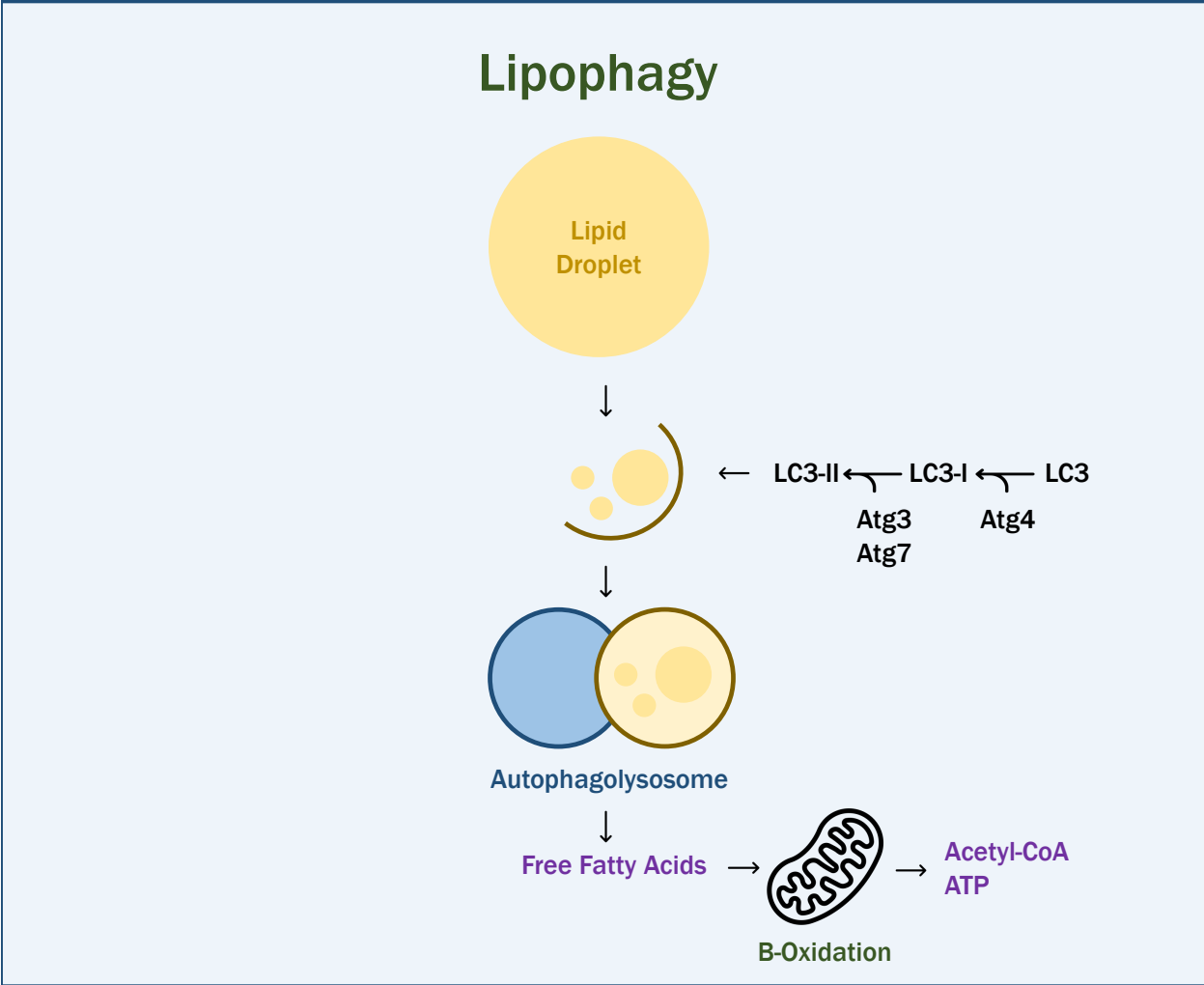


Figure 3.4 Lipophagy. An overview of the key steps and outcomes of lipophagy. Portions of lipid droplets are sequestered into autophagosomes. Autophagosomes fuse with lysosomes and the neutral lipids stored in lipid droplets are released as free fatty acids which then can be shuttled into mitochondria and undergo beta-oxidation, the products of which are acetyl-CoA and ATP. Key metabolic intermediates required for efficient DENV2 replication are indicated in purple.

As with glucose metabolism, DENV2 has been implicated in the disruption of lipophagy (Heaton and Randall, 2010; Jordan and Randall, 2017). NS4A and NS4B were found to have key roles in the induction of lipophagy during DENV2 infection (Zhang et al., 2018). NS4A, in the presence of NS4B, was found to interact with ancient ubiquitous protein 1 (AUP1), a protein which localizes on the surface of lipid droplets

and regulates induction of lipophagy through acyltransferase activity (Zhang et al., 2018). Despite this identification of the role of viral non-structural protein dysregulation of metabolic enzymes, the upstream mechanisms by which these metabolic enzymes are transcriptionally regulated during DENV2 infection has not been previously described. Beyond metabolic pathways, there are many other critical cellular pathways which are differentially regulated at the level of transcription during infection with DENV2. Each of these pathways has the potential, when manipulated, to promote or restrict viral replication. We were interested in understanding the mechanisms of transcriptional regulation of these pathways, specifically the type I interferon (IFN) response, due to the well-established importance of type I IFNs in restricting viral replication.

3.2 The Type I Interferon Response

The IFN response is a key innate immunity pathway, allowing host cells to recognize the presence of non-self entities and restrict pathogen replication. The type I interferons, comprised of IFN- β and the multiple isoforms of IFN- α , are primary drivers of antiviral innate immunity. The type I IFN response, while critical for early control of viral infection, must be tightly regulated. An unchecked IFN response can lead to immunopathologies including autoimmune disorders. Each step within pathogen recognition, initiation of type I IFN expression, IFN- α/β receptor (IFNAR) ligation and downstream signaling, and interferon-stimulated gene (ISG) expression is regulated by host factors at multiple levels (Chen et al., 2017a; Ivashkiv and Donlin, 2014). Viruses,

in turn, have multiple mechanisms for evading initiation of type I IFN responses and/or type I IFN signaling (Iwasaki, 2012). Each level of regulation of the type I IFN response is key to understanding not only host antiviral responses but also the mechanism by which viruses evade innate immunity.

3.2a Type I IFN Induction and Signaling Pathways

The type I IFN response is comprised of two phases. The first involves recognition of pathogen-associated molecular patterns (PAMPs) and initiation of type I IFN secretion. In the second phase, secreted type I IFN acts in an autocrine or paracrine fashion to promote the expression of the innate antiviral gene program, the ISGs (Goubau et al., 2013; Honda et al., 2006; Odendall and Kagan, 2017; Takaoka and Yamada, 2019).

Cytoplasmic, double-stranded RNA (dsRNA), either capped or uncapped, is a PAMP which is recognized by pattern-recognition receptors (PRRs). Uncapped, 5' triphosphate dsRNA is recognized by the host cytoplasmic helicase, retinoic acid-inducible gene I (RIG-I), while capped dsRNA is primarily recognized by melanoma differentiation-associated gene 5 (MDA-5). The synthetic, dsRNA mimic, polyinosinic:polycytidylic acid (poly(I:C)) is recognized by both helicases (Gitlin et al., 2006; Hornung et al., 2006; Kato et al., 2006, 2008). Binding of dsRNA to RIG-I or MDA-5 induces a conformational change and allows association with mitochondrial antiviral signaling protein (MAVS, also known as IPS-1), leading to dimerization of MAVS, recruitment of the E3-ubiquitin ligase complex component TNF receptor

associated factor 6 (TRAF6), activation of tank-binding kinase 1 (TBK1), and activating phosphorylation of interferon regulator factors 3 and 7 (IRF3 and IRF7), which allows translocation to the nucleus and activation of expression of type I IFNs (Goubau et al., 2013; Honda et al., 2006; Odendall and Kagan, 2017; Takaoka and Yamada, 2019).

Alternatively, dsRNA in endosomes is recognized by toll-like receptor 3 (TLR3) (Alexopoulou et al., 2001). Ligand-binding of TLR3 initiates dimerization, recruitment of TIR domain-containing adaptor molecular (TRIF) and the E3 ubiquitin ligase TRAF3, activation of TBK1 and inhibitor of nuclear factor kappa-B kinase subunit epsilon (IKK ϵ), and activating phosphorylation of IRF3 and IRF7 (Doyle et al., 2002; Takaoka and Yamada, 2019).

Secreted type I IFNs bind to IFN- α/β receptor (IFNAR). Ligand-binding to IFNAR initiates dimerization and activation of the Janus kinases JAK1 and tyrosine kinase 2 (Tyk2) and recruitment of signal transducer and activator of transcription (STAT), which then becomes phosphorylated and dimerizes. Homo- and heterodimers of the STAT isoforms dimerize in a context-dependent manner. Type I IFN activation of IFNAR canonically leads to STAT1-STAT2 heterodimers. The STAT1-STAT2 heterodimer associates with IRF9, forming the interferon-stimulated gene factor 3 (ISGF3) transcription factor complex which translocates to the nucleus and acts to initiate the transcription of ISGs (Honda et al., 2006; Ivashkiv and Donlin, 2014). Full activation of STATs requires tyrosine phosphorylation upon IFNAR activation, and serine phosphorylation in the transactivation domain upon nuclear translocation (Michalska et al., 2018; Plataniias, 2005). The type I IFN response associated with dsRNA is summarized in Figure 3.5.

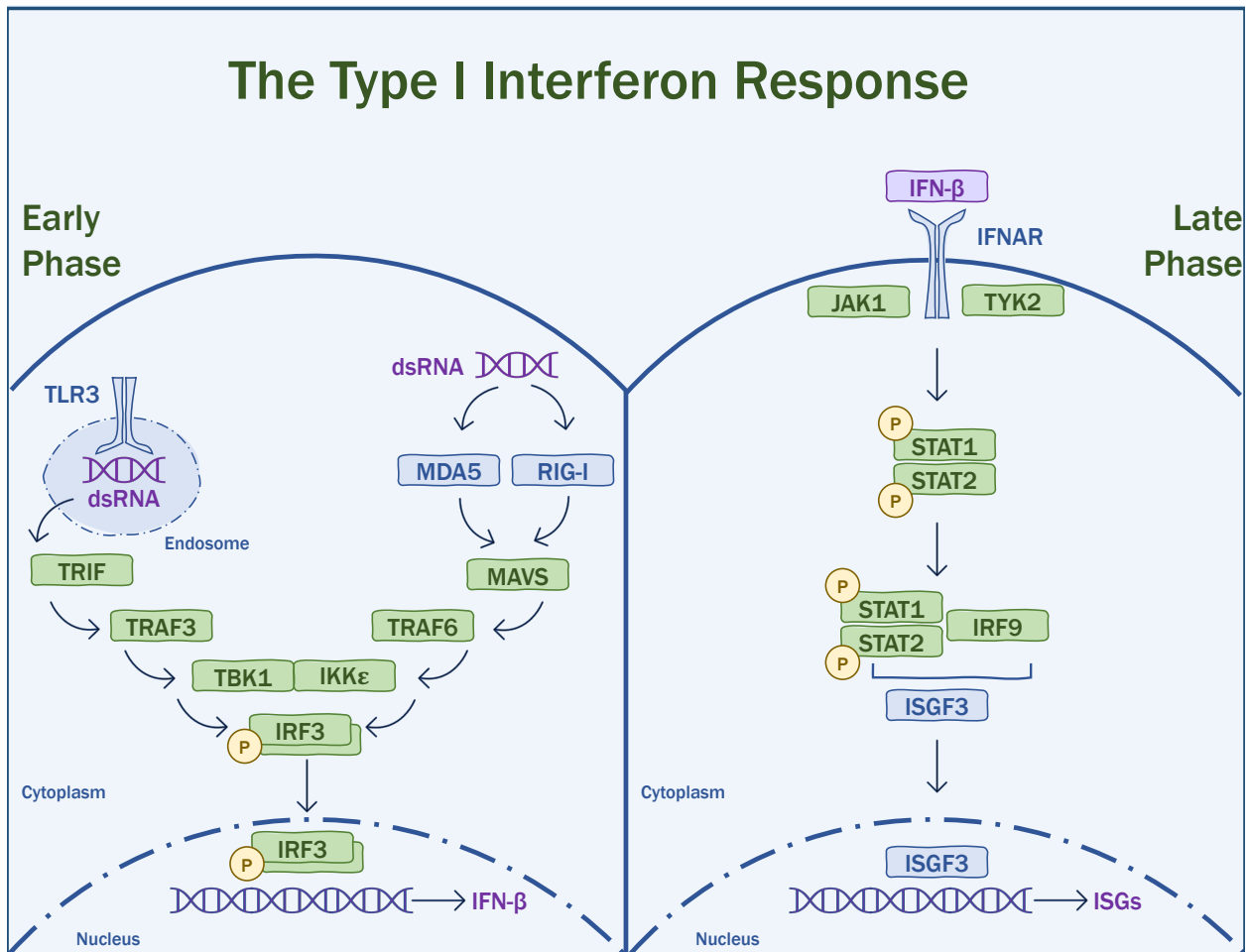


Figure 3.5 The Type I Interferon Response Associated with Double-Stranded RNA. Left panel: dsRNA in the cytoplasm is recognized by MDA-5 and/or RIG-I, allowing association with MAVS, activation of TRAF6, activation of TBK1 and IKK ϵ , and phosphorylation of IRF3. dsRNA in endosomes is recognized by TLR3, allowing activation of TRIF, TRAF3, TBK1 and IKK ϵ , and phosphorylation of IRF3. Phosphorylated IRF3 translocates to the nucleus where, in combination with other transcription factors, promotes the expression of IFN- β , which is then secreted from the cell. Right panel: Secreted IFN- β binds to IFNAR, initiating recruitment and phosphorylation of STAT1/STAT2 and association with IRF9, resulting in the formation of the ISGF3 complex. The ISGF3 complex translocates to the nucleus and promotes transcription of ISGs.

3.2b Type I IFN Evasion by DENV2

IFN- β expression is induced during DENV2 infection by activation and signaling through RIG-I, MDA-5, and TLR3 (Loo et al., 2008; Nasirudeen et al., 2011). Overexpression of any these factors induces greater IFN- β expression and reduced DENV2 replication, while knockout of these factors has the opposite effect (Loo et al., 2008; Nasirudeen et al., 2011). Due to this ability of the type I IFN response to restrict virus replication, DENV2, similar to many other viruses, has multiple mechanisms to reduce IFN signaling and minimize the ability of the host cell to restrict virus replication (Chen et al., 2017c; Green et al., 2014). These mechanisms are primarily executed by DENV2 nonstructural proteins including NS2A, NS4A, NS4B, and NS5 (Ashour et al., 2009; He et al., 2016; Kumar et al., 2013; Munoz-Jordan et al., 2003; Muñoz-Jordán et al., 2005). Inhibition of type I IFN signaling by DENV2 occurs at multiple levels including initial recognition by PRRs, PRR signaling, and JAK/STAT signaling (Ashour et al., 2009; He et al., 2016; Kumar et al., 2013; Munoz-Jordan et al., 2003; Muñoz-Jordán et al., 2005).

3.2c Transcriptional Regulation of IFN- β Expression

Because of the important nature of the type I IFN response in protecting the host from virus infection, and the potential for immunopathology in a dysregulated interferon response, IFN- β expression is tightly regulated at multiple levels. Particularly at the level of IFN- β mRNA expression, transcription of IFN- β relies on the coordinated binding of

multiple transcription factors and coactivators at the IFN- β enhancer region, forming the IFN- β enhanceosome. The IFN- β enhanceosome is formed through cooperative binding of c-Jun/ATF-2, IRFs (including IRF-3 and IRF-7), and the NF κ B subunits RelA and p50 (Du et al., 1993; Thanos and Maniatis, 1995; Wathelet et al., 1998). Cooperative binding of these different elements relies on binding of high-mobility group protein (HMG I(Y)) which induces the necessary conformational change in the enhancer region (Thanos and Maniatis, 1995). Interaction between the enhanceosome components IRF-3 and IRF-7 and p300/CREB-binding protein (CBP) further promotes the transcription of IFN- β (Wathelet et al., 1998).

Appropriately regulated IFN- β expression depends not only on coordinated activation but also proper downregulation to prevent immunopathology associated with over-activation of the type I IFN response. IRF3, as a key link between PRR signaling and IFN- β expression, is targeted by a number of negative regulators to reduce type I IFN signaling. Regulators of IRF3 include Pin1 (peptidyl-prolyl cis-trans isomerase NIMA-interacting 1), Rubicon (Run domain Beclin-1-interacting and cysteine-rich domain-containing protein), and LYAR (cell growth-regulating nucleolar protein) (Kim et al., 2017; Saitoh et al., 2006; Yang et al., 2019). Mechanisms of inhibition of IRF3-dependent IFN- β expression include: reduced phosphorylation of IRF3 by competitive binding to TBK1/IKK ϵ , prevention of IRF3 dimerization, increased proteasomal-mediated degradation of IRF3, and reduced IRF3 binding to the IFN- β enhancer (Kim et al., 2017; Lu et al., 2017; Saitoh et al., 2006; Yang et al., 2019).

IRF3 inhibition and/or downregulation ultimately reduces the expression of IFN- β , but regulation at the level of IRF3 is not the only mechanism by which IFN- β expression,

and therein the perpetuation of the type I IFN response, is resolved. In particular, we were interested in the direct regulation of IFN- β transcription at the promoter, including recruitment of transcription factors and transcription elongation. Of particular interest were the transcriptional regulators, cyclin-dependent kinases 8 and 19 (CDK8 and CDK19) which are known to function primarily in induced states and within innate immunity pathways (Chen et al., 2017b)

3.3 Cyclin-dependent Kinases 8 and 19

Cyclin-dependent kinase 8 (CDK8) is a highly conserved 464-amino acid protein of approximately 53 kDa structured into two lobes (N-lobe and C-lobe) and an activating loop (A-loop) (Schneider et al., 2011; Tassan et al., 1995; Xu et al., 2014). Within the N-lobe, the α B helix is responsible for interaction with the CDK8-activating cyclin, Cyclin C (Schneider et al., 2011). Binding of Cyclin C with CDK8 induces a conformational change in the A-loop, exposing the catalytic cleft (Schneider et al., 2011)

CDK8 orthologs have been identified in a wide range of eukaryotic organisms, while its paralog CDK19 has only been identified in vertebrates (Cao et al., 2014; Tassan et al., 1995). CDK8 and CDK19 share high sequence similarity and identical active sites, but diverge in sequence in the 3' UTR and have both distinct and overlapping functions (Galbraith et al., 2013; Sato et al., 2004; Steinparzer et al., 2019). Both CDK8 and CDK19 function in a gene-specific manner to up- or downregulate transcription (Bancerek et al., 2013; Jeronimo and Robert, 2017; Steinparzer et al., 2019).

A body of recent work illustrating a role for CDK8/19 as regulators of metabolic gene expression (Galbraith et al., 2017; Tang et al., 2018) and as regulators of immunity-related gene expression (Bancerek et al., 2013; Chen et al., 2017b; Johannessen et al., 2017; Steinparzer et al., 2019) led us to investigate the role of CDK8 and CDK19 as transcriptional regulators during DENV2 infection (Chapter 4) and during the type I IFN response (Chapter 5).

3.3a Mechanisms of Transcriptional Regulation by CDK8/19

Mediator is a large, multi-subunit complex which functions as a co-activator and mediates RNA polymerase II-dependent transcription (Jeronimo and Robert, 2017). Individual components of Mediator reversibly associate with the complex; for example, Mediator subunit 12 (Med12), Mediator subunit 13 (Med13), CDK8, and Cyclin C form a submodule which can associate with both the larger Mediator complex and as an independent submodule, termed the CDK8 submodule (Knuesel et al., 2009; Tsai et al., 2013) (Figure 3.6).

The known functional ability of CDK8 to regulate gene expression is determined by phosphorylation targets of CDK8. In the larger mediator complex, CDK8 has been shown to promote expression of immediate early genes within the serum response through phosphorylation of Ser5 and Ser2 on the carboxy-terminal domain of RNA Pol II and recruitment of CDK7, CDK9/PTEF-b (Donner et al., 2010). A similar promotion of pause-release and elongation of transcripts by CDK8 has been shown in the hypoxia response (Galbraith et al., 2013). In this instance, CDK8 activity results in the

recruitment of the super elongation complex (SEC) to stimulate pause-release of RNA Pol II on transcripts of genes responsive to hypoxia-inducible factor 1 alpha (HIF-1 α) (Galbraith et al., 2013).

CDK8 in the submodule has also been shown to regulate gene expression, but through different mechanisms. These include phosphorylation of serine 10 on histone H3, an epigenetic modification which promotes acetylation of lysine 14 on the same histone H3 tail, thereby leading to an open conformation of chromatin and promoting transcriptional activity (Meyer et al., 2008).

In addition, a number of transcription factors have been identified as phosphorylation targets of CDK8. Sterol-regulator element binding protein 1 (SREBP-1), a transcription factor responsible for the upregulation of expression of genes required for lipogenesis, is marked for ubiquitin-dependent degradation as a result of CDK8 phosphorylation (Zhao et al., 2012). This CDK8-mediated degradation of SREBP-1 results in reduced expression of key lipogenic genes including *FAS* (fatty acid synthase), *ACS* (acetyl-coenzyme A synthetase), and *SCD1* (stearyl-CoA desaturase 1) (Zhao et al., 2012).

CDK8 phosphorylation of transcription factors does not always follow this same mechanism of mediating degradation and repressing transcription; rather, the result of CDK8 phosphorylation of transcription factors can have a positive or negative effect on gene expression in a manner that is not only dependent on the transcription factor but on the individual downstream genes. While CDK8 phosphorylation of SREBP-1 results in reduced expression of SREBP-1-dependent genes, CDK8 phosphorylation of signal transducer and activator of transcription 1 (STAT1) has a net positive effect on gene

expression, with some repression on a specific subset of genes (Bancerek et al., 2013). CDK8 phosphorylates STAT1 in the transactivation domain after nuclear localization of STAT1 during activation of JAK/STAT signaling by IFN- γ treatment (Bancerek et al., 2013). Known mechanisms of CDK8 transcriptional regulation are summarized in Figure 3.6.

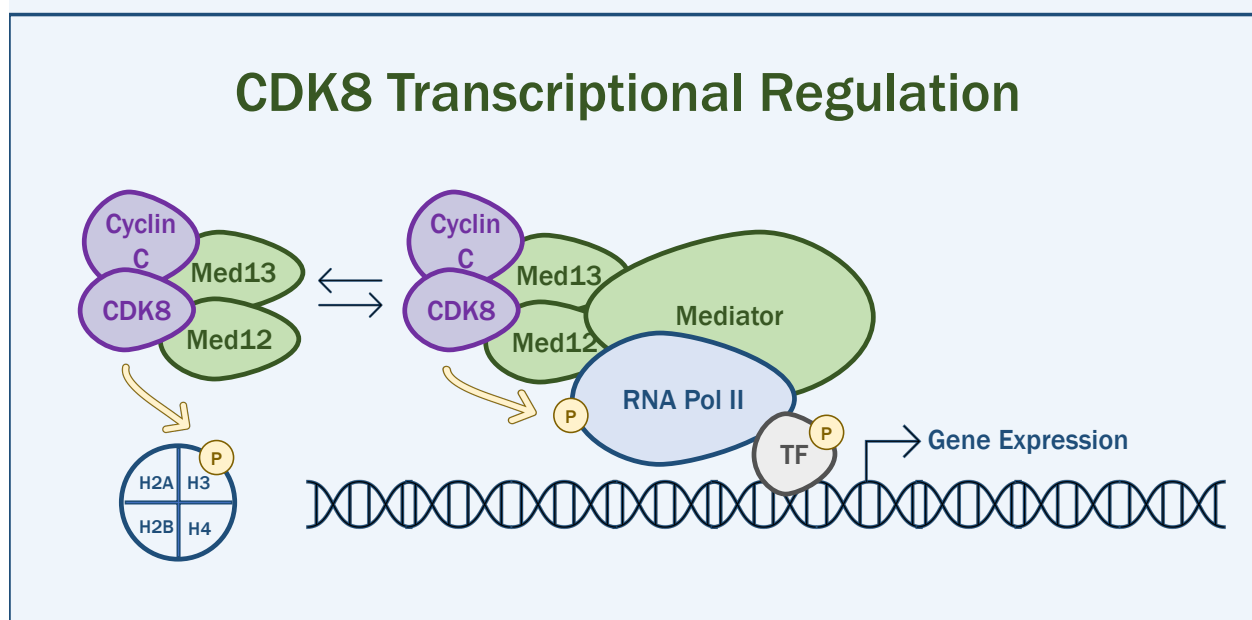


Figure 3.6 Mechanisms of CDK8 Transcriptional Regulation. CDK8, Cyclin C, Med12, and Med13 associate with the larger Mediator complex in conjunction with RNA Pol II and regulate transcription through phosphorylation of the C-terminal domain of RNA Pol II. Separately, CDK8, Cyclin C, Med12, Med13 together form the CDK8 submodule (left) with an identified phosphorylation target of serine 10 on histone H3, a marker of active transcription. Additionally, numerous transcription factors (TF) have also been identified as CDK8 phosphorylation targets. These phosphorylation events have gene-specific up- or downregulatory effects.

These identified functions of CDK8 illustrate the critical role of CDK8 as a transcriptional regulator in induced states rather than a regulator of basal transcription. Induced states in which CDK8 is known to have key regulator functions include: hypoxia (Galbraith et al., 2013, 2017), starvation (Birkenheuer et al., 2015; Donner et al., 2010;

Zhao et al., 2012), and immune signaling activation (Bancerek et al., 2013; Chen et al., 2017b; Johannessen et al., 2017; Steinparzer et al., 2019).

Related to the described functions of CDK8 as a regulator of gene expression in the hypoxia and serum response pathways, CDK8 has been found to be upregulated and/or functionally activated in a number of cancers. These include colorectal cancer, breast cancer, and prostate cancer (Brägelmann et al., 2017; Firestein et al., 2008; McDermott et al., 2017). While the entirety of CDK8 function as an oncogene is not fully understood, CDK8 has been identified as an important co-activator in β -catenin-mediated transformation as well as a regulator of downstream oncogenes in the MAPK signaling pathway (Donner et al., 2010; Firestein et al., 2008). CDK8 knockdown or kinase inhibition has also been shown to affect cancer cell line proliferation and morphology (Galbraith et al., 2017; McDermott et al., 2017). Alterations in cellular metabolism is a hallmark of cancer which allows cellular proliferation and survival in low-nutrient and low-oxygen tumor microenvironments and recent work has demonstrated a critical role for CDK8/19 in metabolic gene expression (Galbraith et al., 2017; Hanahan and Weinberg, 2011; Tang et al., 2018). In addition to the above described role in the regulation of SREBP-dependent lipogenic enzymes, CDK8 was identified as a regulator of select glycolytic gene expression in normoxic and hypoxic states and CDK8 is a transcriptional regulator of autophagic gene expression in both *Drosophila* and mammalian cells (Galbraith et al., 2017; Tang et al., 2018; Zhao et al., 2012).

In summary, CDK8 kinase activity has diverse targets, functions, and effects on gene expression in induced states. The net result of CDK8 kinase activity occurs in a

gene-specific manner and depends on the signaling and/or response pathway leading to CDK8 kinase activity, the association of CDK8 with either the larger Mediator complex or the smaller submodule, and the nature of the phosphorylation target.

3.3b CDK8/19 Chemical Inhibition

Because CDK8 expression is commonly upregulated in human cancers (Brägelmann et al., 2017; Firestein et al., 2008; McDermott et al., 2017; Park et al., 2018), it is currently viewed as an important chemotherapeutic target (Johannessen et al., 2017; Porter et al., 2012). A number of chemical inhibitors of CDK8/19 have been described. Senexin A is a small-molecule active site inhibitor of CDK8 and CDK19, as is its second-generation iteration, Senexin B (McDermott et al., 2017; Porter et al., 2012). Other inhibitors of CDK8/19 kinase activity include cortistatin A and MSC2530818 (Clarke et al., 2016; Pelish et al., 2015; Poss et al., 2016). Recent work has suggested that the result of CDK8/19 kinase inhibition is distinct from CDK8/19 knockdown, suggesting a kinase-independent structural or scaffold role for CDK8 and/or CDK19 in regulation of gene expression (Poss et al., 2016; Steinparzer et al., 2019). This work is complicated by incomplete knockdown of CDK8/19 and/or incomplete inhibition of CDK8/19 by chemical inhibitors and warrants further investigation.

CDK8/19 knockdown and CDK8/19 chemical inhibition are not without challenges. CDK8 knockdown is embryonically lethal, CDK8/19 inhibition has proliferative and morphological consequences *in vitro*, and the use of at least some

CDK8/19 inhibitors has been found to have significant toxicity in mice (Clarke et al., 2016; Galbraith et al., 2017; Westerling et al., 2007).

3.3c Viral Manipulation of CDK8/19

Due to CDK8's role in the regulation of proliferation, cell survival in induced states, and metabolic gene expression, it represents a potentially attractive target for viral manipulation to reshape the host cell environment in a way that is conducive to viral replication. One clear example of viral manipulation of CDK8 is walleye dermal sarcoma virus (WDSV). WDSV is an oncogenic retrovirus of walleye and is associated with seasonal growth and then regression of dermal sarcomas (Rovnak and Quackenbush, 2010). WDSV encodes a cyclin-like protein, retroviral cyclin (RV-cyclin) which has limited homology to host cyclins and interacts with host transcriptional regulators including TATA-binding protein associated factor 9 (TAF9) to alter the gene expression profile of host cells (Quackenbush et al., 2009; Rovnak and Quackenbush, 2006). RV-cyclin directly binds to CDK8, functionally replacing Cyclin C, and ultimately enhancing CDK8 function in the regulation of transcriptional elongation (Birkenheuer et al., 2015; Brewster et al., 2011; Rovnak et al., 2012). This is a mechanism by which a virally encoded protein alters the activity of CDK8 to affect regulation of host gene expression and may suggest CDK8 as a potential target for other viruses, particularly those which are highly dependent on CDK8-regulated genes, including metabolic gene expression.

3.4 Summary and Introduction to Research Aims

3.4a Introduction to Research Aims, Chapter 4

We investigated the role of host transcriptional regulation in establishment of the metabolic environment which is required to support DENV2 replication. In particular, we focused on host transcriptional regulators CDK8 and CDK19 (Galbraith et al., 2017; Tang et al., 2018). We hypothesized that CDK8 and CDK19, as cellular transcriptional regulators during induced states, regulate key host transcriptional changes during DENV2 infection including changes in glucose metabolism and lipophagy which are known to support viral replication (Abernathy et al., 2019; Fernandes-Siqueira et al., 2018; Fontaine et al., 2015; Gullberg et al., 2018; Heaton et al., 2010; Jordan and Randall, 2017; Zhang et al., 2018).

Using a synchronized infection model in a cell line highly permissive to DENV2 infection, our research aims included: characterization of expression changes in CDK8 and CDK19 during the course of infection, characterization of the role of CDK8/19 as pro- or anti-viral, identification of the mechanism by which CDK8 supports DENV2 replication including identification of specific metabolic pathways and genes which are regulated by CDK8 and which are required for efficient DENV2 replication, and ultimately, to characterize the role of CDK8/19 in establishing a cellular metabolic environment conducive to DENV2 replication.

3.4b Introduction to Research Aims, Chapter 5

During the investigation into the role of CDK8/19 as transcriptional regulators of metabolic gene expression during DENV2 infection, we observed a marked effect on the robustness of the type I interferon response in the context of CDK8/19 inhibition. This led to a hypothesis that, in addition to a role for regulating metabolic gene expression, CDK8/19 also have a role in regulation of the innate antiviral response.

However, the DENV2 infection system is not the optimal model for studying regulation of the type I IFN response. Significant limitations of this model include the inability to separate early innate recognition of pathogen-associated molecular patterns (PAMPs) from the later phase of autocrine and paracrine signaling, the known ability of DENV2 to manipulate the type I IFN response (Ashour et al., 2009; Green et al., 2014) and the inability to distinguish CDK8 activity from that of CDK19 activity due to significant reduction in cellular proliferation in the context of knockdown in the cell line used for DENV2 infection studies (Audetat et al., 2017; Birkenheuer et al., 2015; Firestein et al., 2008).

We therefore turned to different cell lines and different stimuli to induce the type I IFN response to address our research aims. These aims included: characterizing the effect of CDK8/19 inhibition and knockdown on induction of the type I IFN response during DENV2 infection in multiple cell lines, further establishing the independence or dependence of DENV2 replication on CDK8/19-dependent regulation of the type I IFN response, distinguishing unique roles for CDK8 and CDK19 as regulators of the type I

IFN response, and identifying distinct pathways of induction of the type I IFN response in which CDK8 and CDK19 differentially regulate IFN- β expression.

CHAPTER 4: CYCLIN-DEPENDENT KINASES 8 AND 19 REGULATE HOST CELL METABOLISM DURING DENGUE VIRUS SEROTYPE 2 INFECTION²

4.1 Summary

Dengue virus infection is associated with the upregulation of metabolic pathways within infected cells. This effect is common to infection by a broad array of viruses. These metabolic changes, including increased glucose metabolism, oxidative phosphorylation and autophagy, support the demands of viral genome replication and infectious particle formation. The mechanisms by which these changes occur are known to be, in part, directed by viral nonstructural proteins that contact and control cellular structures and metabolic enzymes. We investigated the roles of host proteins with overarching control of metabolic processes, the transcriptional regulators, cyclin-dependent kinase 8 (CDK8) and its paralog, CDK19, as mediators of virally induced metabolic changes. Here, we show that expression of CDK8, but not CDK19, is increased during dengue virus infection in Huh7 human hepatocellular carcinoma cells, although both are required for efficient viral replication. Chemical inhibition of CDK8 and CDK19 with Senexin A during infection blocks virus-induced expression of select metabolic and autophagic genes, hexokinase 2 (HK2) and microtubule-associated protein 1 light chain 3 (LC3) and reduces viral genome replication and infectious particle production. The results further define the dependence of virus replication on increased

²Butler, M.; Chotiwan, N.; Brewster, C.D.; DiLisio, J.E.; Ackart, D.F.; Podell, B.K.; Basaraba, R.J.; Perera, R.; Quackenbush, S.L.; Rovnak, J. (2020). Cyclin-Dependent Kinases 8 and 19 Regulate Host Cell Metabolism during Dengue Virus Serotype 2 Infection. *Viruses*. 12, 654.

metabolic capacity in target cells and identify CDK8 and CDK19 as master regulators of key metabolic genes. The common inhibition of CDK8 and CDK19 offers a host-directed therapeutic intervention that is unlikely to be overcome by viral evolution.

4.2 Introduction

According to the World Health Organization, dengue virus (DENV) is endemic in over 100 countries throughout tropical and subtropical regions worldwide. They estimate that 500,000 people with severe dengue require hospitalization each year, with an estimated 2.5% fatality rate (World Health Organization, 2020). The Pan American Health Organization reported 2,733,635 cases in 2019 in Central and South America, the highest number of cases ever recorded in the Americas; 22,127 of these were classified as severe dengue and 1206 people died (Pan American Health Organization and World Health Organization).

Viruses depend on the host cell to provide energy and metabolic precursors to support genome replication and infectious particle production. Viral replication places increased demands for production of ATP and metabolites on the host cell (Mayer et al., 2019; Moreno-Altamirano et al., 2019; Thaker et al., 2019). To meet these demands, viruses manipulate the intracellular environment of the host cell by remodeling cellular structures and by reprogramming cellular metabolism to increase the expression of key metabolic enzymes (Chotiwan et al., 2018; Fernandes-Siqueira et al., 2018; Fontaine et al., 2015; Gullberg et al., 2018; Heaton and Randall, 2010; Heaton et al., 2010; Melo et al., 2018; Perera et al., 2012; Pleet et al., 2018).

Infections with dengue viruses are the most common mosquito-borne diseases worldwide and pose a significant risk to approximately half of the world's population (Bhatt et al., 2013; Pang et al., 2017). There are four distinct serotypes, dengue 1, 2, 3, and 4 (DENV1–4), each causing a similar, acute disease marked by fever and severe joint pain. Sequential infections with different DENV serotypes are associated with dengue hemorrhagic fever (DHF) and dengue shock syndrome (DSS), which are life threatening in 15% of patients (Guzman and Harris, 2015; Halstead, 2007).

Of the four serotypes, DENV2 has been shown to rely on increased glucose uptake and enhanced glucose metabolism to provide necessary metabolic intermediates for viral replication (Fernandes-Siqueira et al., 2018; Fontaine et al., 2015; Silva et al., 2019). DENV2 infection also induces autophagy and lipophagy for efficient replication (Abernathy et al., 2019; Chen et al., 2016; Heaton and Randall, 2010; Jordan and Randall, 2017; Lee et al., 2008; Zhang et al., 2018). Lipophagy releases fatty acids from lipid droplets which are shuttled into mitochondria for β -oxidation and ATP production (Heaton and Randall, 2010; Jordan and Randall, 2017; Zhang et al., 2018).

Recent work has identified interactions between viral non-structural proteins and host metabolic enzymes to modify these processes (Allonso et al., 2015; Heaton et al., 2010; Silva et al., 2019). Beyond protein–protein interactions, it has also been shown that expression of mRNAs encoding specific metabolic enzymes is elevated during DENV2 infection, and this increases the total metabolic capacity of infected cells (Fontaine et al., 2015; Gullberg et al., 2018). We sought to identify host factors that regulate these transcriptional changes in metabolic enzyme expression during DENV2 infection.

Cyclin-dependent kinase 8 (CDK8) is a component of the general transcription factor, Mediator, a large protein complex required for transactivation of all RNA polymerase II (RNA Pol II) transcription. CDK8 regulates transcriptional elongation by phosphorylation of the C-terminal domain of the largest subunit of RNA Pol II, a variety of transcription factors, and serine 10 on histone H3 (H3S10) (Bancerek et al., 2013; Donner et al., 2010; Galbraith et al., 2013; Meyer et al., 2008; Zhao et al., 2012). CDK8 regulates gene expression preferentially during induced states such as hypoxia and serum starvation (Birkenheuer et al., 2015; Donner et al., 2010; Galbraith et al., 2013; Rovnak et al., 2012) and has recently been implicated in the transcription of glycolytic and autophagic genes (Galbraith et al., 2017; Tang et al., 2018).

We have previously shown that CDK8 is directly and very specifically targeted by the oncogenic retrovirus, walleye dermal sarcoma virus (Birkenheuer et al., 2015; Brewster et al., 2011; Rovnak and Quackenbush, 2002; Rovnak et al., 2012) and reasoned that CDK8 is likely targeted, directly or indirectly, by many viruses with metabolic and autophagic demands, as exemplified by DENV2 infection. We found that expression of CDK8 is upregulated during DENV2 infection of Huh7 human hepatocellular carcinoma cells, and that this precedes increased expression of two key genes, hexokinase 2 (HK2) and microtubule-associated protein 1 light chain 3 (LC3).

Knockdown of expression of CDK8, the CDK8 paralog, CDK19, or their activator, Cyclin C, reduced viral genome replication. CDK8 and CDK19 share identical active sites, which allows their specific inhibition with small-molecule competitive inhibitors. We used the active-site inhibitor, Senexin A and its second-generation iteration, Senexin B (McDermott et al., 2017; Porter et al., 2012). These compounds reduced DENV2

induction of HK2 and LC3 expression, viral RNA replication, and the production of infectious particles. Inhibition of CDK8/CDK19 kinase activity also reduced mitochondrial function in infected and uninfected cells. The results identify DENV2 dependence on CDK8 function to regulate host gene expression, a host mechanism that can be targeted for therapeutic interdiction.

4.3 Materials and Methods

4.3a Cell Culture and DENV2 Infection

Huh7 cells, a hepatocellular carcinoma cell line derived from a liver tumor in a 57-year-old Japanese male in 1982 (<https://huh7.com>), were provided by Dr. Rushika Perera and cultured in Dulbecco's modified Eagle medium (DMEM), supplemented with 10% fetal bovine serum (FBS), 1% non-essential amino acids, 1% L-glutamine, 1% penicillin-streptomycin, and 25 mM HEPES. At 24 h prior to infection, 1×10^6 Huh7 cells were plated in 25 cm² flasks. Immediately prior to infection, cells were incubated at 4 C for 15 min, washed with cold Dulbecco's phosphate-buffered saline (D-PBS) and incubated with DENV2 (strain 16681, passage 4) (Kinney et al., 1997) at 4 C for 1 h with rocking. Virus media were removed and replaced with supplemented DMEM with 2% FBS.

4.3b CDK8/19 Small-Molecule Inhibition and Cell Viability Assay

Mock- or DENV2-infected cells were incubated in DMEM with Senexin A (MedChemExpress, Monmouth Junction, NJ, USA) or Senexin B (ProbeChem, Shanghai, China) at indicated concentrations or in media with the volumetric equivalent (final 0.01%) of DMSO solvent for the indicated period of time. Cell viability with Senexin treatment or shRNA transduction was determined by modified MTS assay according to the manufacturer's instructions (CellTiter 96 Aqueous One Solution Cell Proliferation Assay, Promega, Madison, WI, USA).

4.3c qRT-PCR Analysis

At the indicated times post infection or treatment, cells were collected in TRIzol (Thermo Fisher Scientific, Waltham, MA, USA), and total RNA was isolated according to the manufacturer's instructions and treated with Turbo DNase I (Thermo Fisher Scientific, Waltham, MA, USA). cDNA was synthesized with an iScript cDNA synthesis kit (Bio-Rad, Hercules, CA, USA) according to the manufacturer's instructions, and then, subjected to qPCR analysis with iQ SYBR green Supermix in a CFX96 real-time PCR system (Bio-Rad, Hercules, CA, USA). Primer sequences are listed in Table 4.1. Relative expression was normalized to the housekeeping gene, Succinate Dehydrogenase Complex Flavoprotein Subunit A, SDHA (Watson et al., 2007). For genomic equivalent analysis, Cq values were standardized to ten-fold dilutions of in vitro transcribed DENV2 genomic RNA and subject to qRT-PCR.

Table 4.1 PCR Primers.

Gene	Forward	Reverse	Source
CDK8	GGGATCTCTATG TCGGCATGTAG	AAATGACGTTTG GATGCTTAAGC	(Galbraith et al., 2013)
CDK19	GCCACGGCTAGG GCCT	GCGAGAACTGGA GTGCTGATAA	(Galbraith et al., 2013)
Cyclin C	ATGGCAGGGAAC TTTTGGCAG	ACCGTAGCAGTG GCAATAACT	Birkenheuer, unpublished
DENV	ACAAGTCGAACA ACCTGGTCCAT	GCCGCACCATTG GTCTTCTC	(Laue et al., 1999)
HK2	CAAAGTGACAGT GGGTGTGG3	GCCAGGTCCTTC ACTGTCTC3	(Wolf et al., 2011)
LC3	AAGGCTTTCAGA GAGACCCTG	CCGTTTACCCTG CGTTTGTG	(Sinha et al., 2015)
ENO1	GTCTCTTCAGGC GTGCAAGC	GATGAGACACCA TGACGCC	(Galbraith et al., 2017)
PFKL	GGCATTATGTG GGTGCCAAAGTC	CAGTTGGCCTGC TTGATGTTCTCA	(Lee et al., 2017)
PKM2	CCACTTGCAATTA TTTGAGGAA	GTGAGCAGACCT GCCAGACT	(Haas et al., 2015)
GAPDH	GCCATCAATGAC CCCTTCAT	CGCTCCTGGAAG ATGGTG	(Brewster et al., 2011)
SDHA	GACAACTGGAGG TGGCATT	CCGTCATGTAGT GGATGGCA	(Watson et al., 2007)

4.3d Plaque-forming Unit and Extracellular Genome Equivalent Analysis

Media were collected from virus-infected cells at indicated times, centrifuged at 500× g for 15 min to remove cellular debris, and aliquoted into TRIzol LS (Thermo Fisher Scientific, Waltham, MA, USA). RNA was extracted according to the manufacturer's instructions, and cDNA was synthesized with an iScript cDNA synthesis kit (Bio-Rad, Hercules, CA, USA) and subjected to qPCR analysis with iQ SYBR green Supermix in a CFX96 real-time PCR system (Bio-Rad, Hercules, CA, USA). Cq values were compared to ten-fold dilutions of in vitro transcribed DENV2 genomic, as described above.

Plaque assays were performed on BHK cells. Briefly, 10-fold dilutions of clarified supernatant were adsorbed on confluent BHK cells for 1 h. The cells were then overlaid with 3 mL of 1% agarose in MEM supplemented with 5% FBS. After incubation for 8 days, 4% neutral red solution in PBS was added to the agar overlay, and plaques were counted at 18–24 h after staining.

4.3e Lentivirus-mediated shRNA Gene Knockdown

Lentivirus delivery of short hairpin RNAs (shRNA) (Sigma-Aldrich, St. Louis, MO, USA; listed in Table 4.2) was used to knock down expression of CDK8, CDK19, and Cyclin C. A non-target shRNA was used as a control. 293FT cells (Thermo Fisher Scientific, Waltham, MA, USA) were transfected with shRNA and lentivirus packaging constructs, and virus particles were collected after 48 h. Huh7 cells were transduced with shRNA lentiviruses at an MOI of 1 and incubated for 48 h prior to selection with 1 µg/mL puromycin for four days. Selected cells were harvested for protein assay or replated at 1×10^6 cells per 25 cm² flask for DENV2 infection (MOI = 1) for 24 h.

Table 4.2 shRNA sequences.

Gene	Designation	Sequence
CDK8	TRCN000000489	CCGGATGTCCAGTAGCCAAGTTCCACTCGAGTGGAACTTGGCTACTGGACATTTTTT
CDK19	TRCN0000195069	CCGGAGGACTGATAGCTCTTCTTTACTCGAGTAAAGAAGAGCTATCAGTCCTTTTTT
Cyclin C	TRCN0000020189	CCGGGCATCCAAAGTAGAGGAATTTCTCGAGAAATTCCTCTACTTTGGATGCTTTTTT
Nontarget	SHC002	CCGGCAACAAGATGAAGAGCACCAACTCGAGTTGGTGCTCTTCATCTTGTTGTTTTT

4.3f Subcellular Extracts and Protein Analysis

Nuclear extracts were prepared as previously described (Brewster et al., 2011). Briefly, cells were lysed in 0.5% NP-40 in PBS with protease and phosphatase inhibitors (2 µg/mL leupeptin and aprotinin, 1 µg/mL pepstatin, 0.2 mM phenylmethylsulfonyl fluoride [PMSF], 0.2 mM sodium orthovanadate, 2 mM sodium pyrophosphate, and 1 mM glycerophosphate). Nuclei were pelleted at 1500 x g, washed with cold PBS, and then, with buffer A (10 mM HEPES pH 8.0, 10 mM KCl, 1.5 mM MgCl₂, 0.5 mM dithiothreitol (DTT)), prior to extraction overnight with 2.5 nuclear pellet volume buffer C (10 mM HEPES pH8.0, 420 mM KCl, 20% glycerol, 0.1 mM EDTA, 0.5 mM DTT, and protease and phosphatase inhibitors). Extracted nuclei were pelleted for 15 min at 21,000 x g and re-extracted with 1 pellet volume buffer C. Extracts were pooled for analysis. Remaining chromatin-bound proteins were prepared from extracted nuclear pellets after an additional wash with buffer C and equilibration in DNase digestion buffer (100 mM Tris HCl, pH 7.5, 25 mM MgCl₂, and 5 mM CaCl₂) prior to addition of digestion buffer with 1 Unit DNase I /µL and rotation at 4 °C for 72–96 h. Digested chromatin preparations were clarified at 21,000 x g for 15 min.

Mitochondrial extracts were prepared as previously described (Clayton and Shadel, 2014). Briefly, cells were swelled in cold hypotonic buffer (10 mM NaCl, 1.5 mM MgCl₂, 10 mM Tris-HCl pH7.5) and broken in a Dounce homogenizer. Lysates were brought to 210 mM mannitol, 70 mM sucrose, 5 mM Tris-HCl (pH 7.5) and 1 mM EDTA with 2.5X homogenization buffer. Nuclei were removed by centrifugation at 1300 × g for 5 min, and then, mitochondria were pelleted at 15,000 x g for 15 min, washed once in

homogenization buffer and suspended in immunoprecipitation (IP) buffer (1% Triton X-100, 0.5% NP-40, 150 mM NaCl, 10 mM Tris-HCl (pH 7.5), 1 mM EDTA (pH 8.0), 1 mM EGTA, and protease and phosphatase inhibitors).

Protein concentration of each extract was determined with a Pierce BCA protein assay kit (Thermo Fisher Scientific, Waltham, MA, USA) according to the manufacturer's instructions. Equal quantities of total protein were separated by polyacrylamide gel electrophoresis for western blot. Blocked blot segments, separated by molecular weight range, were probed simultaneously with indicated primary antibodies (Tables 4.3 and 4.4) overnight. Antibodies were detected with appropriate horseradish peroxidase-conjugated secondary antibodies and developed with the TMB membrane peroxidase substrate system (3,3',5,5'-Tetramethylbenzidine, KPL). Images were scanned with a Visioneer One Touch 9420 scanner at a gamma value of 1.0, and all contrast adjustments were uniformly applied using Adobe Photoshop. High contrast images were measured using NIH ImageJ gel analysis software to determine band densities.

Table 4.3 Cell Protein Antibodies.

Antibody	Source	Catalog #
Rabbit anti β Actin	Cell Signaling	#4967
Goat anti CDK8	Santa Cruz Biotechnology	sc 1521
Rabbit anti Cyclin C	Novus Biologicals	#NB1202950
Mouse anti Cytochrome C oxidase subunit IV	Molecular Probes	#A21347
Mouse anti Phospho Histone H3 (Ser10)	Cell Signaling	#9706
Rabbit anti Histone H3	Cell Signaling	#9715
Rabbit anti Hexokinase 2	Proteintech	AP#22029
Rabbit anti LC3B	Novus Biologicals	#NBP246892SS

Table 4.4 Virus Protein Antibodies.

Antibody	Source	Catalog #
Mouse anti Flavivirus group antigen protein E, Clone 4G2	Novus Biologicals	#NBP252079
Mouse anti DENV2 NS5 protein	GeneTex	#GTX629447
Rabbit anti DENV capsid protein	GeneTex	#GTX103343
Rabbit anti DENV prM protein	GeneTex	#GTX128093
Mouse anti DENV NS3 protein	GeneTex	#GTX124252

4.3g Mitochondrial and Glycolytic Stress Tests

A Seahorse XFe analyzer (Agilent Technologies, Santa Clara, CA, USA) was used to measure the oxygen consumption rate (OCR) and extracellular acidification rate (ECAR) based on the mitochondrial stress test (Agilent 103015-100) and glycolysis stress test (Agilent 103020-100), respectively. Huh7 cells were plated in XF96 cell culture microplates at 2×10^4 cells per well 16 h prior to infection with DENV2 at an MOI of 10. At 24 or 48 hpi, the culture media were replaced with 180 μ L of XF base medium (Agilent Technologies, Santa Clara, CA, USA) supplemented with 1 mM pyruvate, 2 mM L-glutamine, and with 10 mM glucose for the mitochondrial stress test or without glucose for the glycolysis stress test. The cells were rested for one hour in a non-CO₂ incubator at 37 C, then placed in the Seahorse for analysis. The mitochondrial stress test used sequential injections of oligomycin (1 μ M), p-trifluoromethoxyphenylhydrazine (FCCP, 1.5 μ M), and rotenone and antimycin A (0.5 μ M each). The glycolysis stress test used sequential injections of glucose (10 mM), oligomycin (1 μ M), and 2-

deoxyglucose (50 mM). Measurements were collected at 5-minute intervals; three times before and after injections and six times after the last injection. After analysis, cell numbers were measured by addition of 22 μ L 10 nM Calcein-AM to all wells and absorption read at 520 nm after excitation at 488 nm in a SpectraMax M2e plate reader (Molecular Devices, San Jose, CA, USA). Calcein readings were imported into Wave (Agilent Technologies, Santa Clara, CA, USA) software to normalize OCR and ECAR readings.

Mitochondrial activity was determined as follows: (1) Basal respiration was calculated using the last rate measurement before injection of oligomycin minus the non-mitochondrial respiration rate (defined as the minimum rate measurement after rotenone/antimycin A injection), (2) ATP production was calculated as the last rate measurement before oligomycin injection minus the minimum rate measurement after oligomycin injection, (3) Maximum respiration was calculated using the maximum rate measurement after FCCP injection minus non-mitochondrial rate, (4) Spare capacity was the maximal respiration minus basal respiration, and (5) Proton leak was the minimum rate measurement after oligomycin injection minus non-mitochondrial respiration. Glycolytic function was determined as follows: (1) Glycolysis was the maximum rate measurement before oligomycin injection minus the last rate of measurement before glucose injection, (2) Glycolytic capacity was the maximum rate measurement after oligomycin injection minus the last rate of measurement before glucose injection, (3) Glycolytic reserve was the glycolytic capacity minus glycolysis and (4) Non-glycolytic acidification was the last rate measurement prior to glucose injection.

4.3h Statistics

Statistical analysis was performed on Prism software (Version 8.1.2 (227)).

4.4 Results

4.4a Cyclin-dependent Kinase 8 Is Upregulated during DENV2 Infection

To investigate the role of CDK8 during DENV2 replication, we quantified CDK8 mRNA over time after synchronized infection with a high multiplicity of infection (MOI) to reach complete or near-complete infection of all cells in the culture and mitigate effects from uninfected bystander cells. Huh7 cells were mock-infected, infected at an MOI of 10, or treated with a matched preparation of UV-inactivated DENV2 particles (UV-DENV2). After binding at 4 C, cells were washed and incubated in media at 37 C. Total RNA was harvested at 0, 3, 6, 9, 12, 24 and 48 h post infection (hpi) and virus replication was monitored by qRT-PCR (Figure 4.1A).

We observed a modest increase in CDK8 mRNA levels in infected cells at 3 hpi followed by a steady rise after 12 hpi, coincident with maximal virus replication (Figure 4.1A, 4.1B). We saw the sharpest increase in CDK8 mRNA expression between 24 and 48 hpi in DENV2-infected cells relative to mock-infected cells and cells treated with UV-inactivated virus (Figure 4.1B), and subsequently observed a 2.3-fold increase in CDK8 mRNA levels at 36 hpi in six biological replicates (Figure 4.1C; mean = 2.30 +/- 0.09, $p < 0.0001$). A 2.3-fold increase in CDK8, while modest, may have a profound

reprogramming effect on the host cell due to the cascading nature of CDK8-mediated transcriptional regulation.

Viral RNA from cells treated with UV-DENV2 was taken up by cells (Figure 4.1A) but did not result in viral RNA replication or increased expression of CDK8 (Figure 4.1B), demonstrating that the induction of CDK8 expression is dependent upon uptake of infectious DENV2. In contrast to the increase in CDK8 expression, we found no significant change in CDK19 mRNA expression (Figure 4.1D), suggesting a specific demand for increased CDK8 during DENV2 infection. CDK8 and its paralog CDK19 are highly conserved in their kinase and cyclin-binding domains, but have unique C-terminal domains, suggesting similar but divergent functions (Fant and Taatjes, 2019; Steinparzer et al., 2019).

CDK8 protein levels were also increased in DENV2-infected cells compared to the start of infection (Figure 4.1E). Increased CDK8 was visible in nuclear extracts at 3 hpi, coincident with the first appearance of DENV2 nonstructural protein 5 (NS5) in the nuclei of infected cells (Figure 4.1E). Apparent CDK8 levels in the soluble nuclear fraction remained elevated, relative to Cyclin C, throughout the course of infection and were coincident with a progressive increase in the phosphorylated form of a known CDK8 substrate, H3S10-P (Galbraith et al., 2010; Meyer et al., 2008) relative to total histone H3 (Figure 4.1E). In addition to increased CDK8 in the salt-soluble nuclear fraction, CDK8 in the remaining chromatin fraction began to increase after 6 hpi (Figure 4.1E, see methods for details). Increased chromatin-bound CDK8 was also coincident with increasing NS5 levels in the chromatin fraction. The partition of DENV2 NS5 protein between soluble nuclear and chromatin fractions has been observed previously

(De Maio et al., 2016; Hannemann et al., 2013; Kumar et al., 2013; Tay et al., 2013).

There was also an apparent increase in H3S10-P, relative to H3 levels, in the chromatin fraction (Figure 4.1E). H3S10-P is a mark of active, open chromatin (Galbraith et al., 2010; Meyer et al., 2008).

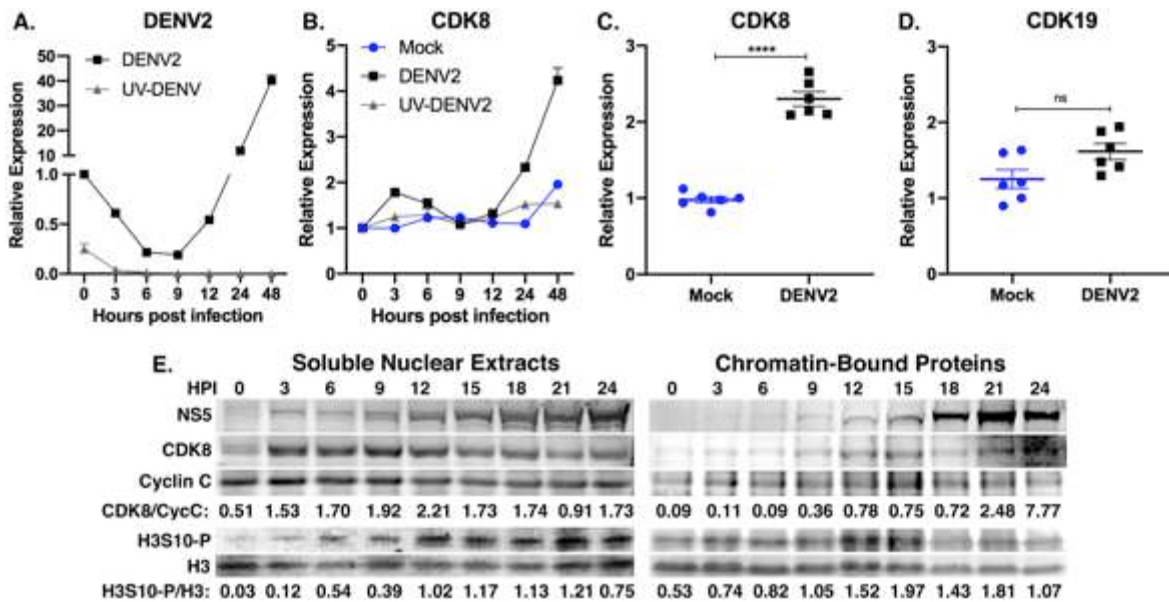


Figure 4.1 CDK8 is upregulated during DENV2 infection. (A,B) Huh7 cells were either mock-infected, infected with DENV2 at MOI 10, or treated with equivalent UV-inactivated DENV2 (UV-DENV) over a time course of 48 h. Total cellular RNA was collected at indicated time points after infection and analyzed by qRT-PCR for DENV RNA (A), and CDK8 mRNA expression (B), relative to the time of infection and normalized to the housekeeping gene, *SDHA*. Results are representative of two independent experiments. (C–D) CDK8 (C) and CDK19 (D) mRNA expression in mock or DENV-infected Huh7 cells after 36 h of infection at MOI 10 (n = 6 biological replicates; **** p < 0.0001 unpaired, two-tailed t test). Error bars represent mean +/- SEM). (E) Western blot analyses of 10 µg of total protein from nuclear extracts (Soluble Nuclear Extracts) and from the remaining, salt-extracted chromatin fraction (Chromatin-Bound Proteins) from cells collected every three hours for 24 h after infection. Antibody specificities are indicated as are the relative band densities of CDK8 versus Cyclin C and histone H3 phosphorylated at serine in position 10 (H3S10-P) versus total histone H3 (H3). Infection was confirmed by presence of nuclear DENV2 NS5. The results are representative of three separate time-course infections.

These data demonstrate that CDK8 mRNA and protein levels increase after DENV2 infection and suggest active CDK8 phosphorylation of histone H3 at serine 10 in

association with increased transcriptional activity. CDK8 chromatin occupancy is also increased during DENV2 infection, an outcome associated with enhanced CDK8-dependent gene expression (Birkenheuer et al., 2015; Donner et al., 2010; Galbraith et al., 2013; Rovnak et al., 2012).

4.4b Knockdowns of CDK8 and CDK19 Reduce DENV2 Replication

To investigate the roles of CDK8 and CDK19 during DENV2 infection, we utilized lentivirus-mediated shRNA knockdowns of CDK8, CDK19, and their activating cyclin, Cyclin C, in Huh7 cells (Figure 4.2A). Huh7 cells were transduced with non-target-shRNA (NT-shRNA) or CDK8-shRNA, selected in puromycin for four days, and then, mock-infected or infected with DENV2. For the purpose of evaluating changes in efficiency of viral replication and transmission within the cell culture, we elected to use an MOI of 1 and quantitated DENV2 genome equivalents (GE) and DENV2 RNA relative to housekeeping gene transcripts in infected cells. Knockdown of CDK8 reduced DENV2 replication 8.5-fold when compared to NT-shRNA controls (NT-shRNA mean = $4.4 \pm 0.9 \times 10^6$ GE vs. CDK8-shRNA mean = $5.2 \pm 0.3 \times 10^5$ GE, $p = 0.002$), and CDK19 knockdown reduced replication 10.5-fold (CDK19-shRNA mean = $4.2 \pm 0.8 \times 10^5$ GE, $p = 0.002$) (Figure 4.2B).

Knockdown of either CDK8 or CDK19 has previously been shown to reduce the proliferation rate of cultured cells (Audetat et al., 2017; Birkenheuer et al., 2015; Firestein et al., 2008) and we observed reduced proliferation of CDK8 and CDK19 knockdowns, compared to NT-shRNA control cells (Figure 4.2C), so we normalized

DENV2 RNA expression to a housekeeping gene to correct for reduced cell numbers.

There was a significant decrease in DENV2 RNA in CDK8 and CDK19 knockdown cells relative to cellular RNA (Figure 4.2D). Knockdown of Cyclin C (CycC-shRNA)

expression (Figure 4.2A), which activates both CDKs and is a proxy for CDK8/19

knockdown (Bancerek et al., 2013) did not affect cell numbers but did reduce DENV2

replication 3.3-fold (NT-shRNA mean = $4.4 \pm 0.9 \times 10^6$ GE vs. CycC-shRNA mean = $1.3 \pm 0.2 \times 10^6$ GE, $p = 0.009$) (Figure 4.2B-D).

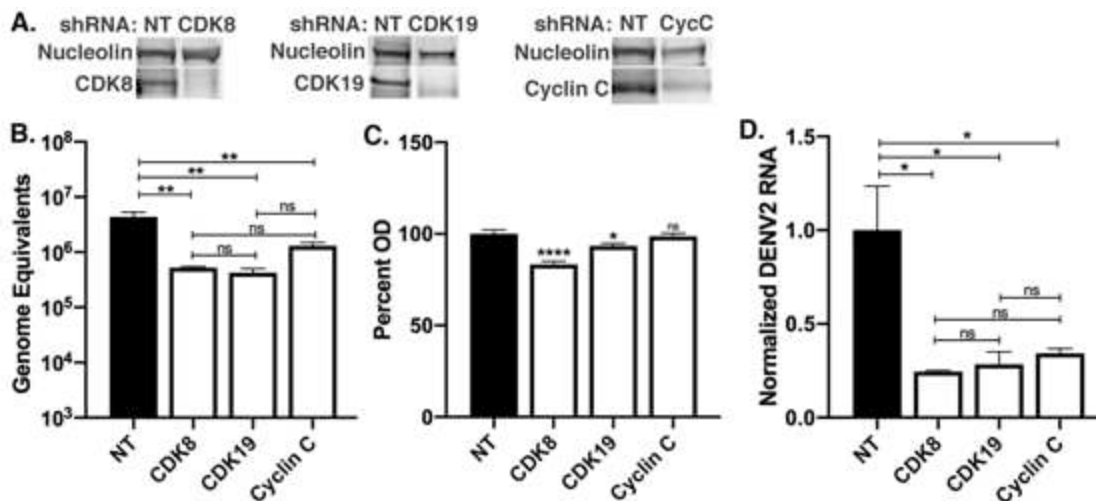


Figure 4.2 Knockdowns of CDK8 and CDK19 reduce DENV2 replication. (A) Western blot analysis of 10 µg of total protein from nuclear extracts of Huh7 cells transduced at an MOI of 1 with lentivirus-mediated non-target control or CDK8-targeted shRNA, CDK19-targeted shRNA, or cyclin C-targeted shRNA. (B) Lentivirus-transduced Huh7 cells were infected with DENV2 at MOI 1 for 24 h, and total cellular RNA analyzed by qRT-PCR for DENV RNA quantification relative to in vitro transcribed DENV genome equivalent (GE) standard curve (n = 3 biological replicates per group; ** p < 0.01; one-way ANOVA with Tukey's multiple comparisons test. Error bars represent mean ± SEM). (C) Relative optical density read in lentivirus-transduced Huh7 cells after four days of selection, then treated with CellTiter 96 Aqueous One Solution. (n = 4 biological replicates. * p < 0.05, **** p < 0.0001; one-way ANOVA with Dunnett's test. Error bars represent mean ± SEM). (D) Lentivirus-transduced Huh7 cells were infected with DENV2 at MOI 1 for 24 h, and total cellular RNA analyzed by qRT-PCR for DENV RNA quantification normalized to the housekeeping gene, SDHA, and relative to expression in non-target controls (n = 3 biological replicates per group; * p < 0.05, one-way ANOVA with Tukey's multiple comparisons test. Error bars represent mean ± SEM).

4.4c CDK8/19 Chemical Inhibition Reduces DENV2 Replication

To better study CDK8 and CDK19 function during DENV2 infection, we utilized a small-molecule CDK8/19 active site inhibitor, Senexin A (Porter et al., 2012). The use of Senexin A does not distinguish CDK8 and CDK19 activities, as their active sites are identical, but Senexin A treatment can be administered exclusively during infection without prior treatment or selection and did not negatively affect Huh7 cell proliferation at the concentrations used in this study (12–25 μM) (Figure 4.3A). Senexin inhibition of CDK8/19, in contrast to knockdowns, exclusively inhibits kinase activity rather than eliminating both kinase- and structure-related functions of CDK8/19 (Porter et al., 2012; Steinparzer et al., 2019). We verified Senexin A inhibition of CDK8 function by inhibiting expression of a known CDK8-dependent serum response gene, *EGR1* (Birkenheuer et al., 2015; Donner et al., 2010) (Figure 4.3B). Cells which were serum-starved and subsequently serum-repleted exhibited the characteristic induction of *EGR1*, while cells treated with Senexin A did not significantly induce *EGR1* expression in response to serum (Figure 4.3B).

Huh7 cells were treated with dimethyl sulfoxide (DMSO) or Senexin A solubilized in DMSO at the start of synchronized infections, and virus replication was assessed at 24 hpi (after one round of virus replication) (Figure 4.3C) and at 36 hpi (coincident with significantly increased CDK8 expression, Figures 4.1C and 4.3D). At 24 hpi, 12 μM Senexin A reduced intracellular virus RNAs 2.7-fold compared to DMSO controls (DMSO mean = $4.1 \pm 0.5 \times 10^5$ GE vs. Senexin A mean = $1.5 \pm 0.2 \times 10^5$ GE, $p = 0.008$) (Figure 4.3C). Senexin A treatment also reduced extracellular virus RNAs 3.2-

fold (DMSO mean = $2.2 \pm 0.5 \times 10^5$ GE vs. Senexin A mean = $6.8 \pm 1.4 \times 10^4$ GE, $p = 0.04$) and infectious virus particles by 8.9-fold (DMSO = $1.9 \pm 0.2 \times 10^4$ PFU/mL vs. Senexin A mean = $2.1 \pm 1.0 \times 10^3$ PFU/mL, $p = 0.0015$) (Figure 4.3C). At 36 h hpi, 25 μ M Senexin A reduced DENV2 intracellular virus RNAs 1.9-fold (DMSO, 1.5×10^6 GE vs. Senexin A, 7.8×10^5 GE), extracellular RNAs by 3.8-fold (DMSO, 1.6×10^6 GE vs. Senexin A, 4.2×10^5 GE) and PFU/mL by 6.8-fold (DMSO, 4.0×10^4 vs. Senexin A, 5.9×10^3) (Figure 4.3C).

We analyzed the viral proteins in Senexin A-treated cells by western blot (Figure 4.3D). Cell-free virus particles, pelleted from equal volumes of infected-cell supernatants, showed reduction in envelope protein, E, prM and capsid levels (Figure 4.3D). Although levels of capsid protein were outside of the linear range of the western analysis, the relative band densities of E at 24 and 48 hpi and of prM at 24 hpi in supernatants from Senexin A-treated cells have approximately 15% of the protein in the untreated cells. The results from Senexin A inhibition of CDK8/19 during DENV2 infection indicate a significant deficit in the synthesis of viral RNA and in the production and packaging of infectious viral particles.

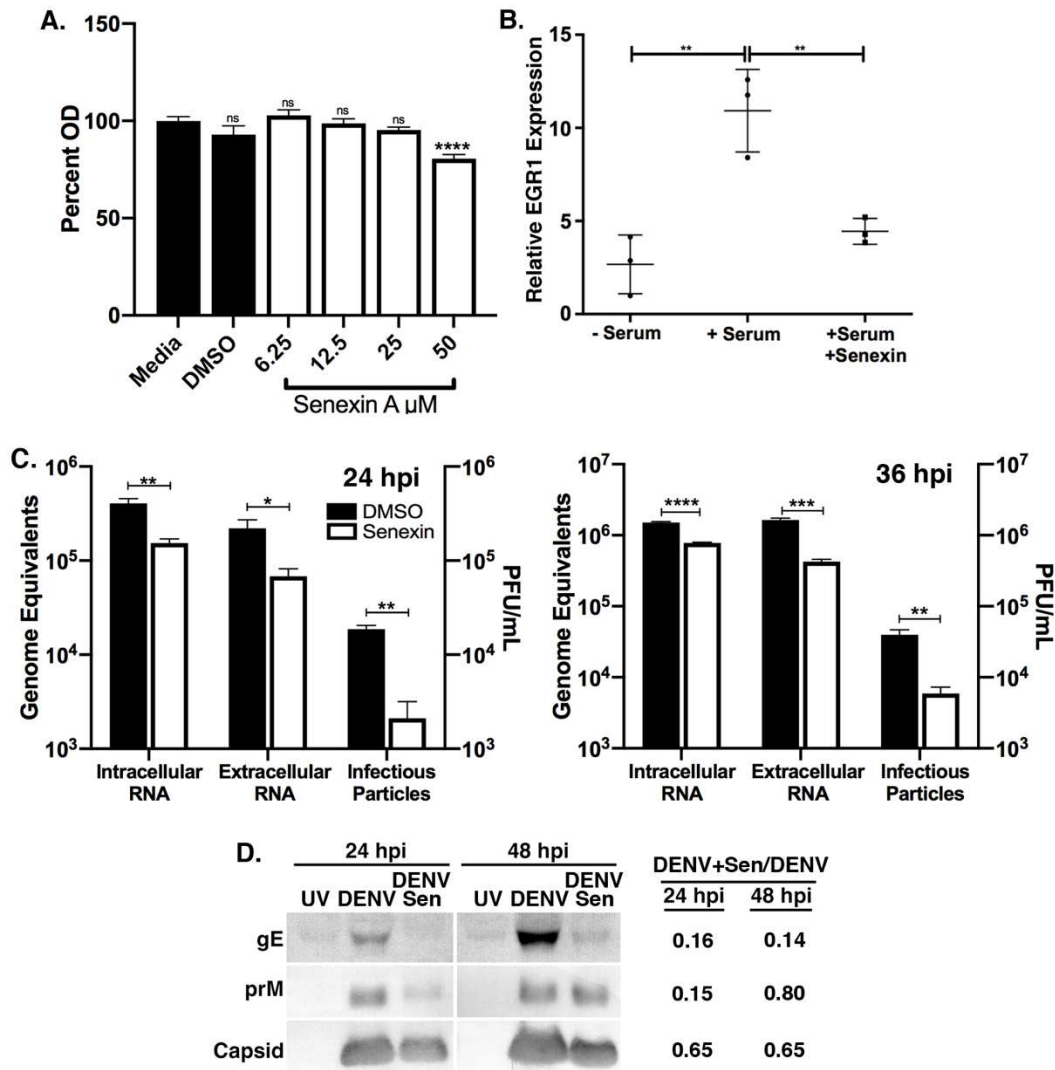


Figure 4.3 CDK8/19 Chemical inhibition reduces DENV2 replication. (A) Relative optical density of Huh7 cells after 72 h treatment with DMSO or Senexin A at indicated doses and addition of CellTiter 96 Aqueous One Solution. (n = 9 biological replicates. **** p < 0.0001 one-way ANOVA with Dunnett's test. Error bars represent mean +/- SEM). (B) EGR1 mRNA levels in serum-starved and serum-stimulated Huh7 cells in the presence of DMSO or 12 μ M Senexin A (n = 3 biological replicates; * p < 0.05, **** p < 0.0001 one-way ANOVA with Dunnett's test; error bars represent mean +/- SEM). (C) DENV2 RNAs in total cellular RNA preparations (Intracellular RNA, GE) and in culture supernatants (Extracellular RNA, GE) were determined by qRT-PCR, and supernatant virus measured by plaque assay (Infectious Particles). Huh7 cells were infected with DENV2 (MOI = 1) for 24 or 36 hpi with DMSO or 12 or 25 μ M Senexin A, respectively (n = 3 biological replicates; * p < 0.05, ** p < 0.01, *** p < 0.001, **** p < 0.0001; unpaired two-tailed t test; Error bars represent mean +/- SEM). (D) Western blot assays of supernatant virus pellets from cells infected with 10 MOI UV-treated DENV2 (UV), or with DENV2 without (DENV) or with 25 μ M Senexin A (DENV/Sen) at 24 and 48 hpi. Antibody specificities are indicated. Relative band densities of DENV2 gE, prM, and

capsid proteins in DENV2-infected, Senexin A-treated versus DENV2-infected virus preparations are indicated to the right of the indicated panels. Results are representative of three biological replicates for each time point.

4.4d Metabolic Gene Expression Is Dependent on CDK8/19 Kinase Activity

CDK8 kinase activity has been shown to control the transcription of select glycolytic genes (Galbraith et al., 2017). We investigated the role of CDK8 and CDK19 as regulators of the metabolic pathways that are induced during DENV2 infection. The early steps in glycolysis are critical for production of metabolites that support DENV2 replication and are marked by an increase in glucose uptake and increased expression of the first rate-limiting enzyme in glycolysis, HK2 (Fernandes-Siqueira et al., 2018; Fontaine et al., 2015). We measured HK2 mRNA expression during the time course of synchronized DENV2 infections and confirmed that it is upregulated compared to mock-infected cells and cells infected with equivalent UV-inactivated DENV2 (Figure 4.4A). Increased HK2 mRNA levels were detected after 12 hpi, coincident with maximal virus RNA replication and with increased CDK8 mRNA expression (Figure 4.1 A–C). HK2 mRNA levels were increased 3.68-fold (± 0.38 , $n = 7$) in DENV-infected Huh7 cells at 48 hpi (Figure 4.4B).

We assessed the impact of Senexin A on HK2 expression during synchronized DENV2 infections and observed inhibition of the virus-induced HK2 expression but not of basal HK2 expression. Senexin A did not entirely block HK2 induction by infection but did reduce it (2.88 ± 0.21 -fold increase over mock vs. a 5.10 ± 0.49 -fold increase in DMSO-treated infected cells; Figure 4.4C). Mock-infected cells showed no difference in HK2 expression with or without Senexin A treatment (Figure 4.4C). While conducting

these experiments, we obtained a second generation CDK8/19 inhibitor, Senexin B (McDermott et al., 2017) and confirmed a similar 2.1-fold reduction in DENV2 genome equivalents with Senexin B treatment as we observed with Senexin A (DMSO GE mean = $6.7 \pm 1.0 \times 10^7$, Senexin B GE mean = $3.2 \pm 0.7 \times 10^7$). As with Senexin A treatment, Senexin B inhibited the induction of HK2 during DENV2 infection, while basal expression of HK2 was unaffected (Figure 4.4C, right panel; DMSO mean fold change over mock: 4.64 ± 0.45 , Senexin B: 3.22 ± 0.45).

In addition to HK2, we evaluated mRNA levels of four other glycolytic genes which have been shown to be responsive to CDK8 function: phosphofructokinase (PFK), glyceraldehyde 3-phosphate dehydrogenase (GAPDH), enolase isoform 1 (ENO1), and pyruvate kinase isoform M2 (PKM2) (Galbraith et al., 2017). Expression of these four genes was not upregulated during DENV2 infection of Huh7 cells (data not shown). This is in line with previous work demonstrating an anapleurotic role for HK2 in the production of metabolic intermediates rather than an ATP-producing role (Fernandes-Siqueira et al., 2018; Fontaine et al., 2015).

HK2 localizes to the outer mitochondrial membrane, where it functions in the regulation of glucose metabolism, protection from apoptosis, and initiation of autophagy (Ahn et al., 2009; Fontaine et al., 2015; John et al., 2011; Roberts and Miyamoto, 2015). We prepared mitochondria-enriched fractions (Clayton and Shadel, 2014) which are also known to be enriched in viral replication complexes and DENV2 proteins (Barbier et al., 2017). We observed increased HK2, relative to levels of a mitochondrial marker protein, cytochrome c oxidase subunit 4 (Cox4), in preparations from DENV2-infected cells compared to mock and UV-DENV2-treated cells, and Senexin A treatment reduced

HK2 abundance to levels in uninfected cells (Figure 4.4D). Senexin A treatment also reduced the apparent levels of NS5 and prM in these preparations to 21% of levels in DENV2-infected cell preparations (Figure 4.4D). Cox4 protein levels were apparently unaffected by Senexin treatment.

Overall, these data indicate that Senexin inhibition of CDK8/19 kinase activity specifically reduces virus-induced but not basal levels of HK2 mRNA and protein expression, and that the expression of the host protein Cox4 is unaffected by both DENV2 infection and by Senexin A treatment.

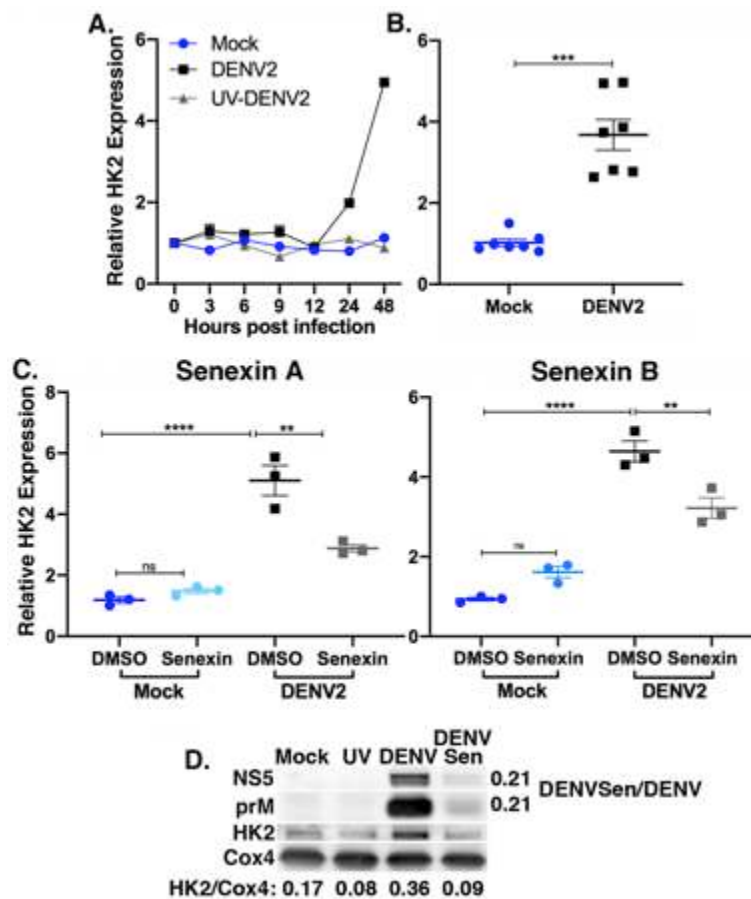


Figure 4.4 Senexin A reduces DENV2 induction of hexokinase 2 expression. (A) Huh7 cells were either mock-infected or infected with DENV2 at MOI 10, and HK2 mRNA expression analyzed by qRT-PCR at indicated time points. Results are representative of two independent experiments. Expression is relative to time of infection and normalized to SDHA. (B) HK2 expression in mock vs. infected cells at 48 hpi (n = 7 biological

replicates; *** $p < 0.001$ unpaired, two-tailed t test with Welch's correction). Error bars represent mean \pm SEM. (C) HK2 mRNA expression in mock-infected and infected Huh7 cells treated with DMSO or 25 μ M Senexin A or 12 μ M Senexin B added at start of infection (MOI 10; 36 hpi). Expression relative to mock-infected, DMSO-treated cells and normalized to SDHA ($n = 3$ biological replicates; ** $p < 0.01$, **** $p < 0.0001$; one-way ANOVA with Tukey's multiple comparisons test). Error bars represent mean \pm SEM. (D) Western blot analysis of cellular and viral protein abundance in 2 μ g mitochondrial-enriched fractions from mock-infected cells (Mock), or cells with 10 MOI UV-treated DENV2 (UV) or DENV2 without (DENV) or with or 25 μ M Senexin A (DENV/Sen). Antibody specificities are indicated as are the relative band densities of HK2 versus Cox4. Relative band densities of DENV2 NS5 and prM proteins in Senexin A-treated versus DMSO-treated, DENV2-infected cell preparations are indicated to the right of the indicated panels. Results are representative of six biological replicates.

4.4e Senexin A Reduces Induction of Lipophagic Gene Expression

In addition to changes in glucose utilization, DENV2 induces lipophagy, the autophagic depletion of lipid droplets for release of free fatty acids to support a metabolic shift to β -oxidation (Heaton and Randall, 2010). LC3 functions in the formation of the autophagosomal membrane on lipid droplets (Singh et al., 2009). LC3 is initially modified to LC3-I by the autophagy factor Atg4, and subsequently modified to the membrane-associated, lipidated form, LC3-II, by autophagy factors Atg3 and Atg7 (Martinez-Lopez and Singh, 2015). Conversion of LC3-I to LC3-II is considered a measure of autophagic activity (Martinez-Lopez and Singh, 2015; Singh et al., 2009), and increased conversion of LC3-I to LC3-II has been observed during DENV2 infection (Lee et al., 2008; Zhang et al., 2018).

We found that the level of LC3 mRNA increased over the course of DENV2 infection coincident with the increases in CDK8 and HK2 (Figures 4.1, 4.4 and 4.5A). LC3 mRNA levels increased 5.6 ± 0.2 -fold ($p < 0.0001$) in DENV2-infected versus mock-infected cells at 48 hpi (Figure 4.5B). As with HK2 (Figure 4.4), the viral induction of LC3 mRNA

expression was significantly reduced in cells treated with Senexin A (DMSO mean fold change over mock: 6.02 ± 0.31 , Senexin A: 3.04 ± 0.26) and with Senexin B (DMSO mean fold change over mock: 6.25 ± 1.70 , Senexin B: 2.41 ± 0.38) (Figure 4.5C). In addition, as observed with HK2 expression, basal LC3 expression was not inhibited by CDK8/19 inhibition. Senexin A, but not Senexin B, actually induced a modest increase in LC3 expression in mock-infected cells (Figure 4.5C).

Western blot analyses of cytoplasmic extracts demonstrated a consistent increase in lipidated LC3-II in DENV2-infected cells compared to mock-infected or UV-DENV2-treated cells, relative to β -actin levels (Figure 4.5D). Senexin A treatment reduced levels of lipidated LC3-II by half (Figure 4.5D). As observed previously, Senexin A treatment also reduced virus protein levels in cellular extracts. In this case, NS3 was 61% and prM 31% of that observed in untreated, DENV2-infected cells. Levels of host actin protein remained unaffected by treatment with Senexin A.

Overall, these data indicate that Senexin inhibition of CDK8 and CDK19 kinase activity specifically reduces infection-induced but not basal levels of LC3 gene expression, and that the expression of host proteins Cox4 (Figure 4.4D) and actin (Figure 4.5D) is unaffected by both DENV2 infection and by Senexin treatment.

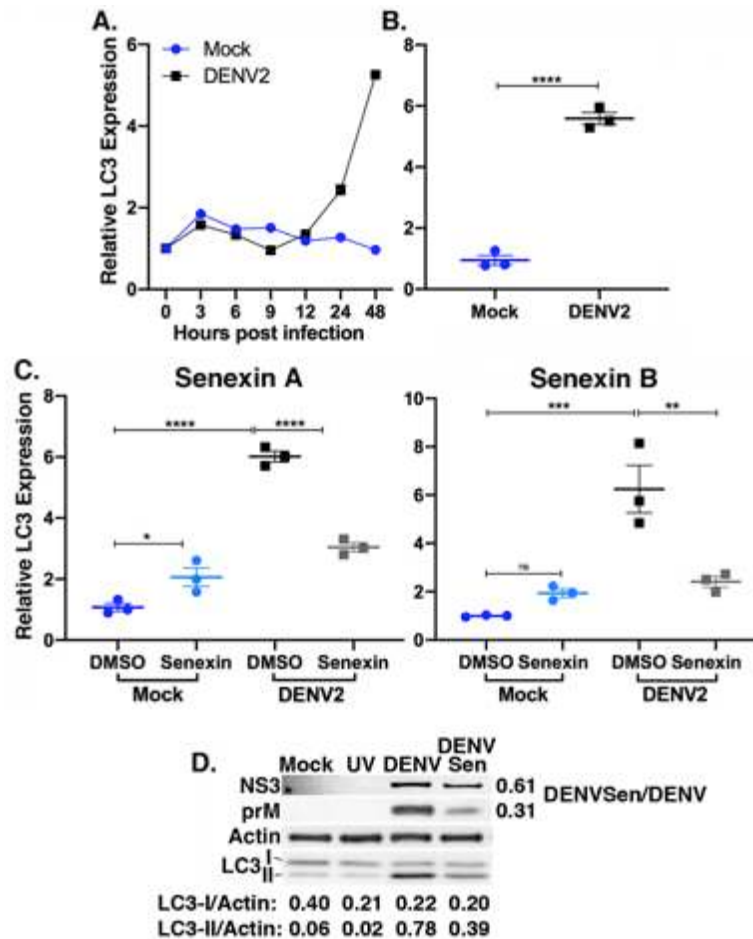


Figure 4.5 Senexin A reduces DENV2 induction of lipophagic gene expression. (A) Huh7 cells were either mock-infected or infected with DENV at MOI 10, and LC3 mRNA expression analyzed by qRT-PCR at indicated time points. Expression relative to time of infection, normalized to *SDHA* and representative of two independent time course experiments. (B) LC3 expression in mock vs. infected cells at 48 hpi (n = 3 biological replicates; *** p < 0.001 unpaired, two-tailed t test with Welch's correction). Error bars represent mean \pm SEM. (C) LC3 mRNA expression in Huh7 cells mock-infected or infected with DENV2 at MOI 10 for 36 h with DMSO or 25 μ M Senexin A or 12 μ M Senexin B added at time of infection (relative to mock-infected, DMSO-treated cells and normalized to *SDHA*; n = 3 biological replicates. ** p < 0.01, *** p < 0.001, **** p < 0.0001; one-way ANOVA with Tukey's multiple comparisons test). Error bars represent mean \pm SEM. (D) Western blot analysis of cellular and viral protein abundance in 2 μ g cytoplasmic extracts from mock-infected cells (Mock), or cells with 10 MOI UV-treated DENV2 (UV) or DENV2 without (DENV) or with or 25 μ M Senexin A (DENV/Sen). Antibody specificities are indicated as are the relative band densities of LC3-I and LC3-II versus *Cox4*. Relative band densities of DENV2 NS3 and prM proteins in Senexin A-treated versus DMSO-treated, DENV2-infected cell preparations are indicated to the right of the indicated panels. Results are representative of six biological replicates.

4.4f Senexin A Inhibits Mitochondrial Respiration

We directly tested the downstream consequences of DENV2 infection and CDK8/19 inhibition by measuring metabolic flux in mock- and DENV2-infected Huh7 cells with and without Senexin A treatment. We used a Seahorse XF metabolic flux analyzer to measure the rates of mitochondrial respiration as indicated by oxygen consumption rate (OCR) following sequential addition of oligomycin (ATP synthase inhibitor), FCCP (uncoupler of oxidative phosphorylation) and rotenone and antimycin A (electron transport chain complex I and III inhibitors) (Figure 4.6) (see methods for details regarding calculations of parameters).

We first evaluated changes in metabolic capacity in DENV2-infected compared to uninfected Huh7 cells. At 24 hpi, there were no significant differences in rate of oxygen consumption between uninfected and DENV2-infected cells (Figure 4.6A; top panel: measurements over time; bottom panels: quantification, see methods for details regarding time points for quantification). However, at 48 hpi, there were substantial increases in basal respiration, ATP production, maximal respiration, and spare capacity in DENV2-infected cells compared to mock-infected cells (Figure 4.6B; top panel: measurements over time, bottom panels: quantification). Only proton leak and non-mitochondrial respiration were unchanged in DENV2-infected cells. These data are in line with our host gene expression data, supporting an increase in metabolic capacity of DENV2-infected Huh7 cells compared to uninfected cells.

We evaluated differences in oxygen consumption between uninfected and DENV2-infected cells with or without Senexin A treatment to determine if CDK8/19 kinase

activity plays a role in the metabolic changes during DENV2-infection. Senexin A reduced basal respiration and ATP production in mock-infected cells after 24 h, but the differences in other parameters and in DENV2-infected cells were not significant (Figure 4.6A). In contrast, we observed significant changes in metabolic flux with Senexin A treatment at 48 hpi (Figure 4.6B). All the parameters of respiration except proton leak were reduced and there were no longer distinguishable differences between DENV2-infected and uninfected cells (Figure 4.6B). Therefore, extended Senexin A inhibition of CDK8/19, from 24 to 48 h, resulted in a profound suppression of mitochondrial respiration, coincident with reduced metabolic gene expression (Figures 4.4 and 4.5).

We also evaluated changes in glycolysis during DENV2 infection, as increased glucose uptake has been previously reported (Fontaine et al., 2015). If increased glucose uptake in DENV2-infected cells was utilized for ATP production, we would expect to see increased extracellular acidification due to the production of lactic acid. We measured the extracellular acidification rate (ECAR) in uninfected and DENV2-infected cells following sequential addition of glucose, oligomycin (ATP synthase inhibitor) and 2-deoxy-glucose (2-DG) (hexokinase inhibitor) (see methods for details regarding calculations of parameters). As evidenced by diminished ECAR, glycolysis, glycolytic capacity and glycolytic reserve were all significantly reduced by DENV2 infection (Figure 4.6C; left panel: measurements over time, right panels: quantification). This supports the conclusion that glucose metabolism during DENV2 infection does not serve an ATP-producing role, but functions in the production of metabolic intermediates (Fernandes-Siqueira et al., 2018).

We also evaluated Senexin A's effects on glycolytic capacity. Senexin A treatment reduced glycolytic and non-glycolytic capacity in both mock- and DENV2-infected samples (Figure 4.6C). However, unlike mitochondrial respiration, cells infected with DENV2 were able to compensate, modestly, for the effects of Senexin A on glycolysis and glycolytic capacity (Figure 4.6C). Together, these data illustrate the dependence of cellular metabolism on CDK8 and/or CDK19 kinase activity and show that this dependence may be manipulated by DENV2 to support the increased metabolic demands required for efficient viral replication.

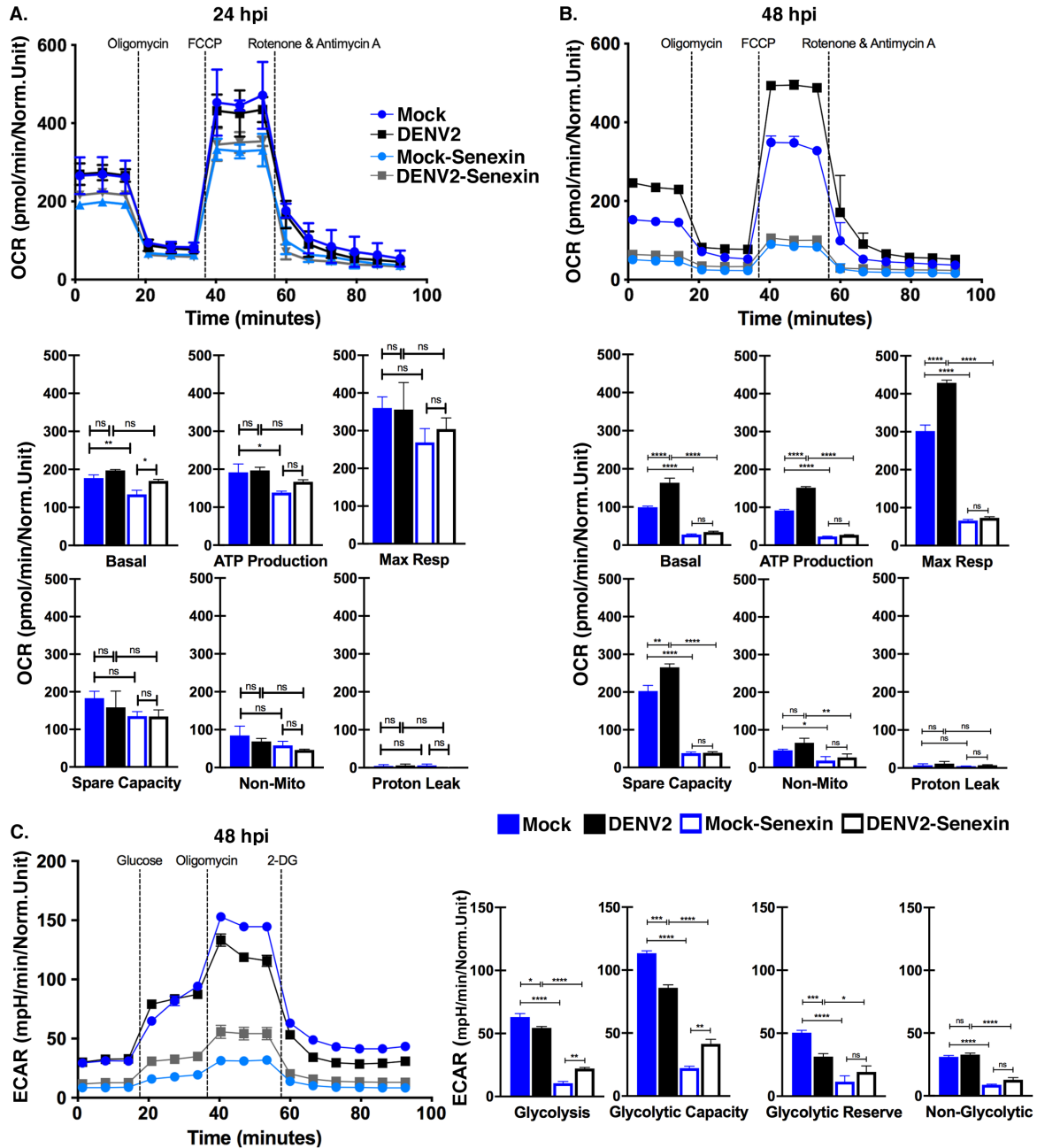


Figure 4.6 Senexin A inhibits mitochondrial respiration. Huh7 cells were either mock-infected or infected with DENV2 at an MOI of 10 with or without DMSO or 12.5 μ M Senexin A for 24 or 48 h. (A,B) Normalized oxygen consumption rate (OCR) was measured over time during mitochondrial stress tests. Specific values determined by the mitochondrial stress test (Basal rate, ATP production, Maximum Respiration, Spare Capacity, Proton Leak, and Non-Mitochondrial Respiration) are presented. (C) Normalized extracellular acidification rate (ECAR) was measured over time during a glucose stress test at 48 hpi. Specific values determined in the glucose stress test (Glycolysis levels, Glycolytic Capacity, Glycolytic Reserve, and Non-Glycolytic Capacity) are presented. Results were normalized to viable cell numbers after metabolic

measurements. Parameters for individual measurements are presented in the methods (* $p < 0.05$, ** $p < 0.01$, *** $p < 0.001$, **** $p < 0.0001$ one-way ANOVA with Tukey's multiple comparisons test. $n = 3$ biological replicates). Error bars represent mean \pm SEM.

4.5 Discussion

Here we show that expression of CDK8, a highly conserved transcriptional regulator, is upregulated during DENV2 infection, suggesting a role for CDK8 in the cellular response to infection. Increased levels of CDK8 are coincident with increased expression of two key metabolic genes, HK2 and LC3, which support DENV2 replication. Manipulation of the host cell environment is critical to support the demands of viral replication, and alterations in metabolism have been the focus of a number of recent papers identifying host factors necessary for DENV replication (Chotiwan et al., 2018; Fernandes-Siqueira et al., 2018; Gullberg et al., 2018; Reid et al., 2018; Rothwell et al., 2009). Autophagy is also a common outcome of flavivirus infection, and lipid droplet metabolism is linked to replication as a source of neutral lipids to meet energy demands, as a source of intermediates for de novo fatty acid synthesis, and as a platform for viral assembly in the case of hepatitis C (Abernathy et al., 2019; Chen et al., 2016; Datan et al., 2016; Heaton and Randall, 2010; Jordan and Randall, 2017; Lee et al., 2008; Martín-Acebes et al., 2015; Martins et al., 2018; Mateo et al., 2013; McLean et al., 2011; Miyanari et al., 2007; Pleet et al., 2018; Randall, 2018; Samsa et al., 2009; Sharma et al., 2014, 2017; Zhang et al., 2018). We show that CDK8/19 kinase activity is required for the altered metabolism observed during DENV2 replication.

We first noted changes in CDK8 mRNA levels during synchronized DENV2 infections but found no significant change in expression of the CDK8 paralog, CDK19 (Figure 4.1). Neither mock-infected or cells with bound, UV-treated DENV2 particles showed increased CDK8, indicating a requirement for virus replication and/or virus protein production. The specific functions of CDK8 remain unclear, but likely include expression of the transcription factors that activate expression of HK2 and LC3 and other proteins that support virus replication.

We used lentivirus-mediated shRNA CDK8 and CDK19 knockdowns to distinguish roles for these transcription cofactors during DENV2 infection and found that both are necessary for robust virus replication (Figure 4.2). However, only CDK8 expression was significantly upregulated during DENV2 infection. This suggests only that CDK19 levels do not need to be increased to support DENV2 replication, as opposed to the clear association of infection with increased CDK8. Basal levels of CDK19 may be sufficient for replication, and the effect of CDK19 knockdown indicates that it does have a supportive role in DENV2 infection. Such a role may include function independent of its kinase activity (Audetat et al., 2017; Fant and Taatjes, 2019; Steinparzer et al., 2019). Further investigation into unique kinase-dependent and kinase-independent roles for CDK8 and CDK19 during DENV2 infection is warranted and will provide insight into functional differences between these two mediator kinases.

Chemical inhibition of CDK8 and CDK19 with the small-molecule inhibitor Senexin A reduced viral genome replication and infectious particle formation (Figure 4.3). CDK8/19 chemical inhibition also reduced the expression of HK2 and LC3 in infected cells to near mock-infected levels (Figures 4.4 and 4.5). As expected, the outcome of the Senexin A

block of HK2 and LC3 induction in DENV2-infected cells was loss of the increased mitochondrial respiration associated with infection (Figure 4.6). What was not expected was the significant decline in mitochondrial respiration in the Senexin A-treated, mock-infected Huh7 carcinoma cells. These data indicate that mitochondrial respiration in Huh7 cells is chronically induced and subject to CDK8/19 regulation without involvement of virus. As little as two-fold over-expression or over-active CDK8 is common in many cancerous cell types, and expanded metabolic capacity plays a role in the establishment and maintenance of many tumors (Firestein et al., 2008; McDermott et al., 2017; Porter et al., 2012). Indeed, the exceptional capacity of hepatic tumor cell lines to support DENV2 replication may lie in their already expanded metabolic activity, which appears to be dependent upon CDK8/19 enzymatic activity. Though not within the scope of this work, investigations into CDK8/19-dependent metabolism in primary cells may yield valuable insight.

The data show that Senexin A has an inhibitory effect on the metabolic capacity of cells, and that this effect cannot be overridden by DENV2 infection. The delay until after 24 h for the full effects of Senexin A suggests that it is acting, as expected, at the level of gene expression; CDK8/19 inhibition blocks the gradual reprogramming of gene expression that results in substantive metabolic changes during maximal virus replication. The timing of DENV2 induction of HK2 and LC3 expression until after 12 hpi, with full induction only after 24 h, and the ability of Senexin A to block HK2 and LC3 induction, supports a role for CDK8/19 specifically in the control of gene expression to regulate metabolism.

CDK8 was recently shown to regulate autophagy in *Drosophila* under starvation conditions by promoting the elongation of mRNAs encoding Atg1 and Atg8, orthologs of mammalian ULK1 and LC3 (Tang et al., 2018). Elongation of the 3' UTR is achieved through CDK8 phosphorylation of the cleavage and polyadenylation specificity factor, CPSF6, a component of the cleavage and polyadenylation (CPA) complex. Tang et al. (Tang et al., 2018) further showed that treatment with Senexin A reduced activation of LC3, which, in accordance with our findings, suggests a conserved role for CDK8 in the regulation of LC3, independent of cellular stressors. Loss of LC3 gene expression is a likely mechanism for reduced mitochondrial respiration in the mock- and DENV2-infected Huh7 cells treated with Senexin A. Dependence of DENV2 replication on increased mitochondrial capacity is consistent with recent reports on the expansion of the mitochondrial compartment during DENV infection (Barbier et al., 2017). Cyclin C has also been implicated in the control of mitochondrial dynamics independently of CDKs (Ježek et al., 2019; Jezek et al., 2019; Stieg et al., 2019). Any of these proposed mechanisms are consistent with the reductions in DENV2 RNA that we observed with the knockdown of CDK8, CDK19, and Cyclin C (Figures 4.2B and 4.2D). Further mechanistic investigations are warranted.

In addition to changes in mitochondrial dynamics, DENV2-infected cells exhibited reduced glycolytic activity, as previously observed, due to diversion of glycolytic intermediates from lactic acid production to anapleurotic roles (El-Bacha et al., 2007; Fernandes-Siqueira et al., 2018). Senexin A treatment reduced the glycolytic activity, in terms of lactic acid production, of both mock- and DENV2-infected cells (Figure 4.6C), indicating CDK8/19 control of glycolytic gene expression. DENV2 infection did allow a

modest increase in glycolysis and glycolytic capacity compared to mock-infected cells in the presence of Senexin A. This compensation may be the result of higher levels of HK2 expression in Senexin A-treated, DENV2-infected cells compared to treated, mock-infected cells (Figure 4.4C) due to an incomplete Senexin A block of CDK8/19 in infected cells. Though we used HK2 and LC3 as measures of CDK8/19-dependent metabolic gene expression during DENV2 infection, these are likely not the only genes regulated by CDK8/19 during viral infection. More investigation into the global picture of CDK8/19-regulated gene expression during DENV2 infection is warranted to understand their complete role.

We previously showed that CDK8 activity is enhanced by a retroviral cyclin (Birkenheuer et al., 2015; Brewster et al., 2011; Rovnak et al., 2012). Interaction between the retroviral cyclin and CDK8 enhances CDK8 function in the serum response to the advantage of the virus, which requires cell proliferation for transmission. We now show that CDK8 is increased during infection with an unrelated virus, DENV2, and that increased CDK8 activity is ultimately beneficial to viral replication. In this case, the support is dependent on metabolic rather than proliferative mechanisms. DENV2 dependence on host metabolism makes it a valuable model to study CDK8/19 control of metabolism.

CDK8 is highly conserved across all metazoan organisms, and metabolic flux and induction of autophagy are common to infections by a broad array of DNA and RNA viruses (Abernathy et al., 2019; Zhang et al., 2018). We propose that many viruses may depend on CDK8 and/or CDK19 function for induced expression of metabolic and autophagic genes. The cellular demands for CDK8/19 function appear to be limited to

proliferative and stress responses as opposed to homeostasis. As such, therapeutics that target CDK8/19 enzyme activity offer promise for virus infection as well as cancer (McDermott et al., 2017).

We observed a reduction in PFUs of almost one log₁₀ copies/mL in the supernatants of Senexin A-treated cells. Waggoner et al. (Waggoner et al., 2020) calculated that the odds of severe dengue disease are increased by 50% for each increase in 1 log₁₀ copies /mL of acute-phase serum. Senexin therapies have the capacity to significantly reduce severe outcomes of DENV infections. In addition to significant reductions in disease severity, there is a minimum mosquito infectious dose in the serum of infected individuals. Nguyen et al. (Nguyen et al., 2013) quantitated the 50% mosquito infectious dose at 6.29–7.52 log₁₀ RNA copies/mL of plasma; a log₁₀ reduction in plasma virus that reduces viral load below this range will effectively reduce the capacity for DENV transmission. Further reductions in viral loads may be achieved with combination therapies of additional host-directed and virus targets, a common strategy to avoid the development of resistance to virus-targeted drugs alone. In summary, we have identified CDK8/19 as a hub of transcriptional regulation during DENV2 infection. CDK8 and CDK19 are responsible for the upregulation of key metabolic genes that enhance glucose metabolism and autophagy to meet the energetic and metabolic demands of viral replication.

CHAPTER 5: CYCLIN-DEPENDENT KINASES 8 AND 19 DIFFERENTIALLY REGULATE THE EARLY PHASE OF THE TYPE I INTERFERON RESPONSE

5.1 Summary

The type I interferon response is a critical component of host defense against viral infection. This response is tightly regulated at all levels, from recognition of viral pathogens, to initiation of interferon production, to autocrine and paracrine signaling, to interferon-stimulated gene expression, and ultimately to resolution. This regulation is essential for both adequate protection from viral pathogens and prevention of autoimmunity or other immunopathology. Cyclin-dependent kinases 8 and 19 (CDK8 and CDK19) are transcriptional regulators which function primarily during induced states to regulate gene expression. Our recent investigation into the role of CDK8 and CDK19 as transcriptional regulators during infection with dengue virus serotype 2, as well as numerous recent reports demonstrating CDK8/19 as transcriptional regulators of the type II interferon response, led us to explore the role of CDK8/19 as regulators of type I interferon response. Here we show that CDK8 and CDK19 are regulators of IFN- β expression in response to viral infection and that in response to treatment with the double-stranded RNA mimic, poly(I:C), CDK8 and CDK19 have roles as transcriptional regulators that are both distinct from the antiviral response and distinct from each other. Understanding transcriptional regulation of the type I interferon response is critical to understand host antiviral responses, resolution of innate immunity, and prevention of immunopathology.

5.2 Introduction

Protection of a host from infectious disease involves multiple levels of a complex immune response. Innate immunity, which relies on recognition of pathogen-associated molecular patterns (PAMPs) rather than immune memory, is critical for an early and rapid response to pathogens. For viral infection in particular, the type I interferon (IFN) response is a key driver of innate immunity. Type I IFNs, comprised of IFN- β and multiple isoforms of IFN- α , are produced and secreted upon initial recognition of PAMPs by pattern recognition receptors (PRRs). In the case of infection with RNA viruses which replicate in the cytoplasm, these PRRs are primarily retinoic acid-inducible gene I (RIG-I), melanoma differentiation-associated gene 5 (MDA-5) and toll-like receptors 3 and 7 (TLR3, TLR7) (Gitlin et al., 2006; Hornung et al., 2006; Iwasaki, 2012; Jensen and Thomsen, 2012; Kato et al., 2006, 2008). Pathogen recognition leads to initiation of type I IFN expression, IFN- α/β secretion, IFN- α/β receptor ligation on neighboring cells, and ultimately interferon-stimulated gene (ISG) expression. Each step of this response is regulated by host factors at multiple levels, including at the level of transcription (Chen et al., 2017a; Ivashkiv and Donlin, 2014).

Beginning with the initial discovery of IFNs, understanding of IFN responses is inextricably linked to the study of the viruses which initiate them (Isaacs and Lindenmann, 1987). During our investigation into the role of the host transcriptional regulator CDK8 and its paralog, CDK19, during dengue virus serotype 2 (DENV2) infection (Butler et al., 2020), we observed a marked effect on the robustness of the type I IFN response in the context of CDK8/19 inhibition. This led to a hypothesis that, in

addition to a role for regulating metabolic gene expression, CDK8/19 also have a role in regulation of the innate antiviral response. This hypothesis was well supported by several recent reports identifying a role for CDK8 and CDK19 in the type II IFN response (Bancerek et al., 2013; Steinparzer et al., 2019). In addition to the type II IFN response, CDK8 has known transcriptional regulatory activity in a number of induced cellular states, such as hypoxia and starvation (Birkenheuer et al., 2015; Donner et al., 2010; Galbraith et al., 2013; Rovnak et al., 2012).

However, there are several limitations of using the DENV2 infection model to address this hypothesis. These include: the inability to separate early innate recognition of PAMPs from the later phase of autocrine and paracrine signaling, the known ability of DENV2 to manipulate the type I IFN response (Ashour et al., 2009; Green et al., 2014), and the inability to distinguish CDK8 activity from that of CDK19 activity due to significant reduction in cellular proliferation in the context of CDK8/19 knockdown in the cell line used for DENV2 infection studies (Audetat et al., 2017; Birkenheuer et al., 2015; Firestein et al., 2008).

To address these limitations, we employed the dsRNA mimic, polyinosinic:polycytidylic acid (poly(I:C)), which activates PRRs in a manner similar to DENV2 through the cytoplasmic helicases RIG-I and MDA-5 (Gitlin et al., 2006; Hornung et al., 2006; Kato et al., 2006, 2008). Using distinct delivery methods of poly(I:C), we were able to distinguish unique roles for CDK8 and CDK19 as regulators of the early phase of the type I IFN response. We show that induction of IFN- β mRNA expression by poly(I:C) added directly to cell culture media is negatively regulated by CDK8, while induction by poly(I:C) added to cell culture media in combination with a

transfection reagent is negatively regulated by CDK19. This suggests unique roles for CDK8 and CDK19 as regulators of the type I IFN response, which is itself tightly controlled through a variety of signaling pathways distinct for each stimulus. This work contributes not only to further understanding of the intricate and complex regulation of the critical antiviral protection afforded by the type I IFN response, but also expands the known role of CDK8/19 as key transcriptional regulators for host stress responses.

5.3 Materials and Methods

5.3a Cell Culture, DENV2 Infection, and Poly(I:C) treatment

Huh7, HCT116, and Vero cells were subject to synchronized infection as previously described (Butler et al., 2020). Briefly, at 24 h prior to infection, 1×10^6 cells were plated in 25 cm² flasks. Immediately prior to infection, cells were incubated at 4 C for 15 min, washed with cold Dulbecco's phosphate-buffered saline (D-PBS) and incubated with DENV2 (strain 16681, passage 4) (Kinney et al., 1997) at 4 C for 1 h with rocking. Virus media were removed and replaced with supplemented DMEM with 2% fetal bovine serum (FBS). Mock- or DENV2-infected Huh7 cells were incubated in DMEM with Senexin A (MedChemExpress, Monmouth Junction, NJ, USA) or Senexin B (ProbeChem, Shanghai, China) at indicated concentrations or in media with the volumetric equivalent (final 0.01%) of DMSO solvent for the indicated period of time. HCT116 cells were cultured in Dulbecco's modified Eagle medium (DMEM) supplemented with 10% FBS, 1% L-glutamine, and 25 mM HEPES. 24 h prior to

poly(I:C) treatment, 5×10^6 HCT116 cells were plated in 10 cm dishes. Poly(I:C) treatment at indicated concentrations was either directly added to cell culture media (“pure poly(I:C)”) or transfected with Lipofectamine 2000 (Thermo Fisher Scientific, Waltham, MA, USA) (“transfected poly(I:C)”).

5.3b qRT-PCR Analysis

At the indicated times, cells were collected in TRIzol (Thermo Fisher Scientific, Waltham, MA, USA), and total RNA was isolated according to the manufacturer’s instructions and treated with Turbo DNase I (Thermo Fisher Scientific, Waltham, MA, USA). cDNA was synthesized with an iScript cDNA synthesis kit (Bio-Rad, Hercules, CA, USA) according to the manufacturer’s instructions, and then, subjected to qPCR analysis with iQ SYBR green Supermix in a CFX96 real-time PCR system (Bio-Rad, Hercules, CA, USA). Primer sequences are listed in Table 5.1. Relative expression was normalized to the housekeeping gene, Succinate Dehydrogenase Complex Flavoprotein Subunit A, *SDHA* (Watson et al., 2007).

Table 5.1 PCR Primers.

Gene	Forward	Reverse	Source
CDK8	GGGATCTCTATG TCGGCATGTAG	AAATGACGTTTG GATGCTTAAGC	(Galbraith et al., 2013)
CDK19	GCCACGGCTAG GGCCT	GCGAGAACTGG AGTGCTGATAA	(Galbraith et al., 2013)
DENV2	ACAAGTCGAACA ACCTGGTCCAT	GCCGCACCATT GGTCTTCTC	(Laue et al., 1999)
IFN- β	CGCCGCATTGA CCATCTA	GACATTAGCCAG GAGGTTCTCA	(Bender et al., 2015)
OAS1	CAGCGTCAACTA TCACTTCACT	AACTCTACTTTG CAGAACCTCAC	Rovnak, unpublished
SDHA	GACAACTGGAG GTGGCATT	CCGTCATGTAGT GGATGGCA	(Watson et al., 2007)

5.3c Establishment of Knockdown Cell Lines

Lentivirus delivery of short hairpin RNA (shRNA) (Sigma-Aldrich, St. Louis, MO, USA, Table 5.2) was used to knock down expression of CDK8 and CDK19. 293FT cells (Thermo Fisher Scientific, Waltham, MA, USA) were transfected with shRNA and lentivirus packaging constructs, and virus particles were collected after 48 h. HCT116 cells were transduced with a dilution series of shRNA lentiviruses and incubated for 48 h prior to selection with 1 μ g/mL puromycin for 5 days. Colonies were selected, cultured in puromycin, and screened for knockdown.

Table 5.2 shRNA Sequences.

Gene	Designation	Sequence
CDK8	TRCN00000 00489	CCGGATGTCCAGTAGCCAAGTTCCACTCGAGTG GAACTTGGCTACTGGACATTTTTT
CDK19	TRCN00001 95069	CCGGAGGACTGATAGCTCTTCTTTACTCGAGTAA AGAAGAGCTATCAGTCCTTTTTT

5.3d Subcellular Extracts and Protein Analysis

Nuclear extracts were prepared as previously described (Brewster et al., 2011). Briefly, cells were lysed in 0.5% NP-40 in PBS with protease and phosphatase inhibitors (2 µg/mL leupeptin and aprotinin, 1 µg/mL pepstatin, 0.2 mM phenylmethylsulfonyl fluoride [PMSF], 0.2 mM sodium orthovanadate, 2 mM sodium pyrophosphate, and 1 mM glycerophosphate). Nuclei were pelleted at 1500 x g, washed with cold PBS, and then, with buffer A (10 mM HEPES pH 8.0, 10 mM KCl, 1.5 mM MgCl₂, 0.5 mM dithiothreitol (DTT)), prior to extraction overnight with 2.5 nuclear pellet volume buffer C (10 mM HEPES pH8.0, 420 mM KCl, 20% glycerol, 0.1 mM EDTA, 0.5 mM DTT, and protease and phosphatase inhibitors). Extracted nuclei were pelleted for 15 min at 21,000 x g and re-extracted with 1 pellet volume buffer C. Extracts were pooled for analysis.

Protein concentration of each extract was determined with a Pierce BCA protein assay kit (Thermo Fisher Scientific, Waltham, MA, USA) according to the manufacturer's instructions. Equal quantities of total protein were separated by polyacrylamide gel electrophoresis for western blot. Blocked blot segments, separated by molecular weight range, were probed simultaneously with indicated primary antibodies (Table 5.3) overnight. Antibodies were detected with appropriate horseradish peroxidase-conjugated secondary antibodies and developed with the TMB membrane peroxidase substrate system (3,3',5,5'-Tetramethylbenzidine, KPL). Images were scanned with a Visioneer One Touch 9420 scanner at a gamma value of 1.0, and all contrast adjustments were uniformly applied using Adobe Photoshop.

Table 5.3 Cell Protein Antibodies.

Antibody	Source	Catalog #
Rabbit anti phosphoIRF3	Cell Signaling	#4947
Mouse anti nucleolin	Active Motif	39541

5.3e Statistics

Statistical analysis was performed on Prism software (Version 8.1.2 (227)).

5.4 Results

5.4a CDK8/19 Chemical Inhibition Reduces IFN- β and OAS1 Expression during DENV2 Infection

During an investigation into the role of the host transcriptional regulators CDK8 and CDK19 during infection with dengue viruses, we observed reduced viral replication when cells were treated with the CDK8/19 chemical inhibitors Senexin A and Senexin B (Butler et al., 2020). Due to the critical role of the type I IFN response in control of viral replication, and previous reports of a role for CDK8/19 in the type II IFN response (Bancerek et al., 2013; Steinparzer et al., 2019), we hypothesized that inhibition of CDK8/19 may promote the type I IFN response through release of an inhibitory role of CDK8/19 on either IFN- β or ISG expression.

We therefore evaluated IFN- β mRNA expression during synchronized DENV2 infection in Huh7 cells treated with the vehicle control, dimethyl sulfoxide (DMSO), or the CDK8/19 inhibitors Senexin A and Senexin B (McDermott et al., 2017; Porter et al.,

2012). As an indicator of ISG expression, we also evaluated mRNA expression of the classic ISG, oligoadenylate synthetase 1 (OAS1).

Contrary to our hypothesis, we observed a marked decrease in both IFN- β and OAS1 expression in Huh7 cells treated with either Senexin A or Senexin B (Figure 5.1). IFN- β expression was reduced by approximately 98% in Huh7 cells treated with 25 μ M Senexin A compared to DMSO (DMSO mean \pm SEM: 1.007 ± 0.004 , Senexin A: 0.021 ± 0.001) (Figure 5.1A). OAS1 expression was reduced by approximately 96% in Huh7 cells treated with Senexin A compared to DMSO (DMSO mean \pm SEM: 1.236 ± 0.1467 , Senexin A: 0.051 ± 0.008) (Figure 5.1B). Treatment with Senexin B, a newer generation, optimized iteration of Senexin A, yielded similar results at a lower concentration (12 μ M). IFN- β expression was reduced by approximately 94% in Senexin B-treated Huh7 cells compared to DMSO (DMSO mean \pm SEM: 1.424 ± 0.242 , Senexin B: 0.087 ± 0.006) (Figure 5.1C). Similarly, OAS1 expression was reduced by approximately 91% (DMSO mean \pm SEM: 1.414 ± 0.305 , Senexin B: 0.132 ± 0.010) (Figure 5.1D). Together, these data suggest a role for CDK8/19 as positive regulators of the type I IFN response. However, given the previously noted reduced viral replication in the context of CDK8/19 inhibition, the reduced robustness of the type I IFN response with Senexin A or Senexin B treatment could be attributed to a less robust stimulus. In addition, these data are complicated by the known ability of DENV2 to interfere with the type I IFN response and the inability to distinguish roles for CDK8 and CDK19 as they are commonly inhibited by Senexin A and Senexin B (Ashour et al., 2009; Green et al., 2014; McDermott et al., 2017; Porter et al., 2012).

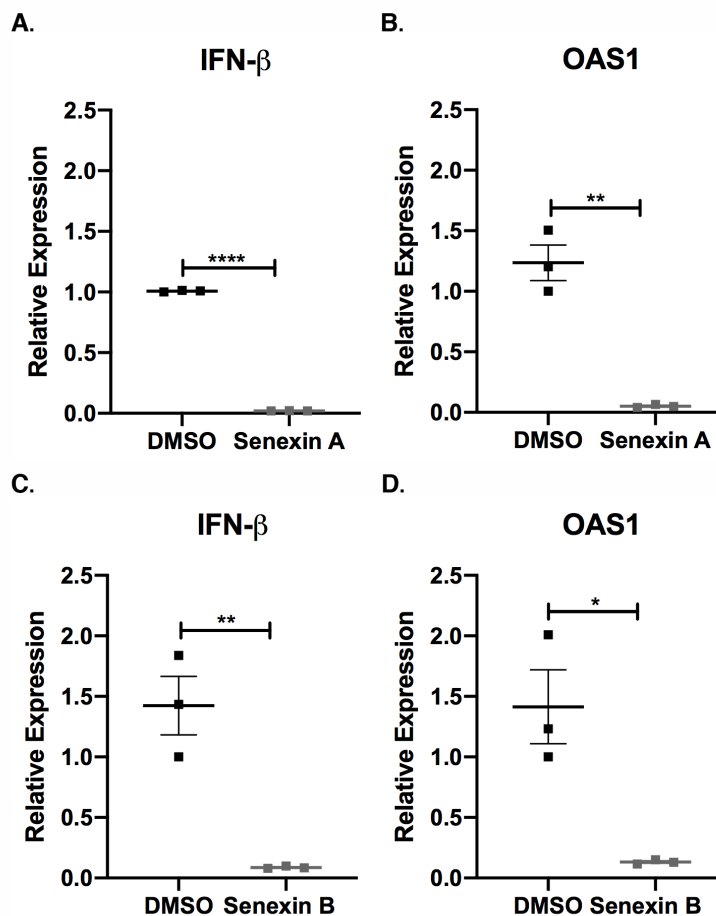


Figure 5.1 CDK8/19 chemical inhibition reduces IFN-β and OAS1 expression during DENV2 infection. Huh7 cells were infected with DENV2 (MOI = 10) for 36 hours and treated with DMSO, 25 μM Senexin A (A, B), or 12 μM Senexin B (C, D) for the duration of infection. Total cellular RNA was analyzed by qRT-PCR for IFN-β (A, C) or OAS1 (B, D). Expression normalized to the housekeeping gene, *SDHA*. n = 3 biological replicates; * p < 0.05, ** p < 0.01, **** p < 0.0001; unpaired two-tailed t test; Error bars represent mean ± SEM.

5.4b The DENV2 Requirement for CDK8 is Independent of the Type I IFN Response

To further investigate this apparently contradictory finding of reduced virus replication in the context of a diminished antiviral response, we evaluated the requirement for CDK8 on DENV2 replication and induction of the type I IFN response in

HCT116 cells which tolerate CDK8 knockdown better than Huh7 cells. We established a CDK8-knockdown HCT116 cell line (8KO) using lentivirus-mediated shRNA targeted to the 3' untranslated region (UTR) of CDK8 which is not present in CDK19 transcripts. CDK8 mRNA expression in the knockdown cell line was approximately 19% of that in wild-type (WT) controls (WT mean \pm SEM: 1.193 ± 0.112 , 8KO: 0.227 ± 0.039) (Figure 5.2A). We confirmed the requirement of DENV2 replication on CDK8, observing an approximately 52% reduction in DENV2 viral RNA in 8KO HCT116 cells compared to WT (WT mean \pm SEM: $43.97 \pm 7.77 \times 10^6$, 8KO: $20.97 \pm 2.68 \times 10^6$) (Figure 5.2B).

Despite this similar outcome of reduced DENV2 replication with both CDK8-knockdown and CDK8/19 chemical inhibition (Figure 5.2B) (Butler et al., 2020), we observed a distinctly different effect on induction of the type I IFN response. While IFN- β expression was reduced in CDK8/19-inhibitor treated cells (Figure 5.1A, 5.1C), IFN- β expression in 8KO HCT116 cells was \sim 2.8 fold greater than in WT HCT116 cells (WT mean \pm SEM: 1.272 ± 0.144 , 8KO: 3.533 ± 0.38) (Figure 5.2C). These data suggest that reduced viral stimulus is not a likely driver of the reduced IFN- β expression in CDK8/19-inhibitor treated cells (Figure 5.1), as reduced viral replication in 8KO HCT116 cells did not show a similar dampening of IFN- β expression (Figure 5.2). In the context of DENV2 infection of Huh7 and HCT116 cells, DENV2 replication was reduced with both CDK8/19 inhibition and with CDK8-knockdown, independent of any changes CDK8/19 inhibition or CDK8-knockdown had on the type I IFN response (Figure 5.1, 5.2) (Butler et al., 2020).

To further confirm that DENV2 dependence on CDK8 is independent of the type I IFN response, we turned to Vero cells which lack the type I IFN locus and therefore do

not produce IFN- β . For this, we used lentivirus-mediated shRNA to transiently knockdown CDK8 expression in Vero cells. Despite less efficient CDK8 knockdown (non-target (NT) control mean \pm SEM: 0.9713 ± 0.015 , CDK8-knockdown: 0.482 ± 0.06) (Figure 5.2D), we still observed a modest but significant reduction in DENV2 viral RNA in CDK8-knockdown Vero cells compared to NT shRNA treated controls (NT mean \pm SEM: $30.9 \pm 1.16 \times 10^5$, CDK8-knockdown: $24.0 \pm 1.10 \times 10^5$) (Figure 5.2E). Together, these data further demonstrate a requirement of DENV2 replication on CDK8, and that this requirement is independent of any regulatory effect that CDK8 may have on the type I IFN response.

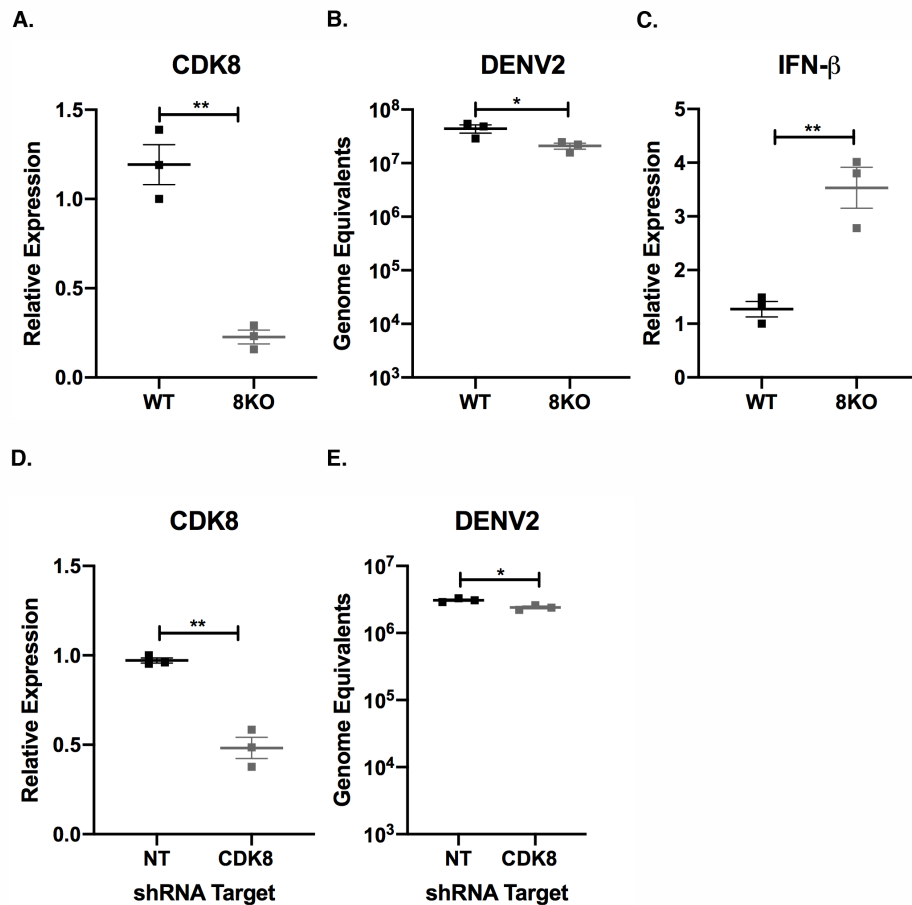


Figure 5.2 DENV2 requirement for CDK8 is independent of the type I IFN response. (A) CDK8 mRNA expression in HCT116 wild-type (WT) and CDK8-knockdown (8KO) cells analyzed by qRT-PCR, expression normalized to the housekeeping gene, *SDHA*. (B-C) HCT116 WT or 8KO cells were infected with DENV2 (MOI = 10) for 36 hours. Total cellular RNA was analyzed by qRT-PCR for DENV2 viral RNA (B) or IFN- β (C). DENV2 RNA quantification relative to in vitro transcribed DENV2 genome equivalent (GE) standard curve (B). IFN- β expression normalized to the housekeeping gene, *SDHA* (C). (D, E) Vero cells transduced with non-target (NT) or CDK8-targeted shRNA (CDK8) were infected with DENV2 (MOI = 1) for 24 hours. (D) CDK8 expression normalized to the housekeeping gene, *SDHA*. (E) DENV2 RNA quantification relative to in vitro transcribed DENV2 genome equivalent (GE) standard curve. n = 3 biological replicates; * p < 0.05, ** p < 0.01; unpaired two-tailed t test; Error bars represent mean \pm SEM.

5.4c CDK19 is a Negative Regulator of the Type I IFN Response during DENV2

Infection

To further distinguish the roles of CDK8 and CDK19 in the type I IFN response, we next established a stable CDK19-knockdown cell line in HCT116 cells using lentivirus-mediated shRNA targeted to a conserved region of CDK19 which is not present in CDK8 transcripts. CDK19 mRNA expression was knocked down approximately 82% in CDK19-knockdown HCT116 cells (19KO) compared to WT controls, and CDK19 expression was unchanged in the CDK8-knockdown HCT116 cells (8KO) (WT mean \pm SEM: 0.98 ± 0.02 , 8KO: 0.92 ± 0.07 , 19KO: 0.18 ± 0.06) (Figure 5.3A). Additionally, we confirmed that CDK8 expression was unchanged in the 19KO cells compared to WT controls (WT mean \pm SEM: 1.01 ± 0.09 , 8KO: 0.24 ± 0.04 , 19KO: 1.16 ± 0.17) (Figure 5.3B).

In contrast to the reduction in DENV2 replication that we observed with CDK8-knockdown, there was not a significant difference in viral RNA production in CDK19-knockdown HCT116 cells compared to WT (WT mean \pm SEM: $6.46 \pm 1.20 \times 10^7$, 19KO:

$4.68 \pm 1.13 \times 10^7$) (Figure 5.3C). Despite this differential effect on the efficiency of DENV2 replication with either CDK8 or CDK19 knockdown, we observed a similar outcome on IFN- β expression. IFN- β mRNA expression was increased approximately 3-fold in CDK19-knocked down HCT116 cells compared to WT (WT mean \pm SEM: 1.09 ± 0.08 , 19KO: 3.11 ± 0.24) (Figure 5.3D). Increased expression of IFN- β after CDK19-knockdown suggests that CDK19 is a negative regulator of the type I IFN response. These data further demonstrate that any effect CDK8 and/or CDK19 may have on DENV2 replication is independent of the robustness of the type I IFN response and provide further evidence that CDK8 and CDK19 are regulators of the type I IFN response in a manner that is context dependent.

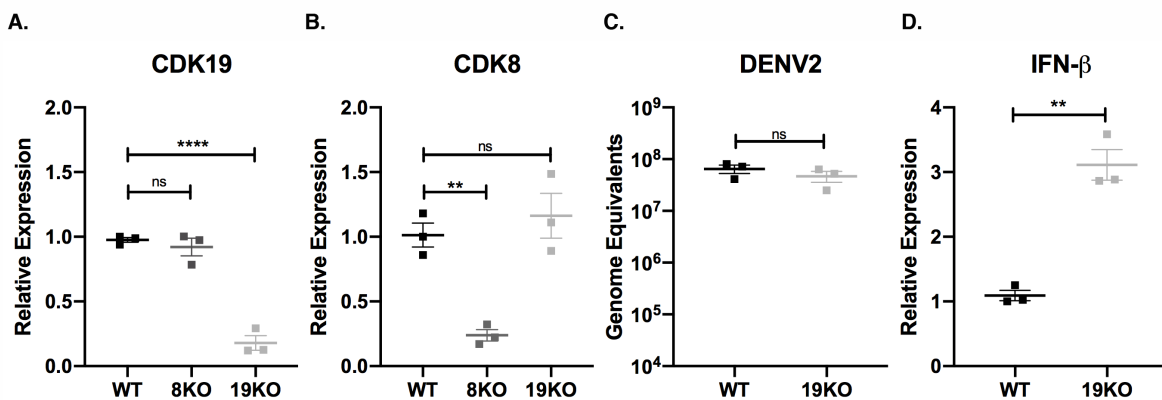


Figure 5.3 CDK19 is a negative regulator of the type I IFN response during DENV2 infection (A) CDK19 and (B) CDK8 mRNA expression in HCT116 wild-type (WT), CDK8-knockdown (8KO), and CDK19-knockdown (19KO) cells analyzed by qRT-PCR. Expression normalized to the housekeeping gene, *SDHA*. (C and D) HCT116 WT or 19KO cells were infected with DENV2 (MOI = 10) for 36 hours. Total cellular RNA was analyzed by qRT-PCR. (C) DENV2 RNA quantification relative to in vitro transcribed DENV2 genome equivalent (GE) standard curve. (D) IFN- β expression normalized to the housekeeping gene, *SDHA*. n = 3 biological replicates; ** p < 0.01, **** p < 0.0001; (A-B) One-way ANOVA with Tukey's multiple comparisons test; (C-D) unpaired two-tailed t test. Error bars represent mean \pm SEM.

5.4d CDK8 and CDK19 Have Distinct Regulatory Roles in Induction of the Type I IFN Response

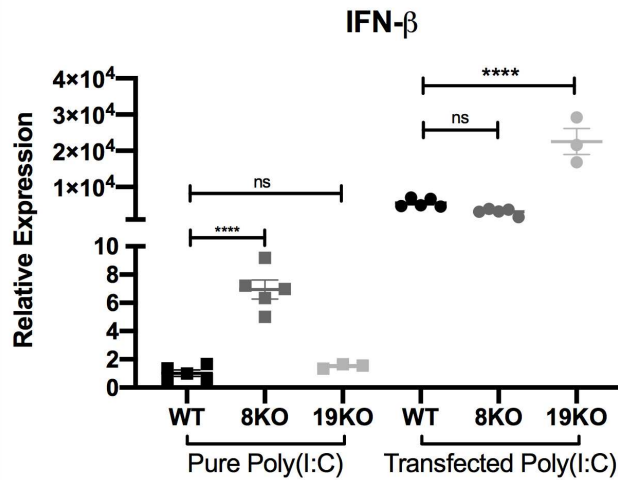
To avoid the complication of DENV2-mediated type I IFN interference, we used the double-stranded RNA mimic poly(I:C) to induce a type I IFN response. Poly(I:C) is recognized by distinct PRRs and initiates distinct signaling pathways dependent on the delivery method into cells (Dauletbaev et al., 2015). Pure poly(I:C), that is poly(I:C) added directly to the cell culture media, is thought to initiate nuclear translocation of both interferon regulator factor 3 (IRF3) and nuclear factor kappa B (NF κ B), while transfected poly(I:C) is thought to primarily initiate nuclear translocation of IRF3 but not NF κ B (Dauletbaev et al., 2015).

We therefore employed differential delivery of poly(I:C) as a way to distinguish roles for CDK8 and/or CDK19 in induction of IFN- β transcription through distinct signaling pathways. We treated wild-type (WT), CDK8-knockdown (8KO), and CDK19-knockdown (19KO) HCT116 cells with pure poly(I:C) or transfected poly(I:C) and evaluated mRNA expression of IFN- β . Transfected poly(I:C) induced a much more robust response than pure poly(I:C) in all cell types, as expected (Figure 5.4A). Pure poly(I:C)-treated 8KO HCT116 cells exhibited an approximately 7-fold greater induction of IFN- β compared to WT cells, while IFN- β expression in 19KO cells was unchanged compared to WT (WT mean \pm SEM: 1.02 ± 0.23 , 8KO: 6.95 ± 0.68 , 19KO: 1.52 ± 0.09) (Figure 5.4A). However, after treatment with transfected poly(I:C), IFN- β expression in 8KO cells was comparable to that in WT cells, while IFN- β expression in 19KO cells was increased approximately 4-fold over WT (WT mean \pm SEM: $5.62 \pm 0.53 \times 10^3$,

8KO: $3.16 \pm 0.39 \times 10^3$, 19KO: $22.56 \pm 3.61 \times 10^3$) (Figure 5.4A). These data suggest that CDK8 and CDK19 have distinct regulatory roles in induction of IFN- β transcription dependent on the nature of the stimulus and subsequent signaling pathway activation.

We next evaluated nuclear translocation of phosphorylated IRF3 (pIRF3) as an indicator of signaling pathway activation. pIRF3 was not detectable by western blot in any of the cell lines tested after treatment with 10 $\mu\text{g/mL}$ of pure poly(I:C), which was not unexpected given the relatively modest induction of IFN- β mRNA expression following this same dose of pure poly(I:C) treatment (Figure 5.4A, Figure 5.4B). pIRF3 in nuclear extracts was readily detectable by western blot in cells treated with 10 $\mu\text{g/mL}$ of transfected poly(I:C), with no discernable difference between WT, 8KO, and 19KO HCT116 cells (Figure 5.4B). This suggests that nuclear translocation of IRF3 is not dependent on CDK8 or CDK19 activity following poly(I:C) treatment. Therefore, the differential induction of IFN- β mRNA expression in 19KO cells compared to WT and 8KO is likely due to regulation at a step downstream of IRF3 activation and nuclear translocation. This is expected, as CDK8 and CDK19 are localized to the nucleus and function at sites of active transcription. The exact mechanism of CDK8/19 regulation on IFN- β mRNA expression is not yet clear but may be due to differential activation of transcription factors and/or recruitment of transcription factors to the IFN- β promoter.

A.



B.

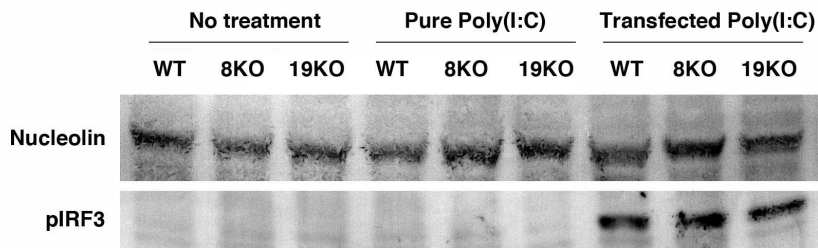


Figure 5.4 CDK8 and CDK19 have distinct regulatory roles in induction of the type I IFN response. HCT116 wildtype (WT), CDK8-knockdown (8KO), or CDK19-knockdown (19KO) cells were treated with 10 μ g/mL pure poly(I:C) or transfected poly(I:C) for 4 hours. (A) IFN- β mRNA expression analyzed by qRT-PCR. Expression normalized to the housekeeping gene, *SDHA*. $n =$ at least 3 biological replicates; **** $p < 0.0001$; One-way ANOVA with Tukey's multiple comparisons test; Error bars represent mean \pm SEM. (B) Western blot analyses of 4 μ g of total protein from nuclear extracts. Antibody specificities are indicated. Results representative of two independent experiments.

5.5 Discussion

Here we show that CDK8 and CDK19 have distinct functions as transcriptional regulators in induction of the type I IFN response. Our initial observations suggesting a role for CDK8/19 as regulators of IFN- β mRNA expression were noted in the course of

describing these kinases as regulators of metabolic gene expression during infection with DENV2 (Butler et al., 2020). This work suggested that CDK8/19 function, through regulation of metabolic gene expression, was ultimately to the benefit of viral replication by providing the necessary metabolic intermediates as building blocks for viral genome copies and viral particle assembly (Fontaine et al., 2015; Gullberg et al., 2018; Heaton and Randall, 2010; Heaton et al., 2010; Jordan and Randall, 2017; Zhang et al., 2018). Therefore, in the context of CDK8/19 inhibition and/or knockdown, we observed reduced viral replication (Butler et al., 2020).

However, we observed a significant reduction in IFN- β and the ISG, OAS1, in the context of CDK8/19 inhibition during DENV2 infection (Figure 5.1). This was an apparently contradictory finding, as a reduced type I IFN response would typically be expected to enhance viral replication. We therefore went on to show that the reduction in viral replication associated with CDK8 knockdown was, in fact, independent of the type I IFN response. In three different cell lines permissive to DENV2 infection, we observed a consistent reduction in viral replication with CDK8 inhibition or knockdown concurrent with 1) reduced IFN- β after CDK8 inhibition in Huh7 cells, 2) increased IFN- β after CDK8 knockdown in HCT116 cells, or 3) an absent type I IFN response in Vero cells (Figures 5.1 and 5.2). This consistent reduction in DENV2 replication in spite of quite different type I IFN responses demonstrates clearly that DENV2 dependence on CDK8 is not tied to the robustness of IFN- β mRNA expression. This is perhaps expected, given the well-documented ability of DENV2 to interfere in the type I IFN response (Ashour et al., 2009; Green et al., 2014) and the well-documented dependence of DENV2 on a supportive metabolic environment in the host cell (Gullberg

et al., 2018; Heaton and Randall, 2010; Heaton et al., 2010; Jordan and Randall, 2017; Zhang et al., 2018).

The significant sequence similarity and active identical sites of CDK8 and CDK19 lend redundant function to these two kinases; however, recent reports suggest that CDK8 and CDK19 have both unique and overlapping functions, and that their roles as transcriptional regulators are dependent on not only their kinase function but their structure as well (Audetat et al., 2017; Galbraith et al., 2013; Steinparzer et al., 2019). Though clearly CDK8 and CDK19's functions are most pronounced in induced states, their roles are known to be cell-type specific, gene-specific, and unique to the nature of the stimulus (Bancerek et al., 2013; Johannessen et al., 2017). While we observed a similar reduction in DENV2 replication after CDK8 and CDK19 knockdown in Huh7 cells (Butler et al., 2020), this was not the case in HCT116 cells (Figures 5.2 and 5.3). CDK8 knockdown reduced DENV2 replication in HCT116 cells while CDK19 did not have a significant effect (Figures 5.2 and 5.3). However, in both CDK8 and CDK19 knockdown, we observed a consistent enhancement of IFN- β mRNA expression during DENV2 infection (Figures 5.2 and 5.3), again suggesting a context-, cell-line- and stimulus-dependent effect of CDK8 and CDK19 knockdown.

To further distinguish the unique roles of CDK8 and CDK19 in the type I IFN response, independent of interference from DENV2, we treated HCT116 cells with poly(I:C), a double-stranded RNA mimic. Delivery of poly(I:C) into cell culture media directly or through transfection activates distinct signaling pathways with the ultimate effect of inducing IFN- β mRNA expression (Dauletbaev et al., 2015). Employing these two delivery methods, we observed a distinct difference between CDK8 and CDK19

knockdown (Figure 5.4). While CDK8 appears to function as a negative regulator of IFN- β mRNA expression upon treatment with pure poly(I:C), CDK19 appears to not have a significant role in this response (Figure 5.4). Conversely, we showed that CDK19 is a negative regulator of IFN- β mRNA expression in response to transfected poly(I:C), while CDK8 knockdown did not have a significant effect. These data clearly show distinct roles for CDK8 and CDK19 as negative regulators of IFN- β mRNA expression dependent on the nature of the stimulus.

Translocation of phosphorylated IRF3, a common transcription factor between pure and transfected poly(I:C) signaling pathways, was not different between CDK8 and CDK19 knockdown cells, suggesting that the differential roles of CDK8 and CDK19 are downstream of IRF3 phosphorylation and nuclear translocation. This is as expected, as CDK8 and CDK19 are localized to the nucleus, and all previously described functions of CDK8 and CDK19 occur in the nucleus. Based on previously described roles for CDK8/19 as negative transcriptional regulators, it seems likely that CDK8/19 function within the type I IFN response is through negative regulation of one or more transcription factors (Johannessen et al., 2017; Zhao et al., 2012). CDK8/19 phosphorylation of the transcription factor sterol regulatory element-binding protein 1 (SREBP) targets SREBP for degradation and negatively regulates expression of genes required for cholesterol biosynthesis (Zhao et al., 2012). Similarly, CDK8 phosphorylation destabilizes c-Jun which has a negative effect on IL-10 production in myeloid cells (Johannessen et al., 2017). Importantly, c-Jun is also involved in IFN- β expression, forming a dimer with Fos to form the transcription factor AP-1 (Du et al., 1993; Panne, 2008; Wathelet et al., 1998). Investigation into the phosphorylation status

of c-Jun, particularly at Ser243, and the stability of c-Jun after poly(I:C) stimulation in cells with knocked-down CDK8 and CDK19, is therefore warranted as a potential mechanism by which CDK8 and CDK19 are negative regulators of IFN- β mRNA expression (Johannessen et al., 2017).

Our work demonstrating distinct roles for CDK8 and CDK19 as transcriptional regulators of the type I IFN response is well in line with numerous recent reports of CDK8/19 as regulators of the type II IFN response, with effects on transcription occurring in a context-, stimulus- and gene-specific manner (Bancerek et al., 2013; Johannessen et al., 2017; Steinparzer et al., 2019). The type I and the type II IFN responses are critical players in the overall immune response and protection from pathogens, but appropriate regulation of these systems is critical to prevent immunopathologies. Understanding key regulators of the IFN response is critical to understand both positive and negative regulation of the immune response, and the balance required between protection from infectious disease and immunopathology.

CONCLUSION

We have identified CDK8 and CDK19 as transcriptional regulators during DENV2 infection and within the type I IFN response. During DENV2 infection, CDK8/19 positively regulate metabolic gene expression, the effect of which establishes a metabolic environment in the host cell that is conducive to efficient viral replication. Identification of host factors on which DENV2 replication is dependent is key to illuminating potential targets for host-directed therapeutic intervention. Despite the significant worldwide burden of dengue disease, current treatment is limited to supportive care as there are no effective antiviral treatments currently in use (Guzman and Harris, 2015). CDK8 and CDK19 are promising targets of host-directed therapy due to their fundamental function as regulators of induced, rather than basal, gene expression.

As is typical for host-directed antiviral therapy, CDK8/19-targeted treatment for DENV2 infection would have greater opportunity for success if given as one component of a combination therapy. Identifying other host factors or viral factors which may be targeted and given in combination with CDK8/19 inhibitors is a potential avenue of future exploration. Beyond the application of CDK8/19 inhibitors for treatment of dengue infection, there is significant interest in development of CDK8/19 inhibitors, also as part of combination therapy, for treatment of cancer (McDermott et al., 2017; Porter et al., 2012).

Beyond the practical applications for CDK8/19 inhibition in the treatment of disease, our work has contributed to the basic understanding of metabolic gene

regulation by host transcriptional regulators. Regulation of metabolism is critical for maintenance of homeostasis, response to stressors including starvation and hypoxia, and infection with a wide variety of pathogens. Our work identified CDK8/19 as key regulators of metabolic gene expression during viral infection, though the full scope of this regulation remains unexplored. Further investigation into characterizing the entire landscape of genes differentially regulated by CDK8/19 during viral infection is warranted. In addition, it is likely that at least a portion of these CDK8/19-dependent gene expression changes may also have an important role, either pro- or anti-viral, in other viral infections beyond DENV2, within the *Flavivirus* genus and beyond (Abernathy et al., 2019; Sanchez and Lagunoff, 2015; Zhang et al., 2018). As such, CDK8/19 could be a target for host-directed therapy against a number of viral infections, among which viral replication depends on the host metabolic environment (Abernathy et al., 2019; Sanchez and Lagunoff, 2015; Zhang et al., 2018).

In addition to characterizing the effect of CDK8/19 regulation on transcription during viral infection, it may be equally informative to identify the mechanism by which this regulation occurs. Previously described mechanisms by which CDK8/19 positively regulate gene expression include: activation of transcription factors, enhancement of transcriptional elongation, and promoter-proximal RNA pol II pause release (Bancerek et al., 2013; Donner et al., 2010; Galbraith et al., 2013). Each of these mechanisms, independently or in combination, should be explored in the context of differential metabolic gene expression by CDK8/19 during viral infection.

In the context of DENV2 infection, our data demonstrated that CDK8/19 act as positive regulators of metabolic gene expression, but in the context of poly(I:C)-

mediated induction of the type I IFN response, CDK8/19 act as negative regulators of IFN- β expression. Resolution of IFN signaling is an essential component of proper regulation of innate immunity, as an uncontrolled IFN response can contribute to immunopathology. Identifying CDK8/19 as negative regulators of IFN- β expression suggests that the mechanism by which CDK8/19 transcriptionally regulate the type I IFN response is distinct from the mechanism(s) of positive regulation on metabolic gene expression.

CDK8/19 negative regulation is most likely to occur on IFN- β promoter with CDK8/19 phosphorylation of transcription factors (Johannessen et al., 2017; Zhao et al., 2012). Phosphorylation of transcription factors by CDK8/19 can lead to degradation, reduced activity, or reduced recruitment of the transcription factors, ultimately leading to diminished activity off of the promoter and reduced expression of IFN- β . As with investigation into mechanisms of CDK8/19 regulation of metabolic gene expression, careful evaluation of each of these potential mechanisms may yield important insight into the ways in which CDK8 and CDK19 transcriptionally regulate critical gene expression during induced states.

DENV2 infection and the type I IFN response are examples of induced states in which we have identified critical roles for CDK8 and CDK19 as transcriptional regulators. However, very little is known regarding the mechanism by which CDK8 and CDK19 are themselves regulated. CDK8 is overexpressed in many types of cancer and during DENV2 infection (Brägelmann et al., 2017; Butler et al., 2020; Firestein et al., 2008; McDermott et al., 2017), and CDK8 and CDK19 both clearly have pronounced function in induced states (Chen et al., 2017b; Donner et al., 2010; Galbraith et al.,

2013; Zhao et al., 2012), but it is currently unknown how this overexpression or enhanced function is initiated.

Our DENV2 infection system offers great opportunity as an experimental model to explore the mechanisms by which CDK8 expression is regulated, as we demonstrated a clear upregulation of CDK8 upon DENV2 infection. It is possible that the upregulation of CDK8 we observed during DENV2 infection was a virus-directed, rather than host-directed, effect. Nuclear NS5 in particular is an interesting candidate for modulating host gene expression (De Maio et al., 2016). If the mechanism of CDK8 upregulation during DENV2 is indeed a result of viral protein activity, this is not a deterrent to understanding the general mechanisms of CDK8 regulation by host cells. Numerous advances in understanding cell biology have been directly the result of viral infection experiments, including the discovery of interferons (Isaacs and Lindenmann, 1987).

In summary, we have shown that CDK8 and CDK19 are transcriptional regulators of metabolic gene expression during viral infection and regulators of the type I IFN response. This work is significant not only in the context of the individual induced states explored here, but in understanding more fully the complex function of CDK8 and CDK19 which have important roles in a wide array of cellular stress responses and are overexpressed in a number of cancers. A number of questions remain unanswered, including the mechanisms by which CDK8 and CDK19 exert regulatory control within these induced states, and the mechanisms by which CDK8 and CDK19 are themselves regulated.

REFERENCES

- Abernathy, E., Mateo, R., Majzoub, K., van Buuren, N., Bird, S.W., Carette, J.E., and Kirkegaard, K. (2019). Differential and convergent utilization of autophagy components by positive-strand RNA viruses. *PLoS Biol* 17, e2006926.
- Acosta, E.G., Castilla, V., and Damonte, E.B. (2008). Functional entry of dengue virus into *Aedes albopictus* mosquito cells is dependent on clathrin-mediated endocytosis. *Journal of General Virology* 89, 474–484.
- Acosta, E.G., Castilla, V., and Damonte, E.B. (2011). Infectious dengue-1 virus entry into mosquito C6/36 cells. *Virus Research* 160, 173–179.
- Aguirre, S., Luthra, P., Sanchez-Aparicio, M.T., Maestre, A.M., Patel, J., Lamothe, F., Fredericks, A.C., Tripathi, S., Zhu, T., Pintado-Silva, J., et al. (2017). Dengue virus NS2B protein targets cGAS for degradation and prevents mitochondrial DNA sensing during infection. *Nat Microbiol* 2, 17037.
- Ahn, K.J., Hwang, H.S., Park, J.H., Bang, S.H., Kang, W.J., Yun, M., and Lee, J.D. (2009). Evaluation of the role of hexokinase type II in cellular proliferation and apoptosis using human hepatocellular carcinoma cell lines. *Journal of Nuclear Medicine* 50, 1525–1532.
- Aktepe, T.E., Liebscher, S., Prier, J.E., Simmons, C.P., and Mackenzie, J.M. (2017). The host protein reticulon 3.1A is utilized by flaviviruses to facilitate membrane remodelling. *Cell Reports* 21, 1639–1654.
- Alayli, F., and Scholle, F. (2016). Dengue virus NS1 enhances viral replication and pro-inflammatory cytokine production in human dendritic cells. *Virology* 496, 227–236.
- Alberti, A., Murgia, C., Liu, S.-L., Mura, M., Cousens, C., Sharp, M., Miller, A.D., and Palmarini, M. (2002). Envelope-induced cell transformation by ovine betaretroviruses. *JVI* 76, 5387–5394.
- Alexopoulou, L., Holt, A.C., Medzhitov, R., and Flavell, R.A. (2001). Recognition of double-stranded RNA and activation of NF- κ B by toll-like receptor 3. *Nature* 413, 732–738.
- Allonso, D., Andrade, I.S., Conde, J.N., Coelho, D.R., Rocha, D.C.P., da Silva, M.L., Ventura, G.T., Silva, E.M., and Mohana-Borges, R. (2015). Dengue virus NS1 protein modulates cellular energy metabolism by increasing glyceraldehyde-3-phosphate dehydrogenase activity. *J. Virol.* 89, 11871–11883.
- Altschul, S.F., Gish, W., Miller, W., Myers, E.W., and Lipman, D.J. (1990). Basic local alignment search tool. *Journal of Molecular Biology* 215, 403–410.

Angleró-Rodríguez, Y.I., Pantoja, P., and Sariol, C.A. (2014). Dengue virus subverts the interferon induction pathway via NS2B/3 protease-Ik β kinase ϵ interaction. *Clin. Vaccine Immunol.* 21, 29–38.

Aravind, L., and Koonin, E.V. (1999). G-patch: A new conserved domain in eukaryotic RNA-processing proteins and type D retroviral polyproteins. *Trends in Biochemical Sciences* 24, 342–344.

Arias, C.F., Preugschat, F., and Strauss, J.H. (1993). Dengue 2 virus NS2B and NS3 form a stable complex that can cleave NS3 within the helicase domain. *Virology* 193, 888–899.

Arnaud, F., Caporale, M., Varela, M., Biek, R., Chessa, B., Alberti, A., Golder, M., Mura, M., Zhang, Y., Yu, L., et al. (2007). A paradigm for virus–host coevolution: sequential counter-adaptations between endogenous and exogenous retroviruses. *PLoS Pathog* 3, e170.

Ashour, J., Laurent-Rolle, M., Shi, P.-Y., and García-Sastre, A. (2009). NS5 of dengue virus mediates STAT2 binding and degradation. *JVI* 83, 5408–5418.

Audetat, K.A., Galbraith, M.D., Odell, A.T., Lee, T., Pandey, A., Espinosa, J.M., Dowell, R.D., and Taatjes, D.J. (2017). A Kinase-independent role for cyclin-dependent kinase 19 in p53 response. *Mol Cell Biol* 37, e00626-16, e00626-16.

Bancerek, J., Poss, Z.C., Steinparzer, I., Sedlyarov, V., Pfaffenwimmer, T., Mikulic, I., Dölken, L., Strobl, B., Müller, M., Taatjes, D.J., et al. (2013). CDK8 kinase phosphorylates transcription factor STAT1 to selectively regulate the interferon response. *Immunity* 38, 250–262.

Bankevich, A., Nurk, S., Antipov, D., Gurevich, A.A., Dvorkin, M., Kulikov, A.S., Lesin, V.M., Nikolenko, S.I., Pham, S., Pribelski, A.D., et al. (2012). SPAdes: A new genome assembly algorithm and its applications to single-cell sequencing. *Journal of Computational Biology* 19, 455–477.

Barbier, V., Lang, D., Valois, S., Rothman, A.L., and Medin, C.L. (2017). Dengue virus induces mitochondrial elongation through impairment of Drp1-triggered mitochondrial fission. *Virology* 500, 149–160.

Barker, C.S., Pickel, J., Tainsky, M., and Hunter, E. (1986). Molecular cloning of the Mason-Pfizer monkey virus genome: Biological characterization of genome length clones and molecular comparisons to other retroviruses. *Virology* 153, 201–214.

Bartelma, G., and Padmanabhan, R. (2002). Expression, purification, and characterization of the RNA 5'-triphosphatase activity of dengue virus type 2 nonstructural protein 3. *Virology* 299, 122–132.

Bartholomeusz, A.I., and Wright, P.J. (1993). Synthesis of dengue virus RNA in vitro: initiation and the involvement of proteins NS3 and NS5. *Archives of Virology* 128, 111–121.

Beatty, J.A., Lawrence, C.E., Callanan, J.J., Grant, C.K., Gault, E.A., Neil, J.C., and Jarrett, O. (1998). Feline immunodeficiency virus (FIV)-associated lymphoma: a potential role for immune dysfunction in tumourigenesis. *Veterinary Immunology and Immunopathology* 65, 309–322.

Beatty, P.R., Puerta-Guardo, H., Killingbeck, S.S., Glasner, D.R., Hopkins, K., and Harris, E. (2015). Dengue virus NS1 triggers endothelial permeability and vascular leak that is prevented by NS1 vaccination. *Sci. Transl. Med.* 7, 304ra141-304ra141.

Begier, E.M., Asiki, G., Anywaine, Z., Yockey, B., Schriefer, M.E., Aleti, P., Ogen-Odoi, A., Staples, J.E., Sexton, C., Bearden, S.W., et al. (2006). Pneumonic plague cluster, Uganda, 2004. *Emerg. Infect. Dis.* 12, 460–467.

Bender, S., Reuter, A., Eberle, F., Einhorn, E., Binder, M., and Bartenschlager, R. (2015). Activation of type I and III interferon response by mitochondrial and peroxisomal MAVS and inhibition by hepatitis C virus. *PLoS Pathog* 11, e1005264.

Bénit, L., Dessen, P., and Heidmann, T. (2001). Identification, phylogeny, and evolution of retroviral elements based on their envelope genes. *J. Virol.* 75, 11709–11719.

Bhatt, S., Gething, P.W., Brady, O.J., Messina, J.P., Farlow, A.W., Moyes, C.L., Drake, J.M., Brownstein, J.S., Hoen, A.G., Sankoh, O., et al. (2013). The global distribution and burden of dengue. *Nature* 496, 504–507.

Birkenheuer, C.H., Brewster, C.D., Quackenbush, S.L., and Rovnak, J. (2015). Retroviral cyclin controls cyclin-dependent kinase 8-mediated transcription elongation and reinitiation. *J. Virol.* 89, 5450–5461.

Boeke, J.D., and Stoye, J.P. (1997). Retrotransposons, endogenous retroviruses, and the evolution of retroelements. In *Retroviruses*, (Cold Spring Harbor, NY, USA: Cold Spring Harbor), p.

Brägelmann, J., Klümper, N., Offermann, A., von Mässenhausen, A., Böhm, D., Deng, M., Queisser, A., Sanders, C., Syring, I., Merseburger, A.S., et al. (2017). Pan-cancer analysis of the mediator complex transcriptome identifies CDK19 and CDK8 as therapeutic targets in advanced prostate cancer. *Clin Cancer Res* 23, 1829–1840.

Brewster, C.D., Birkenheuer, C.H., Vogt, M.B., Quackenbush, S.L., and Rovnak, J. (2011). The retroviral cyclin of walleye dermal sarcoma virus binds cyclin-dependent kinases 3 and 8. *Virology* 409, 299–307.

Buchfink, B., Xie, C., and Huson, D.H. (2015). Fast and sensitive protein alignment using DIAMOND. *Nat Methods* 12, 59–60.

- Burmeister, T. (2001). Oncogenic retroviruses in animals and humans. *Rev. Med. Virol.* *11*, 369–380.
- Butler, M., Chotiwan, N., Brewster, C.D., DiLisio, J.E., Ackart, D.F., Podell, B.K., Basaraba, R.J., Perera, R., Quackenbush, S.L., and Rovnak, J. (2020). Cyclin-dependent kinases 8 and 19 regulate host cell metabolism during dengue virus serotype 2 infection. *Viruses* *12*, 654.
- Byk, L.A., and Gamarnik, A.V. (2016). Properties and functions of the dengue virus capsid protein. *Annu. Rev. Virol.* *3*, 263–281.
- Byk, L.A., Iglesias, N.G., Maio, F.A.D., Gebhard, L.G., Rossi, M., and Gamarnik, A.V. (2016). Dengue virus genome uncoating requires ubiquitination. *MBio* *7*, e00804-16.
- Camacho, C., Coulouris, G., Avagyan, V., Ma, N., Papadopoulos, J., Bealer, K., and Madden, T.L. (2009). BLAST+: architecture and applications. *BMC Bioinformatics* *10*, 421.
- Cao, L., Chen, F., Yang, X., Xu, W., Xie, J., and Yu, L. (2014). Phylogenetic analysis of CDK and cyclin proteins in premetazoan lineages. *BMC Evol Biol* *14*, 10.
- Capella-Gutierrez, S., Silla-Martinez, J.M., and Gabaldon, T. (2009). trimAl: a tool for automated alignment trimming in large-scale phylogenetic analyses. *Bioinformatics* *25*, 1972–1973.
- Carnec, X., Meertens, L., Dejarnac, O., Perera-Lecoin, M., Hafirassou, M.L., Kitaura, J., Ramdasi, R., Schwartz, O., and Amara, A. (2016). The phosphatidylserine and phosphatidylethanolamine receptor CD300a binds dengue virus and enhances infection. *J. Virol.* *90*, 92–102.
- Caspritz, G., and Hadden, J. (1987). The immunopharmacology of immunotoxicology, and immunorestitution. *Toxicol Pathol* *15*, 320–332.
- Chang, Y., Moore, P.S., and Weiss, R.A. (2017). Human oncogenic viruses: nature and discovery. *Phil. Trans. R. Soc. B* *372*, 20160264.
- Chao, C.-H., Wu, W.-C., Lai, Y.-C., Tsai, P.-J., Perng, G.-C., Lin, Y.-S., and Yeh, T.-M. (2019). Dengue virus nonstructural protein 1 activates platelets via Toll-like receptor 4, leading to thrombocytopenia and hemorrhage. *PLoS Pathog* *15*, e1007625.
- Chatel-Chaix, L., Fischl, W., Scaturro, P., Cortese, M., Kallis, S., Bartenschlager, M., Fischer, B., and Bartenschlager, R. (2015). A combined genetic-proteomic approach identifies residues within dengue virus NS4B critical for interaction with NS3 and viral replication. *J. Virol.* *89*, 7170–7186.
- Chatel-Chaix, L., Cortese, M., Romero-Brey, I., Bender, S., Neufeldt, C.J., Fischl, W., Scaturro, P., Schieber, N., Schwab, Y., Fischer, B., et al. (2016). Dengue virus perturbs

mitochondrial morphodynamics to dampen innate immune responses. *Cell Host & Microbe* 20, 342–356.

Chen, H.-R., Chuang, Y.-C., Lin, Y.-S., Liu, H.-S., Liu, C., Perng, G.-C., and Yeh, T.-M. (2016). Dengue virus nonstructural protein 1 induces vascular leakage through macrophage migration inhibitory factor and autophagy. *PLOS Neglected Tropical Diseases* 19.

Chen, H.-R., Lai, Y.-C., and Yeh, T.-M. (2018). Dengue virus non-structural protein 1: a pathogenic factor, therapeutic target, and vaccine candidate. 11.

Chen, K., Liu, J., and Cao, X. (2017a). Regulation of type I interferon signaling in immunity and inflammation: A comprehensive review. *Journal of Autoimmunity* 83, 1–11.

Chen, M., Liang, J., Ji, H., Yang, Z., Altiglia, S., Hu, B., Schronce, A., McDermott, M.S.J., Schools, G.P., Lim, C., et al. (2017b). CDK8/19 Mediator kinases potentiate induction of transcription by NFκB. *Proc Natl Acad Sci USA* 114, 10208–10213.

Chen, S., Wu, Z., Wang, M., and Cheng, A. (2017c). Innate immune evasion mediated by flaviviridae non-structural proteins. *Viruses* 9, 291.

Chen, Y., Maguire, T., Hileman, R.E., Fromm, J.R., Esko, J.D., Linhardt, R.J., and Marks, R.M. (1997). Dengue virus infectivity depends on envelope protein binding to target cell heparan sulfate. *Nat Med* 3, 866–871.

Chotiwan, N., Andre, B.G., Sanchez-Vargas, I., Islam, M.N., Grabowski, J.M., Hopf-Jannasch, A., Gough, E., Nakayasu, E., Blair, C.D., Belisle, J.T., et al. (2018). Dynamic remodeling of lipids coincides with dengue virus replication in the midgut of *Aedes aegypti* mosquitoes. *PLoS Pathog* 14, e1006853.

Cianciolo, G., Copeland, T., Oroszlan, S., and Snyderman, R. (1985). Inhibition of lymphocyte proliferation by a synthetic peptide homologous to retroviral envelope proteins. *Science* 230, 453–455.

Clarke, P.A., Ortiz-Ruiz, M.-J., TePoele, R., Adeniji-Popoola, O., Box, G., Court, W., Czasch, S., El Bawab, S., Esdar, C., Ewan, K., et al. (2016). Assessing the mechanism and therapeutic potential of modulators of the human Mediator complex-associated protein kinases. *ELife* 5, e20722.

Clayton, D.A., and Shadel, G.S. (2014). Isolation of mitochondria from tissue culture cells. *Cold Spring Harbor Protocols* 2014, pdb.prot080002-pdb.prot080002.

Clum, S., Ebner, K.E., and Padmanabhan, R. (1997). Cotranslational membrane insertion of the serine proteinase precursor NS2B-NS3(Pro) of dengue virus type 2 is required for efficient in vitro processing and is mediated through the hydrophobic regions of NS2B. *The Journal of Biological Chemistry* 272, 30715–30723.

- Cousens, C., Minguignon, E., Dalziel, R.G., Ortin, A., Garcia, M., Park, J., Gonzalez, L., Sharp, J.M., and de las Heras, M. (1999). Complete sequence of enzootic nasal tumor virus, a retrovirus associated with transmissible intranasal tumors of sheep. *J. Virol.* *73*, 3986–3993.
- Cross, S., Kapuscinski, M., Perino, J., Maertens, B., Weger-Lucarelli, J., Ebel, G., and Stenglein, M. (2018). Co-infection patterns in individual *Ixodes scapularis* ticks reveal associations between viral, eukaryotic and bacterial microorganisms. *Viruses* *10*, 388.
- Dalrymple, N., and Mackow, E.R. (2011). Productive dengue virus infection of human endothelial cells is directed by heparan sulfate-containing proteoglycan receptors. *Journal of Virology* *85*, 9478–9485.
- Darriba, D., Posada, D., Kozlov, A.M., Stamatakis, A., Morel, B., and Flouri, T. (2020). ModelTest-NG: A new and scalable tool for the selection of DNA and protein evolutionary models. *Molecular Biology and Evolution* *37*, 291–294.
- Datan, E., Roy, S.G., Germain, G., Zali, N., McLean, J.E., Golshan, G., Harbajan, S., Lockshin, R.A., and Zakeri, Z. (2016). Dengue-induced autophagy, virus replication and protection from cell death require ER stress (PERK) pathway activation. *Cell Death Dis* *7*, e2127–e2127.
- Dauletbaev, N., Cammisano, M., Herscovitch, K., and Lands, L.C. (2015). Stimulation of the RIG-I/MAVS pathway by polyinosinic:polycytidylic acid upregulates IFN- β in airway epithelial cells with minimal costimulation of IL-8. *J.I.* *195*, 2829–2841.
- De Maio, F.A., Risso, G., Iglesias, N.G., Shah, P., Pozzi, B., Gebhard, L.G., Mammi, P., Mancini, E., Yanovsky, M.J., Andino, R., et al. (2016). The Dengue virus NS5 protein intrudes in the cellular spliceosome and modulates splicing. *PLoS Pathog* *12*, e1005841.
- Dejarnac, O., Hafirassou, M.L., Chazal, M., Versapuech, M., Gaillard, J., Perera-Lecoin, M., Umana-Diaz, C., Bonnet-Madin, L., Carnec, X., Tinevez, J.-Y., et al. (2018). TIM-1 ubiquitination mediates dengue virus entry. *Cell Reports* *23*, 1779–1793.
- Donehower, L.A., Bohannon, R.C., Ford, R.J., and Gibbs, R.A. (1990). The use of primers from highly conserved pol regions to identify uncharacterized retroviruses by the polymerase chain reaction. *Journal of Virological Methods* *28*, 33–46.
- Donner, A.J., Ebmeier, C.C., Taatjes, D.J., and Espinosa, J.M. (2010). CDK8 is a positive regulator of transcriptional elongation within the serum response network. *Nat Struct Mol Biol* *17*, 194–201.
- Doyle, S.E., Vaidya, S.A., O'Connell, R., Dadgostar, H., Dempsey, P.W., Wu, T.-T., Rao, G., Sun, R., Haberland, M.E., Modlin, R.L., et al. (2002). IRF3 mediates a TLR3/TLR4-specific antiviral gene program. *Immunity* *17*, 251–263.

Du, W., Thanos, D., and Maniatis, T. (1993). Mechanisms of transcriptional synergism between distinct virus-inducible enhancer elements. *Cell* 74, 887–898.

Ecke, D.H., and Johnson, C.W. *Plague in Colorado* (Washington, D.C.: US Government Printing Office).

Edgil, D., Polacek, C., and Harris, E. (2006). Dengue virus utilizes a novel strategy for translation initiation when cap-dependent translation is inhibited. *JVI* 80, 2976–2986.

Egloff, M.-P., Benarroch, D., Selisko, B., Romette, J.-L., and Canard, B. (2002). An RNA cap (nucleoside-2'-O-)-methyltransferase in the flavivirus RNA polymerase NS5: Crystal structure and functional characterization. *The EMBO Journal* 21, 2757–2768.

Egloff, M.-P., Decroly, E., Malet, H., Selisko, B., Benarroch, D., Ferron, F., and Canard, B. (2007). Structural and functional analysis of methylation and 5'-RNA sequence requirements of short capped RNAs by the methyltransferase domain of dengue virus NS5. *Journal of Molecular Biology* 372, 723–736.

El-Bacha, T., Midlej, V., Pereira da Silva, A.P., Silva da Costa, L., Benchimol, M., Galina, A., and Da Poian, A.T. (2007). Mitochondrial and bioenergetic dysfunction in human hepatic cells infected with dengue 2 virus. *Biochimica et Biophysica Acta (BBA) - Molecular Basis of Disease* 1772, 1158–1166.

Falgout, B., Pethel, M., Zhang, Y.M., and Lai, C.J. (1991). Both nonstructural proteins NS2B and NS3 are required for the proteolytic processing of dengue virus nonstructural proteins. *Journal of Virology* 65, 2467–2475.

Falgout, B., Miller, R.H., and Lai, C.-J. (1993). Deletion analysis of dengue virus type 4 nonstructural protein NS2B: Identification of a domain required for NS2B-NS3 protease activity. *Journal of Virology* 67, 2034–2042.

Fant, C.B., and Taatjes, D.J. (2019). Regulatory functions of the Mediator kinases CDK8 and CDK19. *Transcription* 10, 76–90.

Fernandes-Siqueira, L.O., Zeidler, J.D., Sousa, B.G., Ferreira, T., and Da Poian, A.T. (2018). Anaplerotic role of glucose in the oxidation of endogenous fatty acids during dengue virus infection. *MSphere* 3, e00458-17.

Firestein, R., Bass, A.J., Kim, S.Y., Dunn, I.F., Silver, S.J., Guney, I., Freed, E., Ligon, A.H., Vena, N., Ogino, S., et al. (2008). CDK8 is a colorectal cancer oncogene that regulates β -catenin activity. *Nature* 455, 547–551.

Flint, J., Racaniello, V.R., Rall, G.F., and Skalka, A.M. (2015). *Principles of virology* (Washington, D.C.: ASM Press).

Fontaine, K.A., Sanchez, E.L., Camarda, R., and Lagunoff, M. (2015). Dengue virus induces and requires glycolysis for optimal replication. *J. Virol.* 89, 2358–2366.

- Frankel, A.D., and Young, J.A.T. (1998). HIV-1: Fifteen proteins and an RNA. *Annu. Rev. Biochem.* 67, 1–25.
- Fritz, R., Stiasny, K., and Heinz, F.X. (2008). Identification of specific histidines as pH sensors in flavivirus membrane fusion. *Journal of Cell Biology* 183, 353–361.
- Fu, L., Niu, B., Zhu, Z., Wu, S., and Li, W. (2012). CD-HIT: accelerated for clustering the next-generation sequencing data. *Bioinformatics* 28, 3150–3152.
- Galbraith, M.D., Donner, A.J., and Espinosa, J.M. (2010). CDK8: A positive regulator of transcription. *Transcription* 1, 4–12.
- Galbraith, M.D., Allen, M.A., Bensard, C.L., Wang, X., Schwinn, M.K., Qin, B., Long, H.W., Daniels, D.L., Hahn, W.C., Dowell, R.D., et al. (2013). HIF1A employs CDK8-Mediator to stimulate RNAPII elongation in response to hypoxia. *Cell* 153, 1327–1339.
- Galbraith, M.D., Andrysik, Z., Pandey, A., Hoh, M., Bonner, E.A., Hill, A.A., Sullivan, K.D., and Espinosa, J.M. (2017). CDK8 kinase activity promotes glycolysis. *Cell Reports* 21, 1495–1506.
- Germi, R., Crance, J.-M., Garin, D., Guimet, J., Lortat-Jacob, H., Ruigrok, R.W.H., Zarski, J.-P., and Drouet, E. (2002). Heparan sulfate-mediated binding of infectious dengue virus type 2 and yellow fever virus. *Virology* 292, 162–168.
- Gifford, R., Kabat, P., Martin, J., Lynch, C., and Tristem, M. (2005). Evolution and distribution of class II-related endogenous retroviruses. *JVI* 79, 6478–6486.
- Gifford, R.J., Blomberg, J., Coffin, J.M., Fan, H., Heidmann, T., Mayer, J., Stoye, J., Tristem, M., and Johnson, W.E. (2018). Nomenclature for endogenous retrovirus (ERV) loci. *Retrovirology* 15, 59.
- Gillespie, L.K., Hoenen, A., Morgan, G., and Mackenzie, J.M. (2010). The endoplasmic reticulum provides the membrane platform for biogenesis of the flavivirus replication complex. *JVI* 84, 10438–10447.
- Giraldo, M.I., Vargas-Cuartas, O., Gallego-Gomez, J.C., Shi, P.-Y., Padilla-Sanabria, L., Castaño-Osorio, J.C., and Rajsbaum, R. (2018). K48-linked polyubiquitination of dengue virus NS1 protein inhibits its interaction with the viral partner NS4B. *Virus Research* 246, 1–11.
- Gitlin, L., Barchet, W., Gilfillan, S., Cella, M., Beutler, B., Flavell, R.A., Diamond, M.S., and Colonna, M. (2006). Essential role of mda-5 in type I IFN responses to polyriboinosinic:polyribocytidylic acid and encephalomyocarditis picornavirus. *Proceedings of the National Academy of Sciences* 103, 8459–8464.
- Gossmann, T.I., Shanmugasundram, A., Börno, S., Duvaux, L., Lemaire, C., Kuhl, H., Klages, S., Roberts, L.D., Schade, S., Gostner, J.M., et al. (2019). Ice-Age climate

adaptations trap the alpine marmot in a state of low genetic diversity. *Current Biology* 29, 1712-1720.e7.

Goubau, D., Deddouche, S., and Reis e Sousa, C. (2013). Cytosolic sensing of viruses. *Immunity* 38, 855–869.

Graff, S., Moore, D.H., Stanley, W., Randall, H., and Haagensen, C.D. (1949). Isolation of mouse mammary carcinoma virus. *Cancer* 2, 755–762.

Green, A.M., Beatty, P.R., Hadjilaou, A., and Harris, E. (2014). Innate immunity to dengue virus infection and subversion of antiviral responses. *Journal of Molecular Biology* 426, 1148–1160.

Griffin, K.A., Martin, D.J., Rosen, L.E., Sirochman, M.A., Walsh, D.P., Wolfe, L.L., and Miller, M.W. (2010). Detection of *Yersinia pestis* DNA in prairie dog–associated fleas by polymerase chain reaction assay of purified DNA. *Journal of Wildlife Diseases* 46, 636–643.

Gullberg, R.C., Steel, J.J., Pujari, V., Rovnak, J., Crick, D.C., and Perera, R. (2018). Stearoyl-CoA desaturase 1 differentiates early and advanced dengue virus infections and determines virus particle infectivity. *PLoS Pathog* 14, e1007261.

Guzman, M.G., and Harris, E. (2015). Dengue. *The Lancet* 385, 453–465.

Haas, R., Smith, J., Rocher-Ros, V., Nadkarni, S., Montero-Melendez, T., D'Acquisto, F., Bland, E.J., Bombardieri, M., Pitzalis, C., Perretti, M., et al. (2015). Lactate regulates metabolic and pro-inflammatory circuits in control of T Cell migration and effector functions. *PLoS Biol* 13, e1002202.

Halstead, S.B. (2007). Dengue. *The Lancet* 370, 1644–1652.

Hanahan, D., and Weinberg, R.A. (2011). Hallmarks of cancer: The next generation. *Cell* 144, 646–674.

Hannemann, H., Sung, P.-Y., Chiu, H.-C., Yousuf, A., Bird, J., Lim, S.P., and Davidson, A.D. (2013). Serotype-specific differences in dengue virus non-structural protein 5 nuclear localization. *J. Biol. Chem.* 288, 22621–22635.

Hardwicke, K. (2006). Prairie dogs, plants, and pollinators: Tri-trophic interactions affect plant-insect floral visitor webs in shortgrass steppe. Colorado State University.

Hardy, W.D., Old, L.J., Hess, P.W., Essex, M., and Cotter, S. (1973). Horizontal transmission of feline leukaemia virus. *Nature* 244, 266–269.

Hardy, W.D., McClelland, A.J., MacEwen, E.G., Hess, P.W., Hayes, A.A., and Zuckerman, E.E. (1977). The epidemiology of the feline leukemia virus (FeLV). *Cancer* 39, 1850–1855.

Hartmann, K. (2012). Clinical aspects of feline retroviruses: A review. *Viruses* 4, 2684–2710.

Hayward, W.S., Neel, B.G., and Astrin, S.M. (1981). Activation of a cellular onc gene by promoter insertion in ALV-induced lymphoid leukosis. *Nature* 290, 475–480.

He, Z., Zhu, X., Wen, W., Yuan, J., Hu, Y., Chen, J., An, S., Dong, X., Lin, C., Yu, J., et al. (2016). Dengue virus subverts host innate immunity by targeting adaptor protein MAVS. *J. Virol.* 90, 7219–7230.

Heaton, N.S., and Randall, G. (2010). Dengue virus-induced autophagy regulates lipid metabolism. *Cell Host & Microbe* 8, 422–432.

Heaton, N.S., Perera, R., Berger, K.L., Khadka, S., LaCount, D.J., Kuhn, R.J., and Randall, G. (2010). Dengue virus nonstructural protein 3 redistributes fatty acid synthase to sites of viral replication and increases cellular fatty acid synthesis. *Proceedings of the National Academy of Sciences* 107, 17345–17350.

Henzy, J.E., and Coffin, J.M. (2013). Betaretroviral envelope subunits are noncovalently associated and restricted to the mammalian class. *Journal of Virology* 87, 1937–1946.

Hizi, A., and Herschhorn, A. (2008). Retroviral reverse transcriptases (other than those of HIV-1 and murine leukemia virus): A comparison of their molecular and biochemical properties. *Virus Research* 134, 203–220.

Hizi, A., and Herzig, E. (2015). dUTPase: the frequently overlooked enzyme encoded by many retroviruses. *Retrovirology* 12, 70.

Hizi, A., Henderson, L.E., Copeland, T.D., Sowder, R.C., Hixson, C.V., and Oroszlan, S. (1987). Characterization of mouse mammary tumor virus gag-pro gene products and the ribosomal frameshift site by protein sequencing. *Proceedings of the National Academy of Sciences* 84, 7041–7045.

Honda, K., Takaoka, A., and Taniguchi, T. (2006). Type I interferon gene induction by the interferon regulatory factor family of transcription factors. *Immunity* 25, 349–360.

Hoover, E.A., Rojko, J.L., and Olsen, R.G. (1980). Pathogenesis of feline leukemia virus infection. In *Feline Leukemia*, (Boca Raton, FL, USA: CRC Press), pp. 32–51.

Hoover, E.A., Mullins, J.I., Quackenbush, S.L., and Gasper, P.W. (1987). Experimental transmission and pathogenesis of immunodeficiency syndrome in cats. *Blood* 70, 1880–1892.

Hornung, V., Ellegast, J., Kim, S., Brzozka, K., Jung, A., Kato, H., Akira, S., Conzelmann, K.-K., Schlee, M., Endres, S., et al. (2006). 5'-Triphosphate RNA is the ligand for RIG-I. *Science* 314, 994–997.

- Iglesias, N.G., Filomatori, C.V., and Gamarnik, A.V. (2011). The F1 motif of dengue virus polymerase NS5 is involved in promoter-dependent RNA synthesis. *Journal of Virology* 85, 5745–5756.
- Isaacs, A., and Lindenmann, J. (1987). Virus interference. I. The interferon. *Journal of Interferon and Cytokine Research* 7, 429–438.
- Ivashkiv, L.B., and Donlin, L.T. (2014). Regulation of type I interferon responses. *Nat Rev Immunol* 14, 36–49.
- Iwasaki, A. (2012). A virological view of innate immune recognition. *Annu. Rev. Microbiol.* 66, 177–196.
- Jarrett, W.F.H., Martin, W.B., Crichton, G.W., Dalton, R.G., and Stewart, M.F. (1964). Leukaemia in the cat. *Nature* 202, 566–567.
- Jensen, S., and Thomsen, A.R. (2012). Sensing of RNA viruses: A review of innate immune receptors involved in recognizing RNA virus invasion. *Journal of Virology* 86, 2900–2910.
- Jeronimo, C., and Robert, F. (2017). The Mediator Complex: At the Nexus of RNA Polymerase II Transcription. *Trends in Cell Biology* 27, 765–783.
- Ježek, J., Smethurst, D.G.J., Stieg, D.C., Kiss, Z.A.C., Hanley, S.E., Ganesan, V., Chang, K.-T., Cooper, K.F., and Strich, R. (2019). Cyclin C: The story of a non-cycling cyclin. *Biology* 8, 3.
- Jezek, J., Chang, K., Joshi, A.M., and Strich, R. (2019). Mitochondrial translocation of cyclin C stimulates intrinsic apoptosis through Bax recruitment. *EMBO Rep* 20.
- Johannessen, L., Sundberg, T.B., O'Connell, D.J., Kolde, R., Berstler, J., Billings, K.J., Khor, B., Seashore-Ludlow, B., Fassl, A., Russell, C.N., et al. (2017). Small-molecule studies identify CDK8 as a regulator of IL-10 in myeloid cells. *Nat Chem Biol* 13, 1102–1108.
- Johansson, M., Brooks, A.J., Jans, D.A., and Vasudevan, S.G. (2001). A small region of the dengue virus-encoded RNA-dependent RNA polymerase, NS5, confers interaction with both the nuclear transport receptor importin- β and the viral helicase, NS3. *Journal of General Virology* 82, 735–745.
- John, S., Weiss, J.N., and Ribalet, B. (2011). Subcellular localization of hexokinases I and II directs the metabolic fate of glucose. *PLoS ONE* 6, e17674.
- Johnston, E.R., and Radke, K. (2000). The SU and TM envelope protein subunits of bovine leukemia virus are linked by disulfide bonds, both in cells and in virions. *J. Virol.* 74, 2930–2935.

- Jordan, T.X., and Randall, G. (2017). Dengue virus activates the AMP kinase-mTOR axis to stimulate a proviral lipophagy. *J Virol* 91, e02020-16, e02020-16.
- Junhui, Z., Ruifu, Y., Jianchun, L., Songle, Z., Meiling, C., Fengxiang, C., and Hong, C. (1996). Detection of *Francisella tularensis* by the polymerase chain reaction. *Journal of Medical Microbiology* 45, 477–482.
- Junjhon, J., Lausumpao, M., Supasa, S., Noisakran, S., Songjaeng, A., Saraithong, P., Chaichoun, K., Utaipat, U., Keelapang, P., Kanjanahaluethai, A., et al. (2008). Differential modulation of prM cleavage, extracellular particle distribution, and virus infectivity by conserved residues at nonfurin consensus positions of the dengue virus prM junction. *JVI* 82, 10776–10791.
- Kao, J.-C., HuangFu, W.-C., Tsai, T.-T., Ho, M.-R., Jhan, M.-K., Shen, T.-J., Tseng, P.-C., Wang, Y.-T., and Lin, C.-F. (2018). The antiparasitic drug niclosamide inhibits dengue virus infection by interfering with endosomal acidification independent of mTOR. *PLoS Negl Trop Dis* 12, e0006715.
- Kapoor, M., Zhang, L., Ramachandra, M., Kusukawa, J., Ebner, K.E., and Padmanabhan, R. (1995). Association between NS3 and NS5 proteins of dengue virus type 2 in the putative RNA replicase is linked to differential phosphorylation of NS5. *The Journal of Biological Chemistry* 270, 19100–19106.
- Kato, H., Takeuchi, O., Sato, S., Yoneyama, M., Yamamoto, M., Matsui, K., Uematsu, S., Jung, A., Kawai, T., Ishii, K.J., et al. (2006). Differential roles of MDA5 and RIG-I helicases in the recognition of RNA viruses. *Nature* 441, 101–105.
- Kato, H., Takeuchi, O., Mikamo-Satoh, E., Hirai, R., Kawai, T., Matsushita, K., Hiiragi, A., Dermody, T.S., Fujita, T., and Akira, S. (2008). Length-dependent recognition of double-stranded ribonucleic acids by retinoic acid-inducible gene-I and melanoma differentiation-associated gene 5. *Journal of Experimental Medicine* 205, 1601–1610.
- Katoh, K., and Standley, D.M. (2013). MAFFT multiple sequence alignment software version 7: Improvements in performance and usability. *Molecular Biology and Evolution* 30, 772–780.
- Kim, J.-H., Kim, T.-H., Lee, H.-C., Nikapitiya, C., Uddin, M.B., Park, M.-E., Pathinayake, P., Lee, E.S., Chaturanga, K., Herath, T.U.B., et al. (2017). Rubicon modulates antiviral type I interferon (IFN) signaling by targeting IFN regulatory factor 3 dimerization. *J Virol* 91, e00248-17, e00248-17.
- Kinney, R.M., Butrapet, S., Chang, G.-J.J., Tsuchiya, K.R., Roehrig, J.T., Bhamarapravati, N., and Gubler, D.J. (1997). Construction of infectious cDNA clones for dengue 2 virus: strain 16681 and its attenuated vaccine derivative, strain PDK-53. *Virology* 230, 300–308.

- Klema, V.J., Ye, M., Hindupur, A., Teramoto, T., Gottipati, K., Padmanabhan, R., and Choi, K.H. (2016). Dengue virus nonstructural protein 5 (NS5) assembles into a dimer with a unique methyltransferase and polymerase interface. *PLOS Pathogens* 12.
- Knuesel, M.T., Meyer, K.D., Bernecky, C., and Taatjes, D.J. (2009). The human CDK8 subcomplex is a molecular switch that controls Mediator coactivator function. *Genes & Development* 23, 439–451.
- Kotliar, B., Miller, B.J., Reading, R.P., and Clark, T.W. (2006). *The prairie dog as a keystone species* (Washington, D.C.: Island Press).
- Kozak, C.A., and Ruscetti, S. (1992). Retroviruses in rodents. In *The Retroviridae*, (New York, NY: Plenum Press), pp. 405–481.
- Krishnan, M.N., Sukumaran, B., Pal, U., Agaisse, H., Murray, J.L., Hodge, T.W., and Fikrig, E. (2007). Rab 5 is required for the cellular entry of dengue and West Nile viruses. *JVI* 81, 4881–4885.
- Kuhn, R.J., Zhang, W., Rossmann, M.G., Pletnev, S.V., Lenches, E., Jones, C.T., Mukhopadhyay, S., Strauss, E.G., Baker, T.S., and Strauss, J.H. (2014). Structure of dengue virus: Implications for flavivirus organization, maturation, and fusion. 20.
- Kumar, A., Buhler, S., Selisko, B., Davidson, A., Mulder, K., Canard, B., Miller, S., and Bartenschlager, R. (2013). Nuclear localization of dengue virus nonstructural protein 5 does not strictly correlate with efficient viral RNA replication and inhibition of type I interferon signaling. *Journal of Virology* 87, 4545–4557.
- Langmead, B., and Salzberg, S.L. (2012). Fast gapped-read alignment with Bowtie 2. *Nat Methods* 9, 357–359.
- Laue, T., Emmerich, P., and Schmitz, H. (1999). Detection of dengue virus RNA in patients after primary or secondary dengue infection by using the TaqMan automated amplification system. *Journal of Clinical Microbiology* 37, 2543–2547.
- Leamson, R.N., and Halpern, M.S. (1976). Subunit structure of the glycoprotein complex of avian tumor virus. *Journal of Virology* 18, 956–968.
- LeBlanc, J., Weil, J., and Beemon, K. (2013). Posttranscriptional regulation of retroviral gene expression: Primary RNA transcripts play three roles as pre-mRNA, mRNA, and genomic RNA. *WIREs RNA* 4, 567–580.
- Lee, C.M., Xie, X., Zou, J., Li, S.-H., Lee, M.Y.Q., Dong, H., Qin, C.-F., Kang, C., and Shi, P.-Y. (2015). Determinants of dengue virus NS4A protein oligomerization. *J. Virol.* 89, 6171–6183.
- Lee, J.-H., Liu, R., Li, J., Zhang, C., Wang, Y., Cai, Q., Qian, X., Xia, Y., Zheng, Y., Piao, Y., et al. (2017). Stabilization of phosphofructokinase 1 platelet isoform by AKT promotes tumorigenesis. *Nat Commun* 8, 949.

- Lee, Y.-R., Lei, H.-Y., Liu, M.-T., Wang, J.-R., Chen, S.-H., Jiang-Shieh, Y.-F., Lin, Y.-S., Yeh, T.-M., Liu, C.-C., and Liu, H.-S. (2008). Autophagic machinery activated by dengue virus enhances virus replication. *Virology* 374, 240–248.
- Lee, Y.-R., Hu, H.-Y., Kuo, S.-H., Lei, H.-Y., Lin, Y.-S., Yeh, T.-M., Liu, C.-C., and Liu, H.-S. (2013). Dengue virus infection induces autophagy: an in vivo study. 11.
- Letunic, I., and Bork, P. (2019). Interactive Tree Of Life (iTOL) v4: recent updates and new developments. *Nucleic Acids Research* 47, W256–W259.
- Li, H., Clum, S., You, S., Ebner, K.E., and Padmanabhan, R. (1999). The serine protease and RNA-stimulated nucleoside triphosphatase and RNA helicase functional domains of dengue virus type 2 NS3 converge within a region of 20 amino acids. *J. Virol.* 73, 3108–3116.
- Li, K., Zhang, S., Kronqvist, M., Wallin, M., Ekström, M., Derse, D., and Garoff, H. (2008a). Intersubunit disulfide isomerization controls membrane fusion of human T-Cell leukemia virus Env. *JVI* 82, 7135–7143.
- Li, L., Lok, S.-M., Yu, I.-M., Zhang, Y., Kuhn, R.J., Chen, J., and Rossmann, M.G. (2008b). The flavivirus precursor membrane-envelope protein complex: Structure and maturation. 319, 6.
- Li, Y., Li, Q., Wong, Y.L., Liew, L.S.Y., and Kang, C. (2015). Membrane topology of NS2B of dengue virus revealed by NMR spectroscopy. *Biochimica et Biophysica Acta (BBA) - Biomembranes* 1848, 2244–2252.
- Li, Y., Wong, Y.L., Lee, M.Y., Li, Q., Wang, Q.-Y., Lescar, J., Shi, P.-Y., and Kang, C. (2016). Secondary structure and membrane topology of the full-length dengue virus NS4B in micelles. *Angew. Chem. Int. Ed.* 55, 12068–12072.
- Li, Y., Lee, M.Y., Loh, Y.R., and Kang, C. (2018). Secondary structure and membrane topology of dengue virus NS4A protein in micelles. *Biochimica et Biophysica Acta (BBA) - Biomembranes* 1860, 442–450.
- Liao, M., Martín, C.S.-S., Zheng, A., and Kielian, M. (2010). In vitro reconstitution reveals key intermediate states of trimer formation by the dengue virus membrane fusion protein. *JVI* 84, 5730–5740.
- Lobigs, M. (1993). Flavivirus premembrane protein cleavage and spike heterodimer secretion require the function of the viral proteinase NS3. *Proceedings of the National Academy of Sciences* 90, 6218–6222.
- Loo, Y.-M., Fornek, J., Crochet, N., Bajwa, G., Perwitasari, O., Martinez-Sobrido, L., Akira, S., Gill, M.A., García-Sastre, A., Katze, M.G., et al. (2008). Distinct RIG-I and MDA5 signaling by RNA viruses in innate immunity. *JVI* 82, 335–345.

- Lozach, P.-Y., Burleigh, L., Staropoli, I., Navarro-Sanchez, E., Harriague, J., Virelizier, J.-L., Rey, F.A., Desprès, P., Arenzana-Seisdedos, F., and Amara, A. (2005). Dendritic cell-specific intercellular adhesion molecule 3-grabbing non-integrin (DC-SIGN)-mediated enhancement of dengue virus infection is independent of DC-SIGN internalization signals. *J. Biol. Chem.* *280*, 23698–23708.
- Lu, B., Ren, Y., Sun, X., Han, C., Wang, H., Chen, Y., Peng, Q., Cheng, Y., Cheng, X., Zhu, Q., et al. (2017). Induction of INK1T1 by viral infection negatively regulates antiviral responses through inhibiting phosphorylation of p65 and IRF3. *Cell Host & Microbe* *22*, 86-98.e4.
- Luo, D., Xu, T., Hunke, C., Grüber, G., Vasudevan, S.G., and Lescar, J. (2008a). Crystal structure of the NS3 protease-helicase from dengue virus. *JVI* *82*, 173–183.
- Luo, D., Xu, T., Watson, R.P., Scherer-Becker, D., Sampath, A., Jahnke, W., Yeong, S.S., Wang, C.H., Lim, S.P., Strongin, A., et al. (2008b). Insights into RNA unwinding and ATP hydrolysis by the flavivirus NS3 protein. *EMBO J* *27*, 3209–3219.
- Luo, D., Wei, N., Doan, D.N., Paradkar, P.N., Chong, Y., Davidson, A.D., Kotaka, M., Lescar, J., and Vasudevan, S.G. (2010). Flexibility between the protease and helicase domains of the dengue virus NS3 protein conferred by the linker region and its functional implications. *The Journal of Biological Chemistry* *285*, 18817–18827.
- Luo, D., Vasudevan, S.G., and Lescar, J. (2015). The flavivirus NS2B–NS3 protease–helicase as a target for antiviral drug development. *Antiviral Research* *118*, 148–158.
- Ma, L., Jones, C.T., Groesch, T.D., Kuhn, R.J., and Post, C.B. (2004). Solution structure of dengue virus capsid protein reveals another fold. *Proceedings of the National Academy of Sciences* *101*, 3414–3419.
- Mackenzie, J.M., Jones, M.K., and Young, P.R. (1996). Immunolocalization of the dengue virus nonstructural glycoprotein NS1 suggests a role in viral RNA replication. *Virology* *220*, 232–240.
- Maeda, N., Fan, H., and Yoshikai, Y. (2008). Oncogenesis by retroviruses: old and new paradigms. *Rev. Med. Virol.* *18*, 387–405.
- Magden, E., Miller, C., MacMillan, M., Bielefeldt-Ohmann, H., Avery, A., Quackenbush, S.L., and VandeWoude, S. (2013). Acute virulent infection with feline immunodeficiency virus (FIV) results in lymphomagenesis via an indirect mechanism. *Virology* *436*, 284–294.
- Mager, D., and Stoye, J. Mammalian endogenous retroviruses. In *Mobile DNA III*, (Washington, D.C.: ASM Press), p.
- Mammerickx, M., Portetelle, D., de Clercq, K., and Burny, A. (1987). Experimental transmission of enzootic bovine leukosis to cattle, sheep and goats: Infectious doses of blood and incubation period of the disease. *Leukemia Research* *11*, 353–358.

- Markoff, L., Falgout, B., and Chang, A. (1997). A conserved internal hydrophobic domain mediates the stable membrane integration of the dengue virus capsid protein. *Virology* 233, 105–117.
- Martin, M. (2011). Cutadapt removes adapter sequences from high-throughput sequencing reads. *EMBnet J* 17, 10–12.
- Martín-Acebes, M.A., Blázquez, A.-B., and Saiz, J.-C. (2015). Reconciling West Nile virus with the autophagic pathway. *Autophagy* 11, 861–864.
- Martinez-Lopez, N., and Singh, R. (2015). Autophagy and lipid droplets in the liver. *Annu. Rev. Nutr.* 35, 215–237.
- Martins, A.S., Martins, I.C., and Santos, N.C. (2018). Methods for lipid droplet biophysical characterization in flaviviridae infections. *Front. Microbiol.* 9, 1951.
- Mateo, R., Nagamine, C.M., Spagnolo, J., Méndez, E., Rahe, M., Gale, M., Yuan, J., and Kirkegaard, K. (2013). Inhibition of cellular autophagy deranges dengue virion maturation. *J. Virol.* 87, 1312–1321.
- Matsumoto, I., Chambers, J.K., Miwa, Y., Nakayama, H., and Uchida, K. (2017). Anaplastic large T-cell lymphoma in three black-tailed prairie dogs (*Cynomys ludovicianus*). *The Journal of Veterinary Medical Science* 79, 979–983.
- Mayer, K.A., Stöckl, J., Zlabinger, G.J., and Gualdoni, G.A. (2019). Hijacking the supplies: Metabolism as a novel facet of virus-host interaction. *Front. Immunol.* 10, 1533.
- McDermott, M.S.J., Chumanevich, A.A., Lim, C., Liang, J., Chen, M., Altiglia, S., Oliver, D., Rae, J.M., Shtutman, M., Kiaris, H., et al. (2017). Inhibition of CDK8 mediator kinase suppresses estrogen dependent transcription and the growth of estrogen receptor positive breast cancer. *Oncotarget* 8, 12558–12575.
- McLean, J.E., Wudzinska, A., Datan, E., Quaglino, D., and Zakeri, Z. (2011). Flavivirus NS4A-induced autophagy protects cells against death and enhances virus replication. *J. Biol. Chem.* 286, 22147–22159.
- Meertens, L., Carnec, X., Lecoin, M.P., Ramdasi, R., Guivel-Benhassine, F., Lew, E., Lemke, G., Schwartz, O., and Amara, A. (2012). The TIM and TAM families of phosphatidylserine receptors mediate dengue virus entry. *Cell Host & Microbe* 12, 544–557.
- Melo, C.F.O.R., Delafiori, J., Dabaja, M.Z., de Oliveira, D.N., Guerreiro, T.M., Colombo, T.E., Nogueira, M.L., Proenca-Modena, J.L., and Catharino, R.R. (2018). The role of lipids in the inception, maintenance and complications of dengue virus infection. *Sci Rep* 8, 11826.

Meyer, K.D., Donner, A.J., Knuesel, M.T., York, A.G., Espinosa, J.M., and Taatjes, and D.J. (2008). Cooperative activity of cdk8 and GCN5L within Mediator directs tandem phosphoacetylation of histone H3. *EMBO J.*

Michalska, A., Blaszczyk, K., Wesoly, J., and Bluysen, H.A.R. (2018). A positive feedback amplifier circuit that regulates interferon (IFN)-stimulated gene expression and controls type I and type II IFN responses. *Front. Immunol.* 9, 1135.

Miller, B.J., Reading, R.P., Biggins, D.E., Detling, J.K., Forrest, S.C., Hoogland, J.L., Javersak, J., Miller, S.D., Proctor, J., Truett, J., et al. (2007a). Prairie dogs: An ecological review and current biopolitics. *Journal of Wildlife Management* 71, 2801–2810.

Miller, J.L., deWet, B.J.M., Martinez-Pomares, L., Radcliffe, C.M., Dwek, R.A., Rudd, P.M., and Gordon, S. (2008). The mannose receptor mediates dengue virus infection of macrophages. *PLoS Pathog* 4.

Miller, S., Sparacio, S., and Bartenschlager, R. (2006). Subcellular localization and membrane topology of the dengue virus type 2 non-structural protein 4B. *J. Biol. Chem.* 281, 8854–8863.

Miller, S., Kastner, S., Krijnse-Locker, J., Bühler, S., and Bartenschlager, R. (2007b). The non-structural protein 4A of dengue virus is an integral membrane protein inducing membrane alterations in a 2K-regulated manner. *J. Biol. Chem.* 282, 8873–8882.

Miwa, Y., Matsunaga, S., Nakayama, H., Kurosawa, A., Ogawa, H., and Sasaki, N. (2006). Spontaneous lymphoma in a prairie dog (*Cynomys ludovicianus*). *Journal of the American Animal Hospital Association* 42, 151–153.

Miyinari, Y., Atsuzawa, K., Usuda, N., Watashi, K., Hishiki, T., Zayas, M., Bartenschlager, R., Wakita, T., Hijikata, M., and Shimotohno, K. (2007). The lipid droplet is an important organelle for hepatitis C virus production. *Nat Cell Biol* 9, 1089–1097.

Modis, Y., Ogata, S., Clements, D., and Harrison, S.C. (2003). A ligand-binding pocket in the dengue virus envelope glycoprotein. *Proceedings of the National Academy of Sciences* 100, 6986–6991.

Modis, Y., Ogata, S., Clements, D., and Harrison, S.C. (2004). Structure of the dengue virus envelope protein after membrane fusion. *Nature* 427, 313–319.

Modis, Y., Ogata, S., Clements, D., and Harrison, S.C. (2005). Variable surface epitopes in the crystal structure of dengue virus type 3 envelope glycoprotein. *JVI* 79, 1223–1231.

Moreno-Altamirano, M.M.B., Kolstoe, S.E., and Sánchez-García, F.J. (2019). Virus control of cell metabolism for replication and evasion of host immune responses. *Front. Cell. Infect. Microbiol.* 9, 95.

- Mosso, C., Galván-Mendoza, I.J., Ludert, J.E., and del Angel, R.M. (2008). Endocytic pathway followed by dengue virus to infect the mosquito cell line C6/36 HT. *Virology* 378, 193–199.
- Munoz-Jordan, J.L., Sanchez-Burgos, G.G., Laurent-Rolle, M., and Garcia-Sastre, A. (2003). Inhibition of interferon signaling by dengue virus. *Proceedings of the National Academy of Sciences* 100, 14333–14338.
- Muñoz-Jordán, J.L., Laurent-Rolle, M., Ashour, J., Martínez-Sobrido, L., Ashok, M., Lipkin, W.I., and García-Sastre, A. (2005). Inhibition of alpha/beta interferon signaling by the NS4B protein of Flaviviruses. *J. Virol.* 79, 8004–8013.
- Muszynski, K.W., Ohashi, T., Hanson, C., and Ruscetti, S.K. (1998). Both the polycythemia- and anemia-inducing strains of Friend spleen focus-forming virus induce constitutive activation of the Raf-1/mitogen-activated protein kinase signal transduction pathway. *J. Virol.* 72, 919–925.
- Muszynski, K.W., Thompson, D., Hanson, C., Lyons, R., Spadaccini, A., and Ruscetti, S.K. (2000). Growth factor-independent proliferation of erythroid cells infected with Friend spleen focus-forming virus is protein kinase C dependent but does not require Ras-GTP. *J. Virol.* 74, 8444–8451.
- Nasirudeen, A.M.A., Wong, H.H., Thien, P., Xu, S., Lam, K.-P., and Liu, D.X. (2011). RIG-I, MDA5 and TLR3 synergistically play an important role in restriction of dengue virus infection. *PLoS Negl Trop Dis* 5, e926.
- Navarro-Sanchez, E., Altmeyer, R., Amara, A., Schwartz, O., Fieschi, F., Virelizier, J.-L., Arenzana-Seisdedos, F., and Desprès, P. (2003). Dendritic-cell-specific ICAM3-grabbing non-integrin is essential for the productive infection of human dendritic cells by mosquito-cell-derived dengue viruses. *EMBO Reports* 4, 723–728.
- Neufeldt, C.J., Cortese, M., Scaturro, P., Cerikan, B., Wideman, J., Tabata, K., Moraes, T., Oleksiuk, O., Pichlmair, A., and Bartenschlager, R. (2019). ER-shaping Atlastin proteins act as central hubs to promote flavivirus replication and virion assembly. *Nature Microbiology* 4, 2416–2429.
- Ngo, A.M., Shurtleff, M.J., Popova, K.D., Kulsuptrakul, J., Weissman, J.S., and Puschnik, A.S. (2019). The ER membrane protein complex is required to ensure correct topology and stable expression of flavivirus polyproteins. *ELife* 8, e48469.
- Nguyen, N.M., Thi Hue Kien, D., Tuan, T.V., Quyen, N.T.H., Tran, C.N.B., Vo Thi, L., Thi, D.L., Nguyen, H.L., Farrar, J.J., Holmes, E.C., et al. (2013). Host and viral features of human dengue cases shape the population of infected and infectious *Aedes aegypti* mosquitoes. *Proceedings of the National Academy of Sciences* 110, 9072–9077.
- Nitsche, C. (2019). Proteases from dengue, West Nile and Zika viruses as drug targets. *Biophys Rev* 11, 157–165.

Odendall, C., and Kagan, J.C. (2017). Activation and pathogenic manipulation of the sensors of the innate immune system. *Microbes and Infection* 19, 229–237.

Opstelten, D.-J.E., Wallin, M., and Garoff, H. (1998). Moloney murine leukemia virus envelope protein subunits, gp70 and Pr15E, form a stable disulfide-linked complex. *J. VIROL.* 72, 11.

Orosz, C.G., Zinn, N.E., Olsen, R.G., and Mathes, L.E. (1985). Retrovirus-mediated immunosuppression. I. FeLV-UV and specific FeLV proteins alter T lymphocyte behavior by inducing hyporesponsiveness to lymphokines. *The Journal of Immunology* 134, 3396–3403.

Palmarini, M., Sharp, J.M., de las Heras, M., and Fan, H. (1999). Jaagsiekte sheep retrovirus is necessary and sufficient to induce a contagious lung cancer in sheep. *J. Virol.* 73, 6964–6972.

Pan American Health Organization, and World Health Organization Epidemiological update: Dengue.

Pang, T., Mak, T.K., and Gubler, D.J. (2017). Prevention and control of dengue—the light at the end of the tunnel. *The Lancet Infectious Diseases* 17, e79–e87.

Panne, D. (2008). The enhanceosome. *Current Opinion in Structural Biology* 18, 236–242.

Park, M.J., Shen, H., Spaeth, J.M., Tolvanen, J.H., Failor, C., Knudtson, J.F., McLaughlin, J., Halder, S.K., Yang, Q., Bulun, S.E., et al. (2018). Oncogenic exon 2 mutations in Mediator subunit MED12 disrupt allosteric activation of cyclin C-CDK8/19. *J. Biol. Chem.* 293, 4870–4882.

Parkin, D.M. (2006). The global health burden of infection-associated cancers in the year 2002. *Int. J. Cancer* 118, 3030–3044.

Pelish, H.E., Liao, B.B., Nitulescu, I.I., Tangpeerachaikul, A., Poss, Z.C., Da Silva, D.H., Caruso, B.T., Arefolov, A., Fadeyi, O., Christie, A.L., et al. (2015). Mediator kinase inhibition further activates super-enhancer-associated genes in AML. *Nature* 526, 273–276.

Peng, T., Wang, J.-L., Chen, W., Zhang, J.-L., Gao, N., Chen, Z.-T., Xu, X.-F., Fan, D.-Y., and An, J. (2009). Entry of dengue virus serotype 2 into ECV304 cells depends on clathrin-dependent endocytosis, but not on caveolae-dependent endocytosis. *Can. J. Microbiol.* 55, 139–145.

Perera, R., Riley, C., Isaac, G., Hopf-Jannasch, A.S., Moore, R.J., Weitz, K.W., Pasatolic, L., Metz, T.O., Adamec, J., and Kuhn, R.J. (2012). Dengue virus infection perturbs lipid homeostasis in infected mosquito cells. *PLoS Pathog* 8, e1002584.

- Perreira, J.M., Aker, A.M., Savidis, G., Chin, C.R., McDougall, W.M., Portmann, J.M., Meraner, P., Smith, M.C., Rahman, M., Baker, R.E., et al. (2015). RNASEK Is a V-ATPase-associated factor required for endocytosis and the replication of rhinovirus, influenza A virus, and dengue Virus. *Cell Reports* 12, 850–863.
- Plaščzyca, A., Scaturro, P., Neufeldt, C.J., Cortese, M., Cerikan, B., Ferla, S., Brancale, A., Pichlmair, A., and Bartenschlager, R. (2019). A novel interaction between dengue virus nonstructural protein 1 and the NS4A-2K-4B precursor is required for viral RNA replication but not for formation of the membranous replication organelle. *PLoS Pathog* 15, e1007736.
- Platanias, L.C. (2005). Mechanisms of type-I- and type-II-interferon-mediated signalling. *Nat Rev Immunol* 5, 375–386.
- Pleet, M.L., Branscome, H., DeMarino, C., Pinto, D.O., Zadeh, M.A., Rodriguez, M., Sariyer, I.K., El-Hage, N., and Kashanchi, F. (2018). Autophagy, EVs, and infections: A perfect question for a perfect time. *Front. Cell. Infect. Microbiol.* 8, 362.
- Poiesz, B.J., Ruscetti, F.W., Gazdar, A.F., Bunn, P.A., Minna, J.D., and Gallo, R.C. (1980). Detection and isolation of type C retrovirus particles from fresh and cultured lymphocytes of a patient with cutaneous T-cell lymphoma. *Proc Natl Acad Sci USA* 77, 7415–7419.
- Pokidysheva, E., Zhang, Y., Battisti, A.J., Bator-Kelly, C.M., Chipman, P.R., Xiao, C., Gregorio, G.G., Hendrickson, W.A., Kuhn, R.J., and Rossmann, M.G. (2006). Cryo-EM reconstruction of dengue virus in complex with the carbohydrate recognition domain of DC-SIGN. *Cell* 124, 485–493.
- Poli, A., Abramo, F., Baldinotti, F., Pistello, M., Da Prato, L., and Bendinelli, M. (1994). Malignant lymphoma associated with experimentally induced feline immunodeficiency virus infection. *Journal of Comparative Pathology* 110, 319–328.
- Porter, D.C., Farmaki, E., Altiglia, S., Schools, G.P., West, D.K., Chen, M., Chang, B.-D., Puzyrev, A.T., Lim, C. -u., Rokow-Kittell, R., et al. (2012). Cyclin-dependent kinase 8 mediates chemotherapy-induced tumor-promoting paracrine activities. *Proceedings of the National Academy of Sciences* 109, 13799–13804.
- Poss, Z.C., Ebmeier, C.C., Odell, A.T., Tangpeerachaikul, A., Lee, T., Pelish, H.E., Shair, M.D., Dowell, R.D., Old, W.M., and Taatjes, D.J. (2016). Identification of Mediator kinase substrates in human cells using cortistatin A and quantitative phosphoproteomics. *Cell Reports* 15, 436–450.
- Pryor, M.J., Rawlinson, S.M., Butcher, R.E., Barton, C.L., Waterhouse, T.A., Vasudevan, S.G., Bardin, P.G., Wright, P.J., Jans, D.A., and Davidson, A.D. (2007). Nuclear localization of dengue virus nonstructural protein 5 through its importin α/β -recognized nuclear localization sequences is integral to viral infection. *Traffic* 8, 795–807.

Quackenbush, S.L., Linton, A., Brewster, C.D., and Rovnak, J. (2009). Walleye dermal sarcoma virus rv-cyclin inhibits NF- κ B-dependent transcription. *Virology* 386, 55–60.

Randall, G. (2018). Lipid droplet metabolism during dengue virus infection. *Trends in Microbiology* 26, 640–642.

RC Team (2017). R: A language and environment for statistical computing (Vienna, Austria: R foundation for statistical computing).

Reddy, S.B.G., Chin, W.-X., and Shivananju, N.S. (2018). Dengue virus NS2 and NS4: Minor proteins, mammoth roles. *Biochemical Pharmacology* 154, 54–63.

Reid, D.W., Campos, R.K., Child, J.R., Zheng, T., Chan, K.W.K., Bradrick, S.S., Vasudevan, S.G., Garcia-Blanco, M.A., and Nicchitta, C.V. (2018). Dengue virus selectively annexes endoplasmic reticulum-associated translation machinery as a strategy for co-opting host cell protein synthesis. *J Virol* 92, e01766-17, [/jvi/92/7/e01766-17.atom](https://doi.org/10.1128/jvi.92.7.e01766-17).

Richard, A.S., Zhang, A., Park, S.-J., Farzan, M., Zong, M., and Choe, H. (2015). Virion-associated phosphatidylethanolamine promotes TIM1-mediated infection by Ebola, dengue, and West Nile viruses. *Proc Natl Acad Sci USA* 112, 14682–14687.

Richgels, K.L.D., Russell, R.E., Bron, G.M., and Rocke, T.E. (2016). Evaluation of *Yersinia pestis* transmission pathways for sylvatic plague in prairie dog populations in the western U.S. *EcoHealth* 13, 415–427.

Roberts, D.J., and Miyamoto, S. (2015). Hexokinase II integrates energy metabolism and cellular protection: Akt-ing on mitochondria and TORC-ing to autophagy. *Cell Death Differ* 22, 248–257.

Rosenberg, N., and Jolicoeur, P. (1997). *Retroviral pathogenesis* (Cold Spring Harbor, NY, USA: Cold Spring Harbor Laboratory Press).

Rothwell, C., LeBreton, A., Young Ng, C., Lim, J.Y.H., Liu, W., Vasudevan, S., Labow, M., Gu, F., and Gaither, L.A. (2009). Cholesterol biosynthesis modulation regulates dengue viral replication. *Virology* 389, 8–19.

Rous, P. (1911). A sarcoma of the fowl transmissible by an agent separable from the tumor cells. *Journal of Experimental Medicine* 13, 397–411.

Rovnak, J., and Quackenbush, S.L. (2002). Walleye dermal sarcoma virus cyclin interacts with components of the Mediator complex and the RNA Polymerase II holoenzyme. *JVI* 76, 8031–8039.

Rovnak, J., and Quackenbush, S.L. (2006). Walleye dermal sarcoma virus retroviral cyclin directly contacts TAF9. *JVI* 80, 12041–12048.

- Rovnak, J., and Quackenbush, S.L. (2010). Walleye dermal sarcoma virus: Molecular biology and oncogenesis. *Viruses* 2, 1984–1999.
- Rovnak, J., Brewster, C.D., and Quackenbush, S.L. (2012). Retroviral cyclin enhances cyclin-dependent kinase-8 activity. *Journal of Virology* 86, 5742–5751.
- Rubin, H. (2011). The early history of tumor virology: Rous, RIF, and RAV. *Proceedings of the National Academy of Sciences* 108, 14389–14396.
- Saitoh, T., Tun-Kyi, A., Ryo, A., Yamamoto, M., Finn, G., Fujita, T., Akira, S., Yamamoto, N., Lu, K.P., and Yamaoka, S. (2006). Negative regulation of interferon-regulatory factor 3–dependent innate antiviral response by the prolyl isomerase Pin1. *Nat Immunol* 7, 598–605.
- Samsa, M.M., Mondotte, J.A., Iglesias, N.G., Assunção-Miranda, I., Barbosa-Lima, G., Da Poian, A.T., Bozza, P.T., and Gamarnik, A.V. (2009). Dengue virus capsid protein usurps lipid droplets for viral particle formation. *PLoS Pathog* 5, e1000632.
- Sanchez, E.L., and Lagunoff, M. (2015). Viral activation of cellular metabolism. *Virology* 479–480, 609–618.
- Sanford, T.J., Mears, H.V., Fajardo, T., Locker, N., and Sweeney, T.R. (2019). Circularization of flavivirus genomic RNA inhibits de novo translation initiation. *Nucleic Acids Research* 47, 9789–9802.
- Sangiambut, S., Keelapang, P., Aaskov, J., Puttikhunt, C., Kasinrerak, W., Malasit, P., and Sittisombut, N. (2008). Multiple regions in dengue virus capsid protein contribute to nuclear localization during virus infection. *Journal of General Virology* 89, 1254–1264.
- Sato, S., Tomomori-Sato, C., Parmely, T.J., Florens, L., Zybaylov, B., Swanson, S.K., Banks, C.A.S., Jin, J., Cai, Y., Washburn, M.P., et al. (2004). Mediator subunits identified by multidimensional protein identification technology. *Molecular Cell* 14, 685–691.
- Scaturro, P., Cortese, M., Chatel-Chaix, L., Fischl, W., and Bartenschlager, R. (2015). Dengue virus non-structural protein 1 modulates infectious particle production via interaction with the structural proteins. *PLoS Pathog* 11, e1005277.
- van der Schaar, H.M., Rust, M.J., Waarts, B.-L., van der Ende-Metselaar, H., Kuhn, R.J., Wilschut, J., Zhuang, X., and Smit, J.M. (2007). Characterization of the early events in dengue virus cell entry by biochemical assays and single-virus tracking. *Journal of Virology* 81, 12019–12028.
- van der Schaar, H.M., Rust, M.J., Chen, C., van der Ende-Metselaar, H., Wilschut, J., Zhuang, X., and Smit, J.M. (2008). Dissecting the cell entry pathway of dengue virus by single-particle tracking in living cells. *PLoS Pathog* 4, e1000244.

Schneider, E.V., Bottcher, J., Blaesse, M., Neumann, L., Huber, R., and Maskos, K. (2011). The structure of CDK8/CycC implicates specificity in the CDK/Cyclin family and reveals interaction with a deep pocket binder. *Journal of Molecular Biology* 412, 251–266.

Sharma, M., Bhattacharyya, S., Nain, M., Kaur, M., Sood, V., Gupta, V., Khasa, R., Abdin, M.Z., Vрати, S., and Kalia, M. (2014). Japanese encephalitis virus replication is negatively regulated by autophagy and occurs on LC3-I- and EDEM1-containing membranes. *Autophagy* 10, 1637–1651.

Sharma, M., Bhattacharyya, S., Sharma, K.B., Chauhan, S., Asthana, S., Abdin, M.Z., Vрати, S., and Kalia, M. (2017). Japanese encephalitis virus activates autophagy through XBP1 and ATF6 ER stress sensors in neuronal cells. *Journal of General Virology* 98, 1027–1039.

Silva, E.M., Conde, J.N., Allonso, D., Ventura, G.T., Coelho, D.R., Carneiro, P.H., Silva, M.L., Paes, M.V., Rabelo, K., Weissmuller, G., et al. (2019). Dengue virus nonstructural 3 protein interacts directly with human glyceraldehyde-3-phosphate dehydrogenase (GAPDH) and reduces its glycolytic activity. *Sci Rep* 9, 2651.

Singh, R., Kaushik, S., Wang, Y., Xiang, Y., Novak, I., Komatsu, M., Tanaka, K., Cuervo, A.M., and Czaja, M.J. (2009). Autophagy regulates lipid metabolism. *Nature* 458, 1131–1135.

Sinha, R.A., Singh, B.K., Zhou, J., Wu, Y., Farah, B.L., Ohba, K., Lesmana, R., Gooding, J., Bay, B.-H., and Yen, P.M. (2015). Thyroid hormone induction of mitochondrial activity is coupled to mitophagy via ROS-AMPK-ULK1 signaling. *Autophagy* 11, 1341–1357.

Song, Y., Mugavero, J., Stauff, C.B., and Wimmer, E. (2019). Dengue and Zika virus 5' untranslated regions harbor internal ribosomal entry site functions. *MBio* 10, e00459-19.

Sonigo, P., Barker, C., Hunter, E., and Wain-Hobson, S. (1986). Nucleotide sequence of Mason-Pfizer monkey virus: An immunosuppressive D-type retrovirus. *Cell* 45, 375–385.

Stamatakis, A. (2014). RAxML version 8: a tool for phylogenetic analysis and post-analysis of large phylogenies. *Bioinformatics* 30, 1312–1313.

Stehelin, D., Varmus, H.E., Bishop, J.M., and Vogt, P.K. (1976). DNA related to the transforming gene(s) of avian sarcoma viruses is present in normal avian DNA. *Nature* 260, 170–173.

Steinparzer, I., Sedlyarov, V., Rubin, J.D., Eislmayr, K., Galbraith, M.D., Levandowski, C.B., Vcelkova, T., Sneezum, L., Wascher, F., Amman, F., et al. (2019). Transcriptional responses to IFN- γ require Mediator kinase-dependent pause release and mechanistically distinct CDK8 and CDK19 functions. *Molecular Cell* 76, 485-499.e8.

Stern, O., Hung, Y.-F., Valdau, O., Yaffe, Y., Harris, E., Hoffmann, S., Willbold, D., and Sklan, E.H. (2013). An N-terminal amphipathic helix in dengue virus nonstructural protein 4A mediates oligomerization and is essential for replication. *Journal of Virology* 87, 4080–4085.

Stieg, D.C., Chang, K.-T., Cooper, K.F., and Strich, R. (2019). Cyclin C regulated oxidative stress responsive transcriptome in *Mus musculus* embryonic fibroblasts. G3.400077.2019.

Stocks, C.E., and Lobigs, M. (1998). Signal peptidase cleavage at the flavivirus C-prM junction: Dependence on the viral NS2B-3 protease for efficient processing requires determinants in C, the signal peptide, and prM. *J. Virol.* 72, 2141–2149.

Suksanpaisan, L., Susantad, T., and Smith, D.R. (2009). Characterization of dengue virus entry into HepG2 cells. *Journal of Biomedical Science* 16.

Takaoka, A., and Yamada, T. (2019). Regulation of signaling mediated by nucleic acid sensors for innate interferon-mediated responses during viral infection. *International Immunology* 31, 477–488.

Tanaka, A., Takahashi, C., Yamaoka, S., Nosaka, T., Maki, M., and Hatanaka, M. (1990). Oncogenic transformation by the tax gene of human T-cell leukemia virus type I in vitro. *Proceedings of the National Academy of Sciences* 87, 1071–1075.

Tang, H.-W., Hu, Y., Chen, C.-L., Xia, B., Zirin, J., Yuan, M., Asara, J.M., Rabinow, L., and Perrimon, N. (2018). The TORC1-regulated CPA complex rewires an RNA processing network to drive autophagy and metabolic reprogramming. *Cell Metabolism* 27, 1040-1054.e8.

Tassan, J.P., Jaquenoud, M., Leopold, P., Schultz, S.J., and Nigg, E.A. (1995). Identification of human cyclin-dependent kinase 8, a putative protein kinase partner for cyclin C. *Proceedings of the National Academy of Sciences* 92, 8871–8875.

Tassaneetrithep, B., Burgess, T.H., Granelli-Piperno, A., Trumpfheller, C., Finke, J., Sun, W., Eller, M.A., Pattanapanyasat, K., Sarasombath, S., Birx, D.L., et al. (2003). DC-SIGN (CD209) mediates dengue virus infection of human dendritic cells. *Journal of Experimental Medicine* 197, 823–829.

Tay, M.Y.F., Fraser, J.E., Chan, W.K.K., Moreland, N.J., Rathore, A.P., Wang, C., Vasudevan, S.G., and Jans, D.A. (2013). Nuclear localization of dengue virus (DENV) 1–4 non-structural protein 5; protection against all 4 DENV serotypes by the inhibitor Ivermectin. *Antiviral Research* 99, 301–306.

Tay, M.Y.F., Saw, W.G., Zhao, Y., Chan, K.W.K., Singh, D., Chong, Y., Forwood, J.K., Ooi, E.E., Grüber, G., Lescar, J., et al. (2015). The C-terminal 50 amino acid residues of dengue NS3 protein are important for NS3-NS5 interaction and viral replication. *J. Biol. Chem.* 290, 2379–2394.

Tay, M.Y.F., Smith, K., Ng, I.H.W., Chan, K.W.K., Zhao, Y., Ooi, E.E., Lescar, J., Luo, D., Jans, D.A., Forwood, J.K., et al. (2016). The C-terminal 18 Amino Acid Region of Dengue Virus NS5 Regulates its Subcellular Localization and Contains a Conserved Arginine Residue Essential for Infectious Virus Production. *PLoS Pathog* 12, e1005886.

Teo, C.S.H., and Chu, J.J.H. (2014). Cellular vimentin regulates construction of dengue virus replication complexes through interaction with NS4A protein. *Journal of Virology* 88, 1897–1913.

Thaker, S.K., Ch'ng, J., and Christofk, H.R. (2019). Viral hijacking of cellular metabolism. *BMC Biol* 17, 59.

Thanos, D., and Maniatis, T. (1995). Virus induction of human IFN- β gene expression requires the assembly of an enhanceosome. *Cell* 10, 1091–1100.

Thas, I., and Garner, M.M. (2012). A retrospective study of tumours in black-tailed prairie dogs (*Cynomys ludovicianus*) submitted to a Zoological pathology service. *Journal of Comparative Pathology* 147, 368–375.

Theodorou, V., Kimm, M.A., Boer, M., Wessels, L., Theelen, W., Jonkers, J., and Hilkens, J. (2007). MMTV insertional mutagenesis identifies genes, gene families and pathways involved in mammary cancer. *Nat Genet* 39, 759–769.

Tripp, D.W., Rocke, T.E., Runge, J.P., Abbott, R.C., and Miller, M.W. (2017). Burrow dusting or oral vaccination prevents plague-associated prairie dog colony collapse. *EcoHealth* 14, 451–462.

Tsai, K.-L., Sato, S., Tomomori-Sato, C., Conaway, R.C., Conaway, J.W., and Asturias, F.J. (2013). A conserved Mediator–CDK8 kinase module association regulates Mediator–RNA polymerase II interaction. *Nat Struct Mol Biol* 20, 611–619.

Tsatsanis, C., Fulton, R., Nishigaki, K., Tsujimoto, H., Levy, L., Terry, A., Spandidos, D., Onions, D., and Neil, J.C. (1994). Genetic determinants of feline leukemia virus-induced lymphoid tumors: patterns of proviral insertion and gene rearrangement. *Journal of Virology* 68, 8296–8303.

Tsuchiya, M.T.N., Dikow, R.B., and Cassin-Sackett, L. (2020). First genome sequence of the Gunnison's prairie dog (*Cynomys gunnisoni*), a keystone species and player in the transmission of sylvatic plague. *Genome Biology and Evolution* 12, 618–625.

Uchida, L., Espada-Murao, L.A., Takamatsu, Y., Okamoto, K., Hayasaka, D., Yu, F., Nabeshima, T., Buerano, C.C., and Morita, K. (2015). The dengue virus conceals double-stranded RNA in the intracellular membrane to escape from an interferon response. *Sci Rep* 4, 7395.

Umareddy, I., Chao, A., Sampath, A., Gu, F., and Vasudevan, S.G. (2006). Dengue virus NS4B interacts with NS3 and dissociates it from single-stranded RNA. *Journal of General Virology* 87, 2605–2614.

- Waggoner, J.J., Katzelnick, L.C., Burger-Calderon, R., Gallini, J., Moore, R.H., Kuan, G., Balmaseda, A., Pinsky, B.A., and Harris, E. (2020). Antibody-dependent enhancement of severe disease is mediated by serum viral load in pediatric dengue virus infections. *The Journal of Infectious Diseases* 221, 1846–1854.
- Wallin, M., Ekström, M., and Garoff, H. (2004). Isomerization of the intersubunit disulphide-bond in Env controls retrovirus fusion. *EMBO J* 23, 54–65.
- Wang, S.-H., Syu, W.-J., Huang, K.-J., Lei, H.-Y., Yao, C.-W., King, C.-C., and Hu, S.-T. (2002). Intracellular localization and determination of a nuclear localization signal of the core protein of dengue virus. *Journal of General Virology* 83, 3093–3102.
- Wathelet, M.G., Lin, C.H., Parekh, B.S., Ronco, L.V., Howley, P.M., and Maniatis, T. (1998). Virus infection induces the assembly of coordinately activated transcription factors on the IFN- β enhancer in vivo. *Molecular Cell* 1, 507–518.
- Watson, S., Mercier, S., Bye, C., Wilkinson, J., Cunningham, A., and Harman, A. (2007). Determination of suitable housekeeping genes for normalisation of quantitative real time PCR analysis of cells infected with human immunodeficiency virus and herpes viruses. *Virology* 4, 130.
- Welsch, S., Miller, S., Romero-Brey, I., Merz, A., Bleck, C.K.E., Walther, P., Fuller, S.D., Antony, C., Krijnsse-Locker, J., and Bartenschlager, R. (2009). Composition and three-dimensional architecture of the dengue virus replication and assembly sites. *Cell Host & Microbe* 5, 365–375.
- Westerling, T., Kuuluvainen, E., and Mäkelä, T.P. (2007). Cdk8 is essential for preimplantation mouse development. *Molecular Cell Biology* 27, 6177–6182.
- Wilder-Smith, A., Ooi, E.-E., Horstick, O., and Wills, B. (2019). Dengue. *The Lancet* 393, 350–363.
- Wolf, A., Agnihotri, S., Micallef, J., Mukherjee, J., Sabha, N., Cairns, R., Hawkins, C., and Guha, A. (2011). Hexokinase 2 is a key mediator of aerobic glycolysis and promotes tumor growth in human glioblastoma multiforme. *The Journal of Experimental Medicine* 208, 313–326.
- Wootton, S.K., Halbert, C.L., and Miller, A.D. (2006). Envelope proteins of Jaagsiekte sheep retrovirus and enzootic nasal tumor virus induce similar bronchioalveolar tumors in lungs of mice. *Journal of Virology* 80, 9322–9325.
- World Health Organization (2020). Dengue and severe dengue.
- Wright, T.L., Eshar, D., Carpenter, J.W., Lin, D., Padmanabhan, A., Peddireddi, L., and Cino, G. (2017). Suspected hepatitis B virus association with a hepatocellular carcinoma in a black-tailed prairie dog (*Cynomys ludovicianus*). *Journal of Comparative Pathology* 157, 284–290.

- Wu, R.-H., Tsai, M.-H., Chao, D.-Y., and Yueh, A. (2015). Scanning mutagenesis studies reveal a potential intramolecular interaction within the C-terminal half of dengue virus NS2A involved in viral RNA replication and virus assembly and secretion. *J. Virol.* *89*, 4281–4295.
- Xie, X., Gayen, S., Kang, C., Yuan, Z., and Shi, P.-Y. (2013). Membrane topology and function of dengue virus NS2A protein. *Journal of Virology* *87*, 4609–4622.
- Xie, X., Zou, J., Puttikhunt, C., Yuan, Z., and Shi, P.-Y. (2015). Two distinct sets of NS2A molecules are responsible for dengue virus RNA synthesis and virion assembly. *J. Virol.* *89*, 1298–1313.
- Xie, X., Zou, J., Zhang, X., Zhou, Y., Routh, A.L., Kang, C., Popov, V.L., Chen, X., Wang, Q.-Y., Dong, H., et al. (2019). Dengue NS2A protein orchestrates virus assembly. *Cell Host & Microbe* *26*, 606-622.e8.
- Xu, W., Stadler, C.K., Gorman, K., Jensen, N., Kim, D., Zheng, H., Tang, S., Switzer, W.M., Pye, G.W., and Eiden, M.V. (2013). An exogenous retrovirus isolated from koalas with malignant neoplasias in a US zoo. *Proceedings of the National Academy of Sciences* *110*, 11547–11552.
- Xu, W., Amire-Brahimi, B., Xie, X.-J., Huang, L., and Ji, J.-Y. (2014). All-atomic molecular dynamic studies of human CDK8: Insight into the A-loop, point mutations and binding with its partner CycC. *Computational Biology and Chemistry* *51*, 1–11.
- Yang, C., Liu, X., Cheng, T., Xiao, R., Gao, Q., Ming, F., Jin, M., Chen, H., and Zhou, H. (2019). LYAR suppresses beta interferon induction by targeting phosphorylated interferon regulatory factor 3. *J Virol* *93*, e00769-19, /jvi/93/21/JVI.00769-19.atom.
- Yap, T.L., Xu, T., Chen, Y.-L., Malet, H., Egloff, M.-P., Canard, B., Vasudevan, S.G., and Lescar, J. (2007). Crystal structure of the dengue virus RNA-dependent RNA polymerase catalytic domain at 1.85-angstrom resolution. *JVI* *81*, 4753–4765.
- York, D.F., Vigne, R., Verwoerd, D.W., and Querat, G. (1992). Nucleotide sequence of the Jaagsiekte retrovirus, an exogenous and endogenous type D and B retrovirus of sheep and goats. *Journal of Virology* *66*, 4930–4939.
- Yu, I.-M., Zhang, W., Holdaway, H.A., Li, L., Kostyuchenko, V.A., Chipman, P.R., Kuhn, R.J., Rossmann, M.G., and Chen, J. (2008). Structure of the immature dengue virus at low pH primes proteolytic maturation. *Science* *319*, 1834–1837.
- Yu, I.-M., Holdaway, H.A., Chipman, P.R., Kuhn, R.J., Rossmann, M.G., and Chen, J. (2009). Association of the pr peptides with dengue virus at acidic pH blocks membrane fusion. *JVI* *83*, 12101–12107.
- Yusof, R., Clum, S., Wetzel, M., Murthy, H.M.K., and Padmanabhan, R. (2000). Purified NS2B/NS3 serine protease of dengue virus type 2 exhibits cofactor NS2B dependence

for cleavage of substrates with dibasic amino acids in vitro. *J. Biol. Chem.* 275, 9963–9969.

Zavala, G., Pretto, C., Chow, Y.-H.J., Jones, L., Alberti, A., Grego, E., De las Heras, M., and Palmarini, M. (2003). Relevance of Akt phosphorylation in cell transformation induced by Jaagsiekte sheep retrovirus. *Virology* 312, 95–105.

Zhang, J., Lan, Y., Li, M.Y., Lamers, M.M., Fusade-Boyer, M., Klemm, E., Thiele, C., Ashour, J., and Sanyal, S. (2018). Flaviviruses exploit the lipid droplet protein AUP1 to trigger lipophagy and drive virus production. *Cell Host & Microbe* 23, 819-831.e5.

Zhang, Q., Hunke, C., Yau, Y.H., Seow, V., Lee, S., Tanner, L.B., Guan, X.L., Wenk, M.R., Fibriansah, G., Chew, P.L., et al. (2012). The stem region of premembrane protein plays an important role in the virus surface protein rearrangement during dengue maturation. *The Journal of Biological Chemistry* 287, 40525–40534.

Zhang, Y., Zhang, W., Ogata, S., Clements, D., Strauss, J.H., Baker, T.S., Kuhn, R.J., and Rossmann, M.G. (2004). Conformational changes of the flavivirus E glycoprotein. *Structure* 12, 1607–1618.

Zhao, X., Feng, D., Wang, Q., Abdulla, A., Xie, X.-J., Zhou, J., Sun, Y., Yang, E.S., Liu, L.-P., Vaitheesvaran, B., et al. (2012). Regulation of lipogenesis by cyclin-dependent kinase 8–mediated control of SREBP-1. *J. Clin. Invest.* 122, 2417–2427.

Zhao, Y., Soh, T.S., Zheng, J., Chan, K.W.K., Phoo, W.W., Lee, C.C., Tay, M.Y.F., Swaminathan, K., Cornvik, T.C., Lim, S.P., et al. (2015). A crystal structure of the dengue virus NS5 protein reveals a novel inter-domain interface essential for protein flexibility and virus replication. *PLoS Pathog* 11.

Zou, J., Xie, X., Lee, L.T., Chandrasekaran, R., Reynaud, A., Yap, L., Wang, Q.-Y., Dong, H., Kang, C., Yuan, Z., et al. (2014). Dimerization of flavivirus NS4B protein. *Journal of Virology* 88, 3379–3391.

Zou, J., Xie, X., Wang, Q.-Y., Dong, H., Lee, M.Y., Kang, C., Yuan, Z., and Shi, P.-Y. (2015). Characterization of dengue virus NS4A and NS4B protein interaction. *J. Virol.* 89, 3455–3470.